Terms and Conditions of Use of Digitised Theses from Trinity College Library Dublin

Copyright statement

All material supplied by Trinity College Library is protected by copyright (under the Copyright and Related Rights Act, 2000 as amended) and other relevant Intellectual Property Rights. By accessing and using a Digitised Thesis from Trinity College Library you acknowledge that all Intellectual Property Rights in any Works supplied are the sole and exclusive property of the copyright and/or other IPR holder. Specific copyright holders may not be explicitly identified. Use of materials from other sources within a thesis should not be construed as a claim over them.

A non-exclusive, non-transferable licence is hereby granted to those using or reproducing, in whole or in part, the material for valid purposes, providing the copyright owners are acknowledged using the normal conventions. Where specific permission to use material is required, this is identified and such permission must be sought from the copyright holder or agency cited.

Liability statement

By using a Digitised Thesis, I accept that Trinity College Dublin bears no legal responsibility for the accuracy, legality or comprehensiveness of materials contained within the thesis, and that Trinity College Dublin accepts no liability for indirect, consequential, or incidental, damages or losses arising from use of the thesis for whatever reason. Information located in a thesis may be subject to specific use constraints, details of which may not be explicitly described. It is the responsibility of potential and actual users to be aware of such constraints and to abide by them. By making use of material from a digitised thesis, you accept these copyright and disclaimer provisions. Where it is brought to the attention of Trinity College Library that there may be a breach of copyright or other restraint, it is the policy to withdraw or take down access to a thesis while the issue is being resolved.

Access Agreement

By using a Digitised Thesis from Trinity College Library you are bound by the following Terms & Conditions. Please read them carefully.

I have read and I understand the following statement: All material supplied via a Digitised Thesis from Trinity College Library is protected by copyright and other intellectual property rights, and duplication or sale of all or part of any of a thesis is not permitted, except that material may be duplicated by you for your research use or for educational purposes in electronic or print form providing the copyright owners are acknowledged using the normal conventions. You must obtain permission for any other use. Electronic or print copies may not be offered, whether for sale or otherwise to anyone. This copy has been supplied on the understanding that it is copyright material and that no quotation from the thesis may be published without proper acknowledgement.

CHARACTERISATION OF DRUG TRANSPORTERS IN HUMAN RESPIRATORY EPITHELIAL CELLS

by

Sibylle Endter Dipl.-Pharm., M.P.S.I.

A dissertation submitted for the degree of Doctor of Philosophy

at the

University of Dublin, Trinity College.

This research was conducted in the School of Pharmacy and Pharmaceutical Sciences, Trinity College, Dublin 2, Ireland

Under the direction and supervision of

Dr. rer. nat. Carsten Ehrhardt

2010

Declaration

This dissertation is submitted by the undersigned to the University of Dublin, Trinity College, for examination for the degree of Doctor of Philosophy. This work has not been submitted previously as an exercise for a degree at this or any other university and that it is entirely work of the undersigned author with the aid of editorial advice from Dr. Carsten Ehrhardt. The Trinity College Library may lend or copy this dissertation without restriction.

Signed

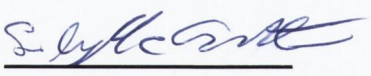

Sibylle Endter

Summary

Cell culture models are an efficient and relatively cheap tool to study isolated mechanisms of an organ. The right cell model, carefully selected to allow highest benefits, can give valuable information in the area of active drug transport, a mechanism hardly understood in the lung. Whereas Caco-2 cells have been demonstrated to be an efficient model for absorption studies in the gastrointestinal region, in the lung a most suitable model for these investigations has not been declared. Little is known about the expression of membrane transporters within lung epithelium, and even less about regional differences that may exist within the different lung epithelial surfaces. My work demonstrated similarities and differences between human lung epithelial cells of different origins. Primary models were compared to cell lines, either isolated from cancer cells or obtained by immortalisation of normal cells. Each model showed a characteristic pattern of expression and activity of the drug transporters tested. Moreover, a number of variations regarding transporter expression in cell models of pulmonary compared to gastrointestinal origin were discovered. Traditional RT-PCR and quantitative RT-PCR analyses characterised mRNA transcript expression of a wide range of membrane carrier transporters in several *in vitro* lung epithelial cell models. Transporters studied included: 11 ABC transporters, 11 SLC transporters, and 9 SLCO transporters. Employed cell culture models included both established cell lines (A549, Calu-3, 16HBE14o-, BEAS-2B) and freshly isolated cells in primary culture (human bronchial and alveolar epithelial cells). Immunofluorescence microscopy confirmed MDR1 protein in hAEpC localised predominantly at the luminal membranes, which was in agreement with immunohistochemical staining for MDR1 performed in normal human lung tissue and resulting in a positive signal

at luminal membranes of ATI cells. Western blot revealed low presence of MDR1 protein in the primary hAEpC at day 8 of culture. Transport of rhodamine-123 (a MDR1 substrate) across the confluent hAEpC monolayers was polarised with net secretion. These findings indicate that hAEpC monolayers might provide a suitable *in vitro* model for studying MDR1 function mechanistically in the distal human lung. Immunofluorescence microscopy confirmed the presence of OCT1, OCT3, OCTN1 and OCTN2 in all cell models tested with highest expression of OCTN1 and OCTN2 in Calu-3 (AIC). Further studies with more specific, ideally monoclonal, antibodies are essential to quantify the proteins. Uptake of the cationic fluorophore 4-[4-(dimethylamino)-styryl]-N-methylpyridinium (ASP^+) was characterised. A549 cells revealed the fastest uptake and Caco-2 cells the highest saturation limit, whereas uptake into Calu-3 and 16HBE14o- cells appeared to be much slower and quicker to saturate. The primary model, hBEpC, showed relatively fast uptake with early saturation. The uptake of ASP^+ was pH- and sodium-dependent in A549 cells and pH-dependent in Calu-3 cells. L- and D-carnitine did not reduce uptake in any cell model tested. Inhibition by formoterol, amantadine and verapamil was of significance in the A549 cell line only. In A549 cells, salmeterol did inhibit the uptake of ASP^+ significantly, but not budesonide and beclomethasone. Bi-directional transport studies revealed net secretion across Calu-3 monolayers and net absorption in the case of 16HBE14o-, whereas hBEpC did not show any directed transport at all. However, whether Calu-3 or 16HBE14o- reflect *in vivo* characteristics is not clear yet, since the commercially obtained hBEpC (as the arguably closest model) showed very peculiar behaviour in our hands. My work could provide a first impression, further transport studies with freshly isolated bronchial epithelium need to clarify this conflict.

Table of contents

1 Introduction

1.1 Lung architecture and epithelial cell types

To enable an efficient and safe gas exchange, the lung is divided in two main functional areas: the conducting zone and the respiratory zone. The conducting area comprises the trachea, bronchi and bronchioles. The respiratory region consists of respiratory bronchioles, alveolar sacs, alveoli and alveolar capillary network. A significant model, shown in figure 1.1, was classified by Weibel [1963] which presents the lung bifurcating into 23 generations, starting with the trachea (generation 0, diameter 1.8 cm), that connects the nasopharyngeal region to the lower respiratory tract lung tissue and branches into the right and left main bronchi.

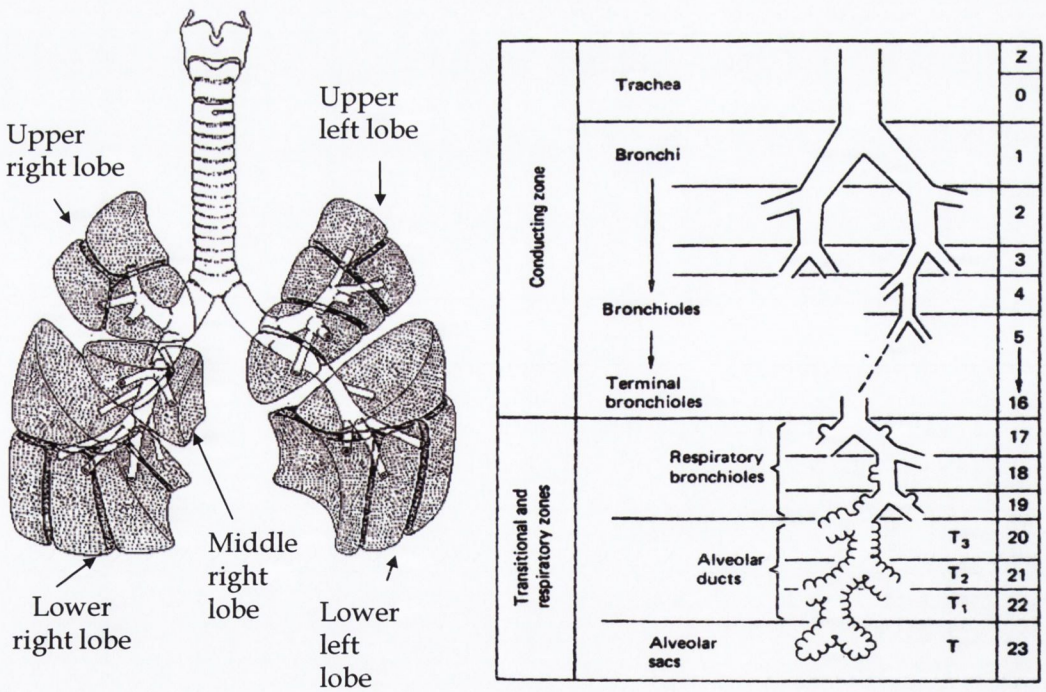

Figure 1.1 Anatomy of the lung (left), model of generations (right) [Weibel ER, 1963]

Generations 0 to 16 compose the conducting zone followed by seven generations of respiratory zone. Cartilages are set in walls of trachea and bronchi to prevent collapse, but disappear after generation 11 (figure 1.2).

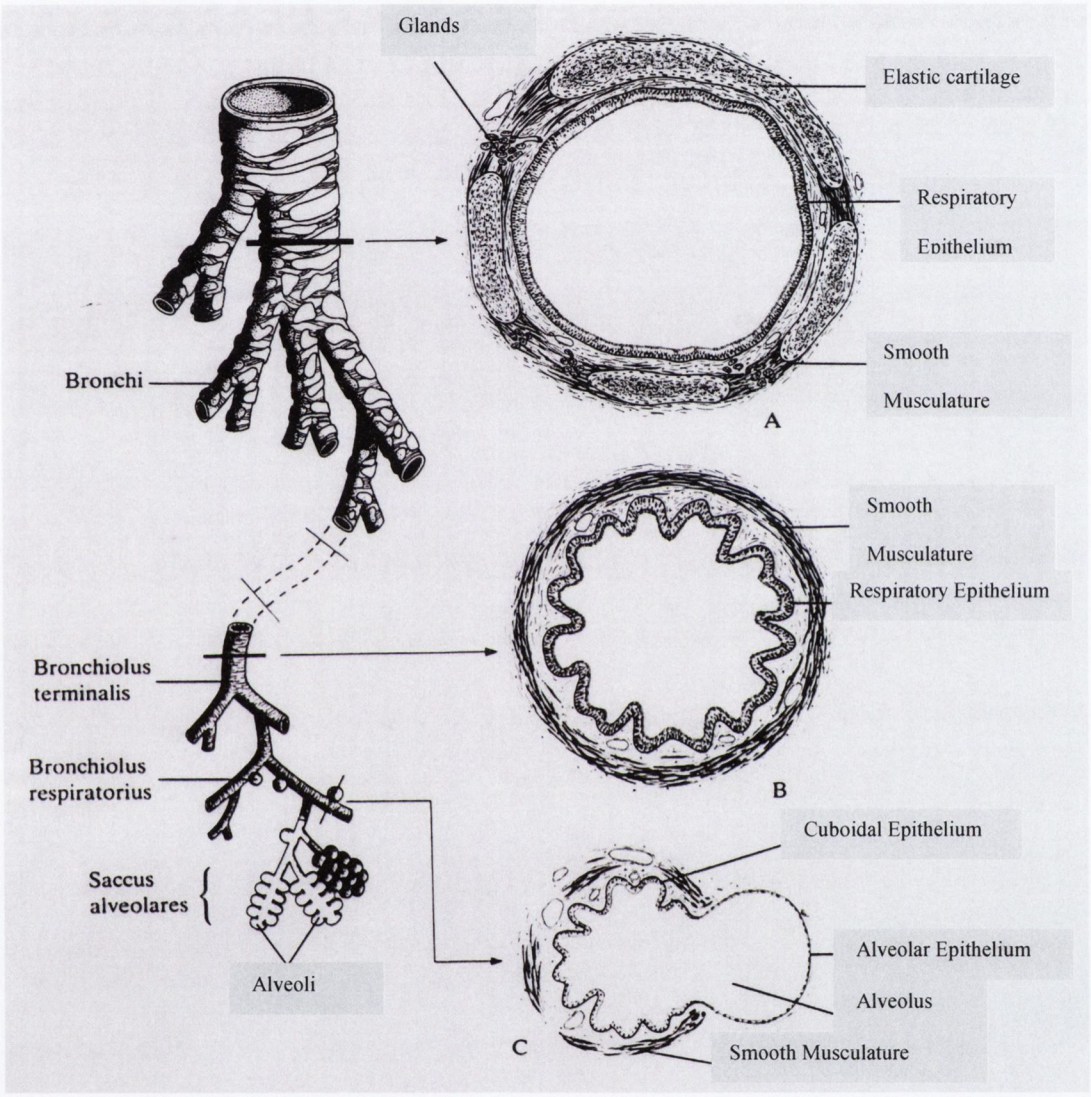

Figure 1.2 Structure of the main sections of the bronchial tree. A = cross section of a bronchus. B = cross section of a bronchiolus with star-shaped lumen. C = cross section of the bronchiolus respiratorius and the alveolus (adapted from [Rohen and Lütjen-Drecoll 2000]).

During 23 generations, morphology and function of the airway epithelium changes remarkably (figure 1.3). There are over 60 cell types in the human lung [Stone 1992], with the main types of the airways being the basal cell, the ciliated cell, the goblet cell, the clara cell, alveolar epithelial type I and II cell (ATI and ATII). Sinuses, pharynx and larynx, forming the first area of the airway, conduct air to generations 0 to 4, trachea and bronchi which feature a pseudostratified epithelium comprising, among others, columnar ciliated and secretory cells next to basal cells. Filtration and conduction of the air to parenchymal area of the lung are essential functions of these generations requiring barrier function of the epithelium (cell depth ~ 50 μm). Goblet cells produce mucus that covers the entire surface of bronchial epithelium and is transported by ciliated cells towards pharynx, where it can be swallowed or coughed out. This mechanism removes particles, bacteria and viruses and therefore is an important part of the unspecific immune system. The monolayer of lung surfactant that coats both airway and alveolar surface is probably only a single molecule thick in most places, but it causes large molecules to aggregate. This aggregation can enhance engulfment by macrophages. Below the molecular layer of lung surfactant the epithelial surface fluids are localised, through which a drug has to diffuse to finally reach the epithelial cell layer. The roles of pH, osmolarity, ions, proteins, lipids, and other constituents of the lining fluid are just beginning to be studied. In the airways the thickness of the surface fluid is thought to average about 5-10 μm [Yoneda 1976], gradually decreasing distally until the vast expanse of the alveoli is reached.

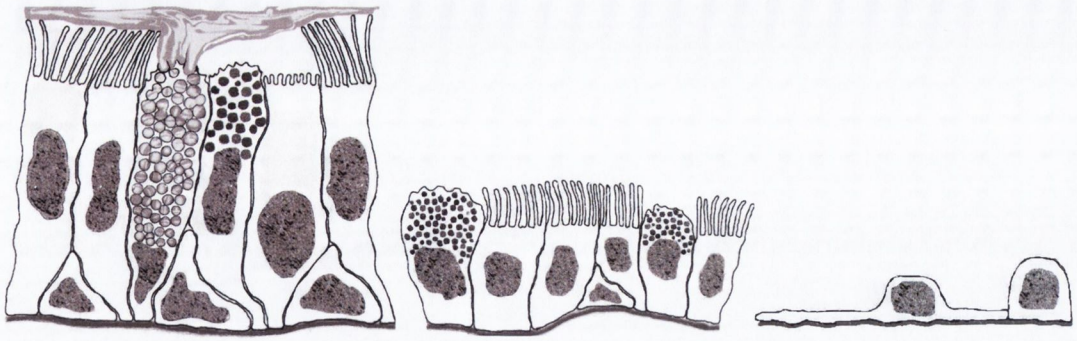

Bronchi Bronchioles Alveoli

Figure 1.3 Major cell types in lung epithelium

During the following 10 generations to the terminal bronchioles, the depth of cells reduces continuously resulting in a thinner epithelium including cuboidal ciliated cells and, additionally, clara cells (cell depth ~ 10 μm). Generations 17 to 23 are the respiratory region composed of respiratory bronchioles, alveolar ducts and alveolar sacs. Alveolar ducts end in groups of alveolar sacs with a diameter of 250 μm. An adult has between 200 and 600 million alveoli. Epithelial cells in this area are extremely thin (cell depth ~ 0.2-4 μm) to allow gas exchange between alveoli and blood. A network of blood capillaries covers the thin basement membrane forming a large area for optimal diffusion of gases. Cell types in this region include mainly alveolar epithelial type I and II cells (ATI and ATII) and macrophages. The estimated area of the epithelial surface of an adult is 140 m^2. The large but thinly stretched ATI cells cover more than 95% of this surface and therefore represent the main part of the air-blood-barrier connected by tight junctions. The cuboidal ATII, although larger in number (67% of cells in number), compose less than 5% of the surface area. They are thicker, include more intracellular organelles and their apical membrane expresses microvilli. Situated in the corners of the alveolus, these cells

serve as progenitor cells for regeneration of ATI cells and produce and secrete surfactant, which covers the alveolar epithelial surface to lower surface tension and prevent collapse. A very thin layer of fluid covers the respiratory area. The average depth of it is about 0.05-0.08 μm, but may also be several microns thick in pooled areas and as thin as 15-20 nm [Weibel 1963; Bastacky et al. 1995]. Little is known about the dynamics of normal fluid in the alveoli.

1.2 Drug delivery to the lung

Drug inhalation is an appreciated and highly developed treatment in therapy of respiratory diseases such as asthma, chronic obstructive pulmonary disease (COPD), cystic fibrosis, and pulmonary infections. Local application leads to high concentrations of drugs in the targeted area within short periods allowing for rapid action and less unwanted side effects due to low systemic exposure. Systemic administration of drugs via the lung is a rather new and challenging method, but initial progress shows it to be a promising pathway. The large surface area of the thin air-blood-barrier with relatively low enzymatic activity appears to be an attractive target for delivery of drugs with low bioavailability after oral administration. For local application, loss of drug inside the inhaler or at areas of the airways not targeted is tolerated because of relative low side effects and costs of drugs used. However, optimisation of inhalers is constantly in process. By control of the aerodynamic properties of the aerosol, deposition in the different region of the respiratory tract can be guided. Large, dense particulates and droplets will not leave the inhaler or will be deposited in the oropharyngal regions to a vast amount because of impaction caused by inertia due to their high mass and high velocity.

Particles intended to reach the respiratory region for systemic absorption should be homogenously small (1-5 μm in diameter) or very light. For therapeutic aerosol particulates the parameter assessing their targeting best is the aerodynamic diameter (d_a). The d_a is the product of the particles geometric diameter and the square root of its mass density. The aerodynamic diameter should be 1-3 μm for deposition in the alveolar region of the lung. The difference between geometric and aerodynamic diameter are demonstrated by the example that even very large (~20 μm in geometric diameter) insulin-loaded PLGA particles were able to reach the alveolar region if they were light and porous enough, resulting in a d_a of ~ 1μm [Edwards et al. 1997]. Particles with aerodynamic diameters <1 μm are not deposited in the lung but expired.

Insulin, morphine, vaccines and therapeutic peptides are just first examples of this emergent systemic delivery via the lung. Inhalation of insulin or morphine is a fast and needle free delivery method of relatively well-controlled doses of these drugs providing an attractive alternative to injections.

The respiratory region provides good conditions for absorption of inhaled macromolecules. Although the surface area of the airways in adult humans is relative small with an average of 2.5 m^2 the large surface area of the alveolar epithelium, varying between 100 and 140 m^2, represents an attractive target for systemic drug delivery. The thin nature of the mucus free air-blood-barrier in this region allows gas exchange over the short distance of 0.5 to 1 μm. Drugs delivered to alveoli can overcome this barrier and enter the blood circulation. Unlike the airways which are limited by a lower regional blood flow the alveolar region is well supplied with blood in dimensions of 5 l/min. Molecules entering the

bloodstream here avoid a first-pass effect which is a challenging part of drug administration via the intestinal route (figure 1.4).

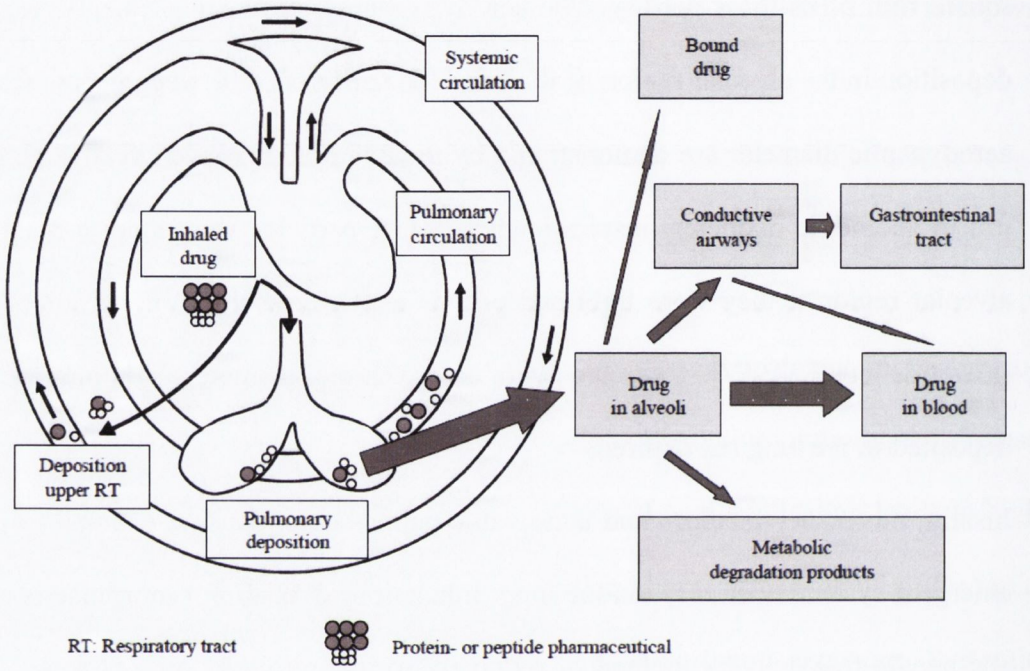

Figure 1.4 Systemic uptake of inhaled drugs after peripheral/alveolar deposition [Siekmeier and Scheuch 2008]

One important factor for the bioavailability of proteins is their size. With a molecular weight up to 30 kDa estimated bioavailability lies between 20 and 50%. Such molecules are absorbed relatively fast compared to larger proteins. However, many other variables can affect the uptake of a molecule leading to an unexpected bioavailability. Apart from size, there are pH-value, electrical charge, surface activity, solubility, stability and enzymatic activity that need to be considered in alveoli. The conducting area is protected by the mucociliar clearance making protein delivery in this region a challenging if not futile task. The lack of this

mechanism in the alveolar area results in a considerable higher bioavailability than in the conducting area that makes this the preferable area. To date, four absorption mechanisms are known to be involved in protein delivery via the alveolar epithelium: phagocytosis by alveolar macrophages, paracellular diffusion via tight junction, vesicular endocytosis or pinocytosis and receptor dependent transcytosis. The functional role of barriers and transport mechanisms is very different and underlies control by physiological and pharmacological factors. External influences on the air-blood-barrier including cigarette smoke can increase permeability leading to faster absorption of insulin in smokers. The opposite effect has been demonstrated in decreased absorption due to alveolar inflammation potentially caused by the inhalation therapy itself [Siekmeier and Scheuch 2008].

Inhaled drugs need to cross the mucus layer and the alveolar lining fluid. Mucus is composed of lipids and glycoproteins. This layer is covered with the thin surfactant form the lower respiratory tract. Depending on the area of the airways its composition, amount and thickness varies, but also can be influence by inflammation or neural factors. The effects of inflammation and pulmonary diseases must be considered for systemic drug delivery in each individual case, since the actual impacts of these diseases on drug absorption are difficult to prognosticate. The monolayer of lung surfactant that coats both airway and alveolar affect stability and solubility of large molecules causes them to aggregate. Macrophages are a primary barrier to the pulmonary absorption of macromolecules, as they are an important part of the unspecific immune system with rapidly increase of number in case of inflammation. Normally, they are the only type of phagocytic cells within the lower respiratory tract. Their release of mediators of inflammation causes an inflammatory cascade. ATI cells can express

carboxypeptidase on their membrane, which degrades several peptides and proteins. Additionally, proteases and proteolytic enzymes are secreted by lymphocytes. The use of protease inhibitors can increase the bioavailability. In normal lung tight junctions inhibit uptake of proteins allowing only small molecules to pass, but cellular damage can open this barrier and enable permeation of large molecules. After passing the epithelium, tight junctions of the endothelium allow permeation of larger molecules. Membrane pores are assumed to exist in different and even flexible sizes for permeation of a range of fluids and macromolecules. Vesicular transport of ATI cells is pressure independent and enables the uptake of fluids and macromolecules. Surfactant secreted by ATII cells is absorbed together with macromolecules by ATI cells via vesicles. Vesicles of this cell type have a diameter of about 35 nm and allow the transcellular transport of large macromolecules. The functional capacity of this mechanism is not estimated easily due to variable number vesicles depending on fluid volume in the lung, specific or unspecific binding of the glycocalix, hardly understood mechanism of movement of the vesicles in the cells, variations between different types of vesicles and insufficient knowledge of mechanisms of membrane displacement and fusion of the vesicles. The role of transporters is hardly understood in this area. Neither uptake nor efflux has been reported.

Sabin and co-workers were among the first who vaccinated by inhalation on a larger scale [Sabin et al. 1983]. An aerosolised vaccine revealed many advantages for a mass vaccination against measles. In developing countries, organisation and funding of sterile consumables for many injections is rather complicated leading to a limited success of such campaigns. Inhalation allows supply to a larger group. Another and more important advantage is the "blood free" nature of this application

preventing the spread of many diseases transmitted by blood, such as the human immunodeficiency virus (HIV) and hepatitis B. Aerosol infection is a common route for many diseases. Therefore, immunisation via the airways induces protection at the site of transmission. Maternal antibodies have been shown to cause problems when vaccinating young children. Aerosolised vaccination can avoid these. Apart from measles, several diseases are suitable candidates: Influenza, rubella plus measles, anthrax, plague, tularaemia and smallpox are just some examples. The choice of excipients needs to be considered, since allergenic and irritating effects can compromise safety of inhaled vaccination in particular for asthmatics [Laube 2005].

Contamination of facemask or mouthpiece with saliva of the vaccinee represents another safety issue that needs to be considered. It could lead to the spread of pathogens.

Gene delivery by inhalation has been reported as a desirable therapy for cystic fibrosis (CF) and lung cancer. Clinical trials utilised three gene-transfer agents to achieve recovery of CFTR and normal chloride channel function in the lungs. Adenovirus, adeno-associated virus 2 and cationic liposomes successfully transferred the normal gene into the airway; however, the transfer efficiency observed was below the limed leading to clinical benefit [Laube 2005]. The polypeptide polyethyleneimine demonstrates sufficient stability during nebulisation. Aerosol delivery of polyethyleneimine DNA complexes results in substantial gene expression in the lungs of mice, and aerosol polyethylenimine-p53 therapy and aerosol polyethyleneimine interleukin-12 therapy significantly reduce the number and size of osteosarcoma lung metastases in mice [Laube 2005].

However, due to the complex nature of the lung, further development of this route is a rather challenging assignment. Due to these challenges, many substances listed in table 1.1 have no fully developed application to assure save and efficient application methods for successful pulmonary delivery. Isolated perfused lung is an effective method and reduces some of this complexity, [Tronde et al. 2008] but further simplification for initial studies, such as cell culture models, can reduce costs and improve research efficiency.

The complex structure of the lung does not allow differentiating between absorption in the different pulmonary regions, when investigating the mechanisms of drug uptake in *in vivo* or *in situ* experiments. Therefore, *in vitro* models based on pulmonary epithelial cells may help to elucidate the underlying processes.

However, comparatively little is known about the potential impact of membrane transporters upon the drug absorption and disposition process. Active transport mechanisms within the respiratory tract also have the potential to modify the biodistribution of therapeutic drugs and environmental xenobiotics that enter the body by other routes such as the gastrointestinal tract, which may alter the retention or accumulation within the lung and ultimately result in toxicity [Ayrton and Morgan 2001;2008]. However, it is clear that the impact of a transporter such as MDR1 on the absorption and disposition of a given substrate will also depend on the substrate's physicochemical properties such as its overall permeability profile (i.e. high or low permeability drug).

Substance group	Substance	Molecular Weight[1)]	Indication
Ergotamine	Dihydroergotamine mesilate	700	Migraine, vascular cephalgia, orthostatic hypotension
	Ergotamine tartrate	1300	Migraine, vascular cephalgia, orthostatic hypotension
Heparin	Fractionated heparin (low molecular weight heparin)	mean MW: 4000-6000	Prevention of deep venous thrombosis, myocardial infarction
	Unfractionated heparin	Mean molecular weight: 15000	Prevention of deep venous thrombosis, myocardial infarction, migraine
Hormones (protein hormones and their analogs)	Calcitonin	4500	Osteoporosis, Paget's disease of the bone
	Cetrorelix	1430	Gonadorelin receptor antagonist, increase of fertility
	Epoetin α	14700	Anaemia
	Epoetin β, γ, δ, ε, ω	18200	Anaemia
	Follicle-stimulating hormone (FSH)	36000	Hormone replacement therapy
	Glucagon	3600	Hormone replacement therapy
	Growth hormone (somatotropin)	22100	Growth hormone deficiency
	Insulin	6000	Diabetes mellitus
	Leuprolide	1200	Endometriosis, pubertas praecox, prostate carcinoma
	Prolactin	23000	Hormone replacement therapy
	Releasing hormones (different hormones)	variable	Different diseases
	Granulocyte-colony stimulating factor (rhGCSF)	18800	Chronic granulocytopenia, AIDS
	PEGylated rhG-CSF	24000-36000	Chronic granulocytopenia, AIDS

	Granulocyte macrophagecolony stimulating factor (GM-CSF)	14600	Tumour therapy of lung metastases, granulocytopenia, infection
	Oxytocin	1000	Hormone replacement therapy
	Parathormone 1-34 (PTH)	4300	Osteoporosis, Paget's disease of the bone
	Parathormone 1-84 (PTH)	9400	Hormone replacement therapy
	Thyroid-stimulating hormone (TSH)	24000-30000	Hypothyreosis
	Vasopressin-analogon (dDAVP)	1100	Enuresis
Other hormones/ neurotransmitters	Adrenaline (Epinephrine)	180	Anaphylactic reaction
	Adrogolide	440	Parkinson's disease
	Estrogens (different estrogens)	270-290	Hormone replacement therapy, slow release application
	Nicotine	160	Smoking cessation, nicotine deprivation
	Testosterone	290	Hormone replacement therapy
Immuno-modulators and suppressors	Cyclosporine A	1200	Graft rejection (especially lung)
	α-Interferons	19000-22000	Chronic hepatitis B and C, tumour therapy (lung cancer or lung metastases of tumours)
	β-Interferons	19000-22000	Multiple sclerosis, tumour therapy (lung cancer or lung metastases of tumours)
	γ-Interferon	16000-25000	Tumour therapy
	Consensus interferon (rCON-IFN)	19600	Hepatitis C
Liposomes	Cyclosporine A	1200	Graft rejection (especially lung)
	Desoxyribonucleic acid (DNA)	variable	Gene therapy (e. g. cystic fibrosis, lung metastases)

	Fentanyl	340	Pain therapy (e.g., cancer)
	Guanylate cyclase agonists	not available	Primary pulmonary hypertension
	Insulin	6000	Diabetes mellitus
	Interleukin-2 (IL-2)	15400	Tumour therapy (predominantly pulmonary metastases of renal cell carcinoma, but also melanoma, lung cancer and breast cancer), chronic hepatitis C
	Leuprolide	1200	Endometriosis, pubertas praecox, prostate carcinoma
	9-nitrocampothecin	393	Tumour therapy (primary or metastatic lung cancer)
	Paclitaxel	854	Tumour therapy (e.g., pulmonary metastases of renal cell carcinoma)
NO donators	Nitroglycerin	230	Primary pulmonary hypertension
	Sodium nitroprusside	300	Primary pulmonary hypertension
Opioids	Fentanyl	340	Pain therapy (e.g., cancer)
	Morphine (hydrochloride or sulphate)	380 or 760	Dyspnea, pain therapy (e.g. cancer)
	Δ-9-tetrahydrocannabinol (THC; dronabinol)	314	Pain therapy, anorexia, nausea, migraine
PDE inhibitors	Dipyramidol	500	Primary pulmonary hypertension
	Pentoxifylline	280	Primary pulmonary hypertension
	Sildenafil	470	Primary pulmonary hypertension
	Tolafentrine	510	Primary pulmonary hypertension

	Zaprinast	270	Primary pulmonary hypertension
Peptides/proteins	Bactericidal/permeability -increasing protein (BPI)	55000	Gram-negative infections of the respiratory tract
	Fab fragments	50000-100000	Vaccination
	Factor IX	57000	Haemophilia B
	Hirudin	7000	Anticoagulant
	Polyamino acids	5000-20000	Experimental
	Protein C	60000	Thrombophilia
	Renin-inhibitory peptides	1000	Hypertonia
	RGD peptides	500-1000	Anti-adhesion molecules
Prostaglandins	Iloprost	360	Primary pulmonary hypertension
	Prostaglandins E_1 and I_2	360	Primary pulmonary hypertension
Tranquiliser	Midazolam	330	Sedation
Vaccines	Influenza virus vaccine, measles virus vaccine, vaccines against inhaled bioterrorism agents	variable	Vaccination against systemic diseases

Table 1.1 Examples of aerosol inhalation for systemic treatment including clinical or experimental studies in animals, off-label use and applications not approved for human use. [Siekmeier and Scheuch 2008]

[1)]Approximated values; data in part for non-glycosylated monomers of peptides and protein

1.3 Drug transporters

The phylogeny, molecular biology and functional characteristics of membrane transporters have been major focuses in biopharmaceutical and cell physiology research over the last 15 years. Particular attention has been paid to transporter

expression within biological barriers such as the blood-brain barrier, liver, kidney and intestine [Sai et al. 2004]. Little is known about the expression of membrane transporters within lung epithelium, and even less about regional differences that may exist within the different lung epithelial surfaces (e.g. alveolar vs. bronchial).

1.3.1 ABC superfamily

ABC transporters are transmembrane proteins that use the energy of ATP hydrolysis to actively transport a wide variety of substrates across extra- and intracellular membranes. Proteins are classified as ABC transporters based upon the sequence and organisation of their ATP or nucleotide binding domains; the functional protein typically contains two nucleotide-binding domains. An ABC protein comprises one to three transmembrane domains, each comprising five to six membrane spanning segments (figures 1.5, 1.6 and 1.7) [Schinkel and Jonker 2003]. The ABC superfamily is divided into seven subfamilies (A-G) based upon similarity of gene structure, the order of the membrane spanning domain, and the sequence homology in the nucleotide binding domain and the transmembrane domains. Substrates include physiological metabolic products, lipids, sterols and a wide range of drugs. [Dean et al. 2001]

ABC transporter family members that are of particular significance with respect to drug absorption and disposition include: MDR1, the multidrug resistance related proteins (MRP1-9) and breast-cancer-related protein (BCRP) (table 1.2) [Cordon-Cardo et al. 1990; Thomas et al. 1994; Ejendal and Hrycyna 2002].

Protein name	Aliases
MDR1	ABCB1, PGY1, P-glycoprotein (P-gp), GP170
MRP1	ABCC1; MRP; ABCC; GS-X; MRP1; ABC29; DKFZp781G125; DKFZp686N04233
MRP2	ABCC2, cMOAT, cMRP
MRP3	ABCC3, MOAT-D, cMOAT-2
MRP4	ABCC4, MOAT-B
MRP5	ABCC5, MOAT-C, pABC11
MRP6	ABCC6, MOAT- E, MLP-1
MRP7	ABCC10
MRP8	ABCC11
MRP9	ABCC12
WHITE1	ABCG1, ABC8
BCRP	ABCG2, MXR, ABCP

Table 1.2 Clinically relevant ABC transporters

MDR1

MDR1 was the first human ABC transporter to be cloned and characterised (figure 1.5). It causes multidrug resistance of cancer cells, but is also expressed in healthy tissues. MDR1 is found to be mainly expressed at the apical aspect of epithelial cells in the liver and blood-brain barrier, epithelial cells of the intestine and the kidney and in adrenal glands.

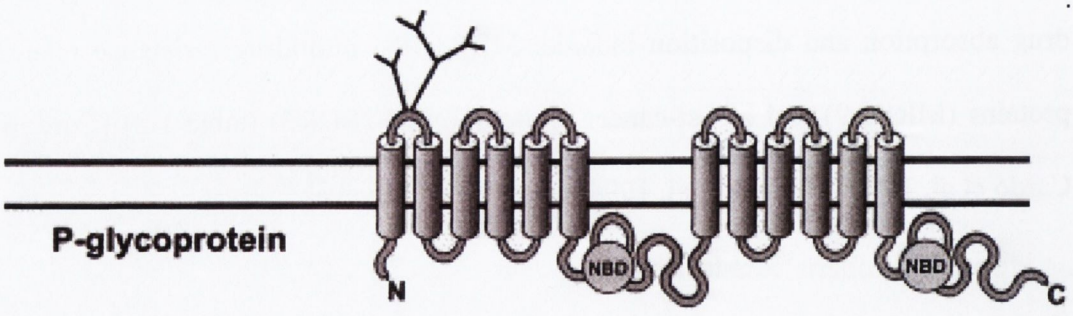

Figure 1.5 Predicted secondary structures of MDR1 [Schinkel and Jonker, 2003]

Within the lung, previous work has localised MDR1 to the bronchial and alveolar epithelial cells [Campbell et al. 2003; van der Deen et al. 2005]. Functionality of MDR1 has also been demonstrated in lung epithelial continuous cell lines, as well as in rat and human primary alveolar cells [Campbell et al. 2003]. MDR1 substrates are usually organic molecules of variable sizes with aromatic groups or non-aromatic linear or cyclic molecules. The wide variety of substrates includes colchicines, cimetidine, doxorubicin, vinblastine, digoxin, saquinavir, rhodamine 123, lipids and steroids (table 1.3). Although it protects the body from various toxins, MDR1 is not essential to sustain life [Schinkel and Jonker 2003].

Substrates		**Inducers**	**Inhibitors**
Anticancer agents	*Anti-human immunodeficiency virus (HIV) agents*	Amiodarone	Amiodarone
Actinomycin D		Amprenavir	Astemizole
Daunorubicin	Amprenavir	Bromocriptine	Atorvastatin
Docetaxel	Indinavir	Chlorambucil	Bepridil
Doxorubicin	Nelfinavir	Cisplatin	Biricodar
Docetaxel	Ritonavir	Clotrimazole	Bromocriptine
Etoposide	Saquinavir	Colchicine	Carvedilol
Imatinib		Cyclosporine	Chlorpromazine
Irinotecan	*Anticonvulsants*	Daunorubicin	Clarithromycin
Mitomycin C	Phenobarbital	Dexamethasone	Cortisol
Mitoxantrone	Phenytoin	Diltiazem	Cyclosporine
Paclitaxel		Doxorubicin	Diltiazem
Teniposide	*Anti-emetics*	Erythromycin	Dipyridamole
Topotecan	Domperidon	Etoposide	Elacridar
Vincristine	Ondansetron	Flurouracil	(GF120918)
Vinblastine		Hydroxyurea	Erythromycin
	H_2-antagonists	Insulin	Felodipine
Antihypertensive agents	Cimetidine	Indinavir	Fluoxetine
	Ranitidine	Methotrexate	Itraconazole
Celiprolol		Midazolam	Ketoconazole
Diltiazem	*Immunosuppressants*	Mitoxantrone	LY335979
Losartan	Cyclosporine	Morphine	Midazolam
Talinolol	Sirolimus	Nelfinavir	Nicardipine
	Tacrolimus	Nifedipine	Nitrendipine
Anti-arrhythmics	Valspodar	Phenobarbital	OC144-093
Digoxin		Phenothiazine	Paroxetine
		Phenytoin	Progesterone

Quinidine Verapamil *Antidepressants* Amitriptyline *Antimicrobial agents* Doxycycline Erythromycin Itraconazole Ketoconazole Levofloxacin Rifampin Sparfloxacin Tetracycline	*Neuroleptics* Chloropromazine Phenothiazine *Steroid hormones* Aldosterone Cortisol Dexamethasone Methylprednisolone *Opioids* Loperamide Morphine Pentazocine *Others* Digoxin Ivermectin Terfenadine Vecuronium	Probenecid Reserpine Retinoid acid Rifampicin Ritonavir St John's wort Tacrolimus Tamoxifen Verapamil Vinblastine Vincristine Yohimbine	Propafenone Quinidine Quinine R101933 Reserpine Ritonavir Sertraline Tacrolimus Tamoxifen Terfenadine Tetrabenzine Valinomycin Valspodar (PSC833) Verapamil Vinblastine XR9051

Table 1.3 Substrates, inducers and inhibitors of MDR1 [Zhou 2008]

MRPs

MRP1, MRP5, MRP7, MRP8 and MRP9 show a wide expression. MRP1 is almost ubiquitous with high expression found in lung, bladder, spleen, testis, and adrenal gland. Expressions of MRP5, MRP7, MRP8 and MRP9 are moderate to low with highest levels for MRP5 in skeletal muscle and brain, for MRP7 in pancreas, liver, placenta, lung, kidney, brain, ovary, lymph node, spleen, heart, leukocytes and colon; for MRP8 and liver, brain, placenta, breast and testis and for MRP9 in testis, ovary, brain, prostate and breast [Toyoda et al. 2008; Cole et al. 1992; Kool et al. 1997]. MRP2 and MRP6 are mainly expressed in the liver and kidneys [Kuo et al. 1996; Kool et al. 1999]. MRP3 is found in the liver, lung, intestine, adrenal gland, pancreas and kidney [Schinkel and Jonker 2003; Kool et al. 1997]. MRP4 is expressed in lung, prostate, kidney, bladder, gallbladder, tonsil, skeletal muscle,

pancreas, spleen, thymus, testis, ovary and small intestine [Schinkel and Jonker; Kool et al. 1997].

In the lung, reports are contradictory. On transcript level highest expression was found for MRP1 and MRP5 in two studies [Kool et al. 1997; Langmann et al. 2003], but Bleasby and co-workers [2006] reported these two transporters to be moderately expressed, whereas MRP7 seemed to be highly expressed. Reports of expression of MRP2 are conflicting, with two studies agreeing in absence of this transporter [Bleasby et al. 2006; Kool et al. 1997] in contrast to Langmann and co-workers [2003], who found low expression of this transporter. MRP3, MRP4 and MRP6 showed low to moderate expression in all three studies. MRP8 and MRP9 were reported to be expressed on moderate level [Bleasby et al. 2006] in discrepancy to Langmann et al. [2003] who did not find these transporters. Substrate selectivities of MRP1, MRP2 and MRP3 are broad and overlapping (table 1.4). All three proteins transport glutathione- and glucuronate-conjugated organic anions with varying affinities. Expression of theses transporters can lead to resistance to several drugs including vinca alkaloids, anthracyclines and camptothecins. Methotrexate is actively transported by MRP1, MRP2, MRP3 and MRP4 [Kruh and Belinsky 2003]. MRP4, MRP5 and MRP8 are smaller than MRP1, MRP2, MRP3, MRP6 and MRP7, as they lack one N-terminal transmembrane domain (figure 1.6). Due to this difference, substrate selectivities do not conform to the other transporters. They include nucleoside analogues, prostaglandins, conjugated steroids and bile acids as well as the drugs mitoxantrone, topotecan and doxorubicin [Kruh and Belinsky 2003]. MRP6 is known to transport glutathione conjugates such as LTC_4.

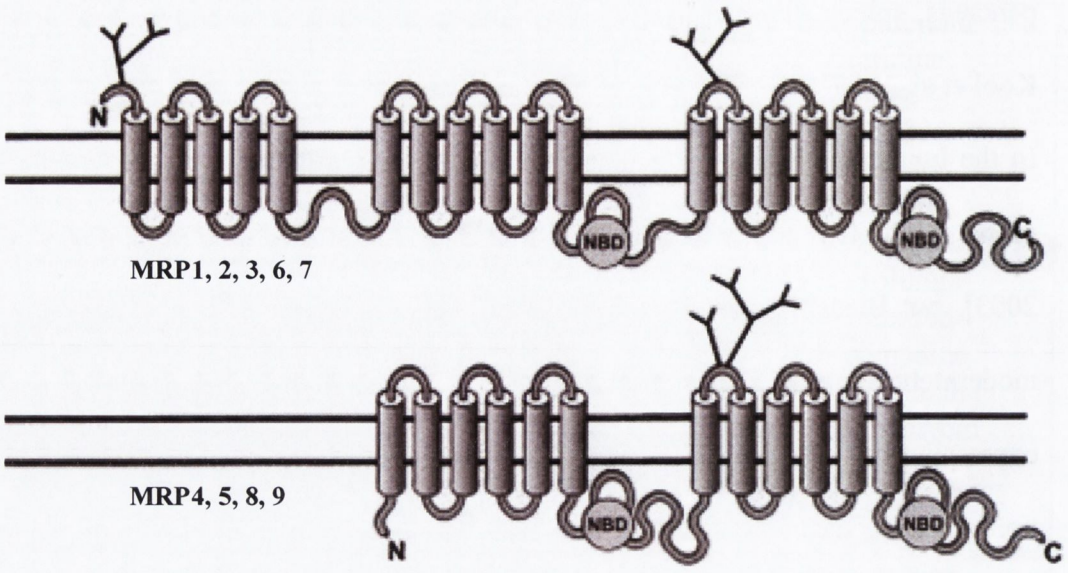

Figure 1.6 Predicted secondary structures of MRP1-9 [Schinkel and Jonker, 2003].

These studies established that MRP7 is a lipophilic anion transporter that has the facility for conferring resistance to some natural product anticancer agents. A distinctive feature of MRP7 is that it is capable of conferring high levels of resistance (9-13-fold) to docetaxel, a microtubule-stabilizing agent. In addition, three- to fourfold levels of resistance were observed for another taxane, paclitaxel, as well as for the microtubule destabilizing agents vincristine and vinblastine [Kruh et al. 2007].

Substrates	MRP1	MRP2
Antiarrhythmics	Quinidine	
Anthracyclines	Doxorubicin, Daunorubicin, Epirubicin, Idarubicin	
Folate based	Methotrexate	
Kinase inhibitors	Imatinib (Gleevec)	
Plant alkaloids	Etoposide, Vincristine, Vinblastine, Irinotecan, SN-38	Reserpine
Taxanes	Paclitaxel, Ortataxel	
CNS active drugs		Chlorprotixene, Flupentixol, Thioridazine
Antivirals	Saquinavir, Ritonavir	Lopinavir
Antibiotics and antifungals	Difloxacin, Grepafloxacin	Rifampicin
Antimalarials and antiparasites	Chloroquine	Ivermectin
Calcium channel blockers	Nifedipine	Isradipine, Diltiazem
Fluorescent dyes	BCECF, Calcein, Fluo-3, SNARF	
Folates	Folic acid, L-leucovorin	
Flavonoids	Quercetin, Kaempferol, Naringenin	Quercetin Silymarin
Hormones	Sulfate or Glucuronide Conjugates of Estradiol and Estrone	Diethylstilbestrol, Tamoxifen
Immunosuppressants	Cyclosporin A	Cyclosporin A
Peptides	GSH, GSSG	
Toxicants	Aflatoxin B1, Methoxychlor, Fenitrothion, Chlorpropham	
Other		Dipyridamole, GF120918, Loperamide, MK571, Terfenadine, Benzbromarone, Taurolithocholic acid, Bromosulfalein, Lansoprazole, P-aminohippuric acid

Table 1.4 Pharmacologically relevant substances interacting with MRP1 and MRP2 [Szaka´cs et al. 2008] [Matsson et al. 2009]

WHITE1 and BCRP

WHITE1 is found to be expressed in the heart, spleen, brain, liver, lung, skeletal muscle, kidney and placenta. It is thought to be involved in intracellular free cholesterol regulation through cholesterol efflux [Klucken et al. 2000; Dean et al. 2001].

BCRP (figure 1.7) is found in drug-resistant cell lines and tumours, stem cells, placenta (syncytiotrophoblast plasma membrane), liver, small intestine, colon, kidney, adrenal and sweat glands. Expression in lung was initially maintained to be limited to cancer tissues, but more recent publications localised it to normal lung as well [Langmann et al. 2003; Bleasby et al. 2006; Fetsch et al. 2006].

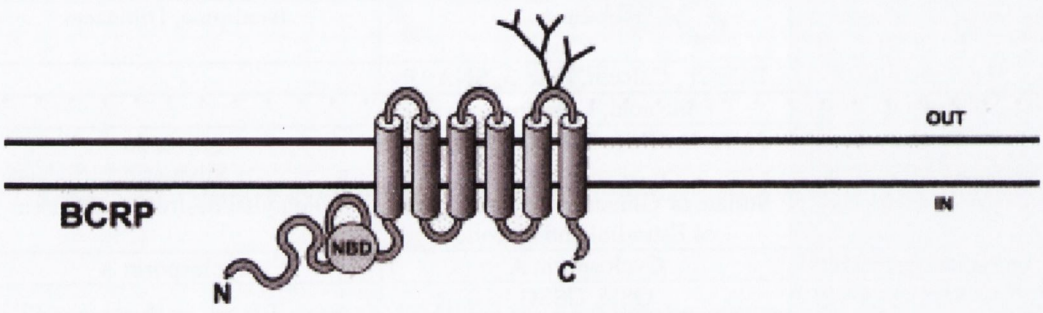

Figure 1.7 Predicted secondary structures of BCRP [Schinkel and Jonker, 2003].

Substrates, overlapping with those of MDR1, MRP1 and MRP2, include antivirals (zidovudine (AZT), lamivudine, abacavir), HMG-CoA reductase inhibitors (rosuvastatin, pitavastatin, cerivastatin), antibiotics (ciprofloxacin, ofloxacin, norfloxacin, erythromycin, nitrofurantoin), calcium channel blockers (azidopine, dipyridamole, nitrendipene), sulfasalazine, cimetidine, riboflavin, vitamin K_3, glyburide, rhodamine123 and flavopiridol (table 1.5) [Robey et al. 2009].

Substrates	ABCG2
Antiarrhythmics	Amiodarone
Antineoplastics	Gefitinib
Anthracyclines	Mitoxantrone
Folate based	Methotrexate
Kinase inhibitors	Imatinib (Gleevec), Flavopiridol
Plant alkaloids	Irinotecan, SN-38, Topotecan, Reserpine
Taxanes	Ortataxel
CNS active drugs	Chlorprotixene, Flupentixol, Thioridazine, Chlorpromazine
Antivirals	Lopinavir, Nelfinavir, Delavirdine, Ritonavir, Saquinavir, Tipranavir
Antibiotics and antifungals	Ciprofloxacin, Ofloxacin, Norfloxacin
Antimalarials and antiparasites	Ivermectin, Amodiaquine
Calcium channel blockers	Nicardipine, Isradipine, Felodipine, Nitrendipine, Verapamil
Fluorescent dyes	BCECF-AM, Hoechst 33342
Folates	Folic acid
Flavonoids	Quercetin, Chrysin, Silymarin, Apigenin, Naringenin
Hormones	Sulfate or Glucuronide Conjugates of Estradiol and Estrone, Diethylstilbestrol, Tamoxifen, 17β-estradiol f, Medroxyprogesterone, Mifepristone, Progesterone
Immunosuppressants	Cyclosporin A
Toxicants	Aflatoxin B1
Other	Dipyridamole, GF120918, Loperamide, MK571, Terfenadine, Benzbromarone, Biochanin A, Chrysin, Ergocristine, Genistein, Glibenclamide, Ketoconazole, Ko143, Simvastatin, Fumitremorgin C, Omeprazole, Prazosin

Table 1.5 Pharmacologically relevant substances interacting with MRP1 and MRP2 [Szaka´cs et al. 2008] [Matsson et al. 2009]

1.3.2 SLC superfamily

The SLC superfamily of transporters is organised into 47 families [Sai and Tsuji, 2004].

- http://ghr.nlm.nih.gov/geneFamily=slc
- http://www.bioparadigms.org/slc/menu.asp

Solutes transported by the various SLC group members are extraordinarily diverse and include charged and uncharged organic molecules, inorganic ions, di- and tri-peptides as well as a variety of structurally related drugs and pro-drugs [Sai and Tsuji, 2004]. Both uptake and efflux SLCs influence physiologic and

pathophysiologic function as well as the absorption and disposition of xenobiotics [Sai and Tsuji, 2004]. The SLC superfamily includes among others, the organic cation transporters (OCT) and organic anion transporters (OAT) (SLC22 family) (table 1.6) which play critical roles in renal and hepatic transport and the detoxification of a wide variety of compounds including drugs, toxins, hormones and neurotransmitter metabolites [Koepsell and Endou, 2004].

Protein name	Aliases
PEPT1	SLC15A1; HPECT1; HPEPT1
PEPT2	SLC15A2
OCT1	SLC22A1, hOCT1; oct1_cds
OCT2	SLC22A2, MGC32628
OCT3	SLC22A3, EMT; EMTH
OCTN1	SLC22A4, MGC34546; MGC40524
OCTN2	SLC22A5, CDSP, FLJ46769
OAT1	SLC22A6, PAHT; HOAT1; ROAT1; MGC45260
OAT2	SLC22A7, MGC24091; MGC45202
OAT3	SLC22A8, MGC24086
OAT4	SLC22A11, hOAT4; MGC34282

Table 1.6 Clinically relevant SLC transporters

PEPT1 and PEPT2

PEPT1 is mainly expressed in the apical plasma membrane of enterocytes in the small intestine, in renal proximal tubular cells of the S1 segment and in bile duct epithelial cells. Transport activity similar to PEPT1 was also observed in lysosomal membranes of liver cells and PEPT1-immunoreactivity was shown in the nuclei of vascular smooth muscle cells and recently in bronchial epithelial cells [Daniel and Kottra 2004, Søndergaard et al. 2008]. PEPT2 (figure 1.8) is expressed more

widely than PEPT1. It is found in kidney, brain, lung (bronchial epithelial cells, type II pneumocytes) and mammary glands.

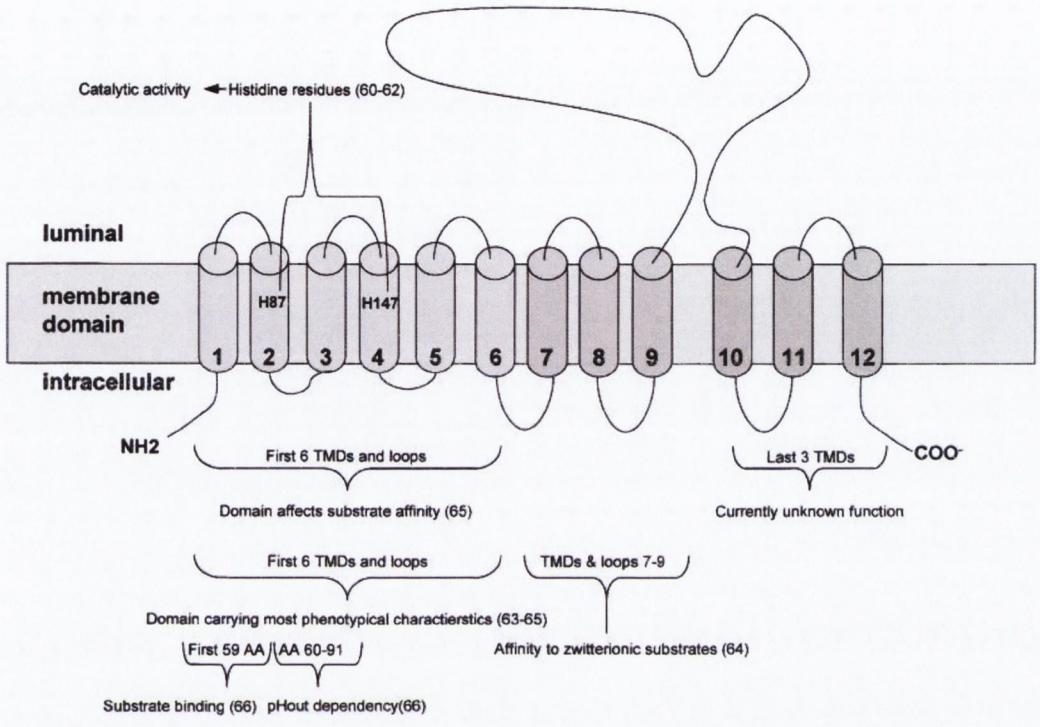

Figure 1.8 Functionally relevant domains of PEPT2 as revealed by chimeric and mutant proteins. To identify functionally relevant domains of PEPT2, chimeric transporter proteins were constructed using distinct sequences of PEPT1 and PEPT2. Also, mutant transporter proteins were constructed containing single amino acid changes [Groneberg et al. 2004].

The physiological role of PEPT1 and PEPT2 in lung epithelium is not yet known but may involve the uptake of peptides, which are products of the luminal protein metabolism via endo- and ecto-peptidases (figure 1.9).

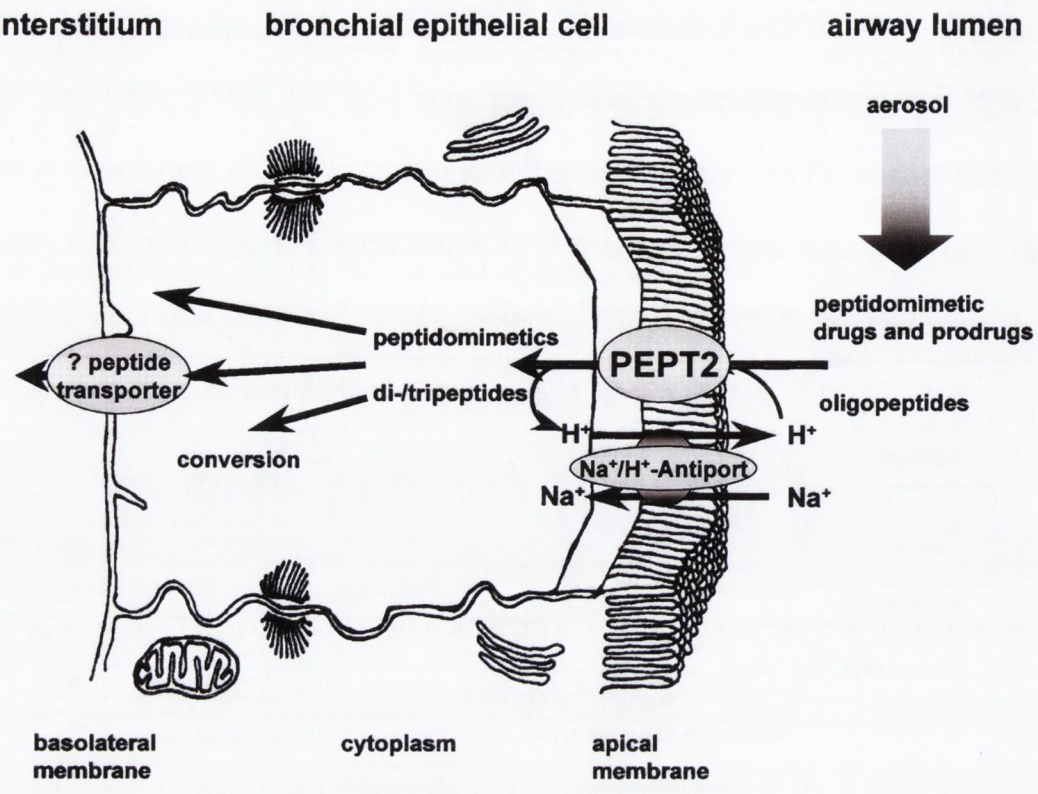

Figure 1.9 Airway epithelial peptidomimetic and peptide transport. Aerosol-administered drugs are transported along with other peptides here by the transporter protein PEPT2 into the airway epithelial cells. The translocation of the substrate is performed using the transmembrane electrochemical proton gradient from the airway lumen to the epithelial cell as driving force. The proton gradient is maintained by Na^+/H^+ exchanging systems such as NHE-1 in the apical membrane [Groneberg et al. 2004].

The relative broad spectrum of transport substrates includes glycylsarcosine, β-lactam antibiotics, ACE (angiotensin-converting enzyme) inhibitors (captopril, enalapril, fosinopril), antiviral drugs (valaciclovir) and dopamine receptor interactors (table 1.7) [Sai and Tsuji 2004; Daniel and Kottra 2004].

	PEPT1		PEPT2	
	Substrate	**Competitor**	**Substrate**	**Competitor**
β-lactam antibiotics	Ciclacillin Cefadroxil Cefixime Ceftibuten	Cephalexin	Cefadroxil	Ciclacillin Cephalexin Cefixime Ceftibuten
Angiotensin-converting enzymes (ACE) inhibitors	Captopril Fosinopril	Enalapril	Captopril Fosinopril	Enalapril
Antitumour agents	Bestatin	Floxuridine as pro-drug	Bestatin	
Antivirals	Acyclovir	Zidovudine		Acyclovir
Dopamine receptor interactors	Sulpiride L-DOPA as pro-drugs			
Photosensitizing agents	5-Aminolevulinic acid		5-Aminolevulinic acid	
Hypotensives		Midodrine		
Others		S 86 2033, S 86 3390 Thrombin inhibitors		

Table 1.7 Selected drugs shown to interact with the Substrate binding sites of the peptide transporters PEPT1 and/or PEPT2. [Rubio-Aliaga and Daniel 2008]

SLC22 family

In humans, the SLC22 family includes, among others, the organic cation transporters OCT1 – OCT3, the organic anion transporters OAT1 – OAT4 and the transporters of carnitine and/or cations OCTN1 and OCTN2.

OCT1, OCT2 and OCT3

OCT1 (figure 1.10) is expressed in various tissues including stomach, intestine (figure 1.11), liver, spleen, lung, trachea, kidney, urinary bladder, brain heart and placenta. In humans, highest concentrations in the liver have been reported where it is assumed to play a role in modulation of uptake and release of cationic drugs hepatocytes across the sinusoidal membrane (figure 1.12). OCT1 is also located in

alveolar epithelial cells [Lips et al. 2007]. OCT2 is predominantly localised in kidney where it plays an important role in renal excretion of xenobiotics (figure 1.13). Additionally, it has been detected in placenta, thymus, adrenal gland, neurons and choroid plexus.

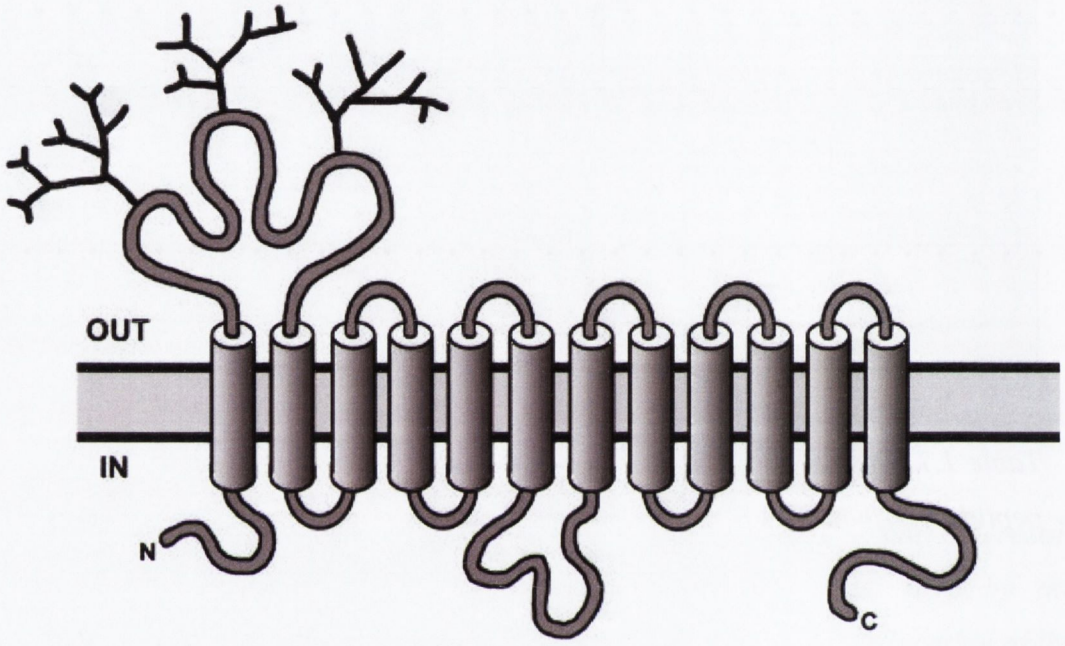

Figure 1.10 Predicted topology of the OCT1 [Jonker and Schinkel 2004]

In human lung, OCT2 is expressed in the luminal membrane of epithelial cells and all over the plasma membrane of basal and intermediate cells in the respiratory epithelium of trachea and bronchi [Lips et al. 2005; Lips et al. 2007]. OCT3 is expressed in skeletal muscle, smooth muscle, liver, placenta, kidney, heart, intestine, spleen, lung, neurons of the brain and sympathetic ganglia, glial cells and the choroid plexus [Koepsell et al. 2007]. Expression in lung has been located in smooth muscle cells of bronchi, blood vessels and alveolar epithelial cells [Kummer et al. 2006; Lips et al. 2007].

All three transporters show a broad substrate specificity including the model cations MPP, tetraethylammonium (TEA) and tetrapropylammonium (TPrA), neurotransmitters (serotonin, histamine, dopamine) and various drugs (quinidine, quinine, aciclovir, ganciclovir, metformin, norepinephrine, epinephrine, amantadine, memantine, cimetidine, famotidine, ranitidine, cisplatin and debrisoquine) (table 1.8) [Koepsell et al. 2007].

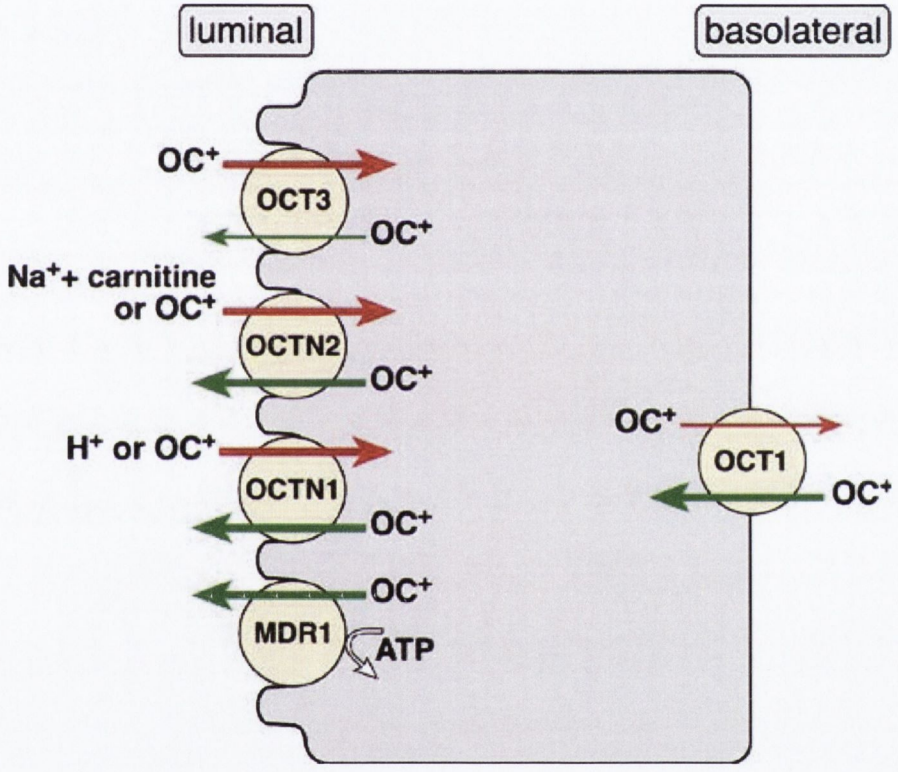

Figure 1.11 Organic cation transporters in enterocytes of human small intestine. Transporter activities involved in cation absorption and cation secretion are indicated as red and green arrows, respectively.

OCT1 and OCT2 are probably involved in non-neuronal autocrine and paracrine cholinergic regulation that influences beat frequency of cilia and regeneration of the epithelial cells. Bronchial ciliated epithelial cells have a relatively high

cytosolic concentration of acetylcholine but do neither contain storage vesicles for acetylcholine nor the vesicular acetylcholine transporter that loads such vesicles [Lips et al. 2005; Kummer et al. 2006].

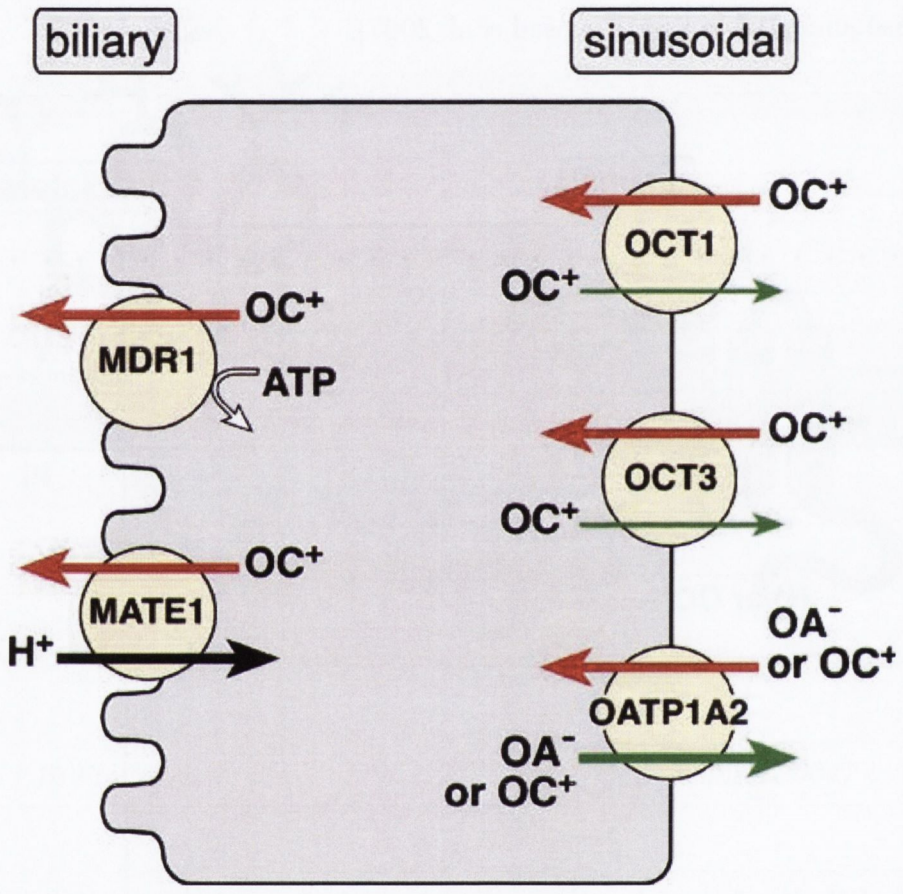

Figure 1.12 Organic cation transporters in human liver. Transporter activities that mediate biliary excretion are indicated in red. Green arrows indicate the release of organic cations from hepatocytes into sinusoids. [Koepsell 2007]

OCT1 and OCT3 are electrogenic cation uniporters that transport cations in both directions and are driven by the electrochemical potential. In the presence of a normal membrane potential of -60 mV cation uptake (thick arrows) is preferred,

however, OCTs may mediate cation efflux (thin arrows) if the intracellular concentration of the respective cation is about ten times higher compared to the extracellular cation concentration. OCTN1 operates as secondary active proton-cation antiporter or as cation exchanger. OCTN2 can function as Na^+-carnitine cotransporter but can also mediate cation uptake or cation efflux. MDR1 is a primary active extrusion pump [Koepsell 2007].

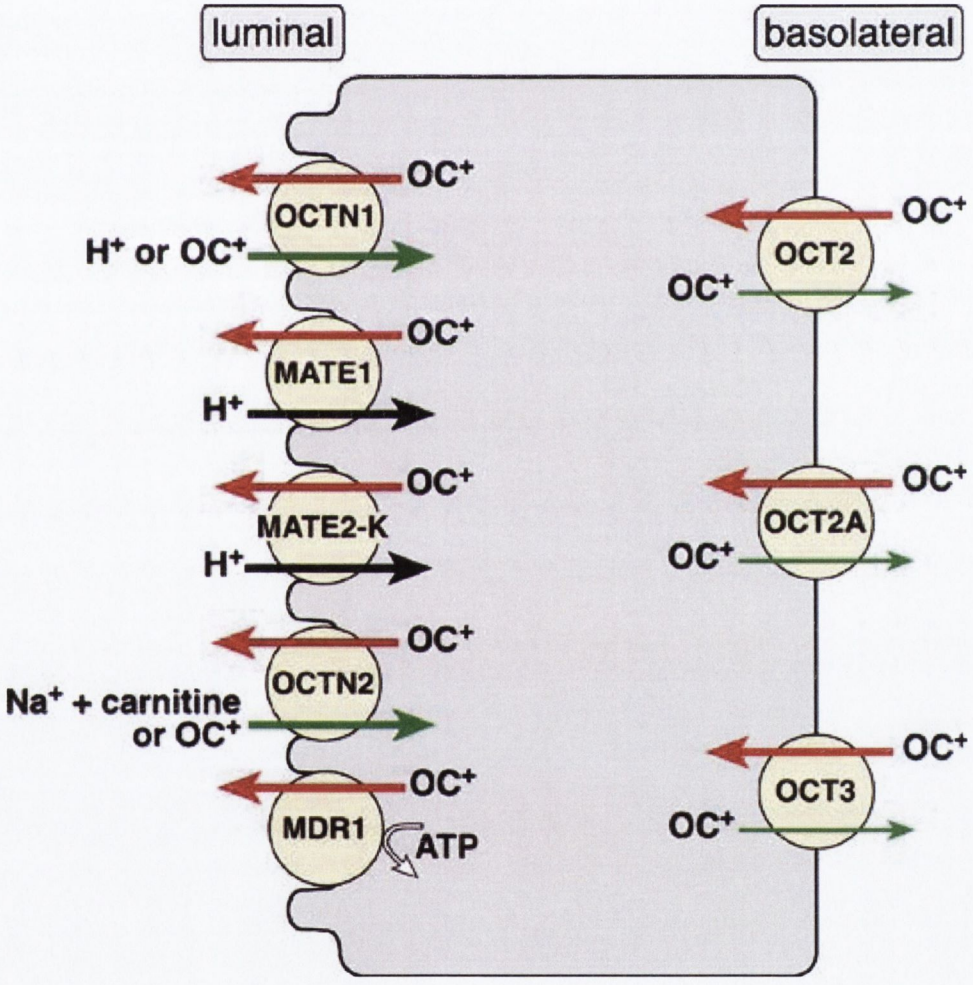

Figure 1.13 Organic cation transporters in plasma membranes of human renal proximal tubules. Red arrows indicate transport activities that are involved in cation secretion whereas green arrows indicate transport activities involved in cation reabsorption. OCT2A is a splice variant of OCT2. [Koepsell 2007]

	OCT1		OCT2		OCT3	
Class	**Substrate**	**Inhibitor**	**Substrate**	**Inhibitor**	**Substrate**	**Inhibitor**
Metabolites		Choline Creatinine L-Carnitine Guanidine Acetylcholine Dopamine Epinephrine Histamine Nor-epinephrine Serotonin	Choline Acetyl-choline Dopamine Epinephrine Histamine Nor-epinephrine	Choline Creatinine L-Carnitine Guanidine Acetyl-choline Serotonin	Dopamine Epinephrine Histamine Nor-epinephrine	Choline Creatinine L-Carnitine Guanidine Acetyl-choline Serotonin
Hormones	Prosta-glandin E_2 Prosta-glandin F_2	Cortico-sterone Proge-sterone Testo-sterone	Prosta-glandin E_2 Prosta-glandin F_2	Cortico-sterone Proge-sterone Testo-sterone		Cortico-sterone Proge-sterone Testo-sterone
Miscellaneous		Agmatine	Agmatine	Agmatine	Agmatine	
Receptor antagonists						
Acetylcholine receptor (muscarinic)		Atropine	Mepiper-phenidol	Atropine		Atropine
α-Adrenoceptor		Phenoxy-benzamine Prazosin		Phenoxy-benzamine Prazosin		Phenoxy-benzamine Prazosin
β-Adrenoceptor		Acebutolol				
Histamine H_1 receptor		Diphenyl-hydramine		Diphenyl-hydramine		Diphenyl-hydramine
Histamine H_2 receptor		Cimetidine Famotidine Ranitidine	Famotidine Ranitidine	Cimetidine Famotidine Ranitidine		Cimetidine Famotidine Ranitidine
NMDA receptor		Amantadine Ketamine Memantine	Amantadine	Amantadine Ketamine Memantine		Amantadine Ketamine Memantine
Receptor agonists						
Acetylcholine receptor (nicotinic)		Nicotine		Nicotine		Nicotine
α-Adrenoceptor		Clonidine Etilefrine		Clonidine Etilefrine	Etilefrine	Clonidine Etilefrine
β-Adrenoceptor		O-Methyl-isoprenaline		O-Methyl-isoprenaline		O-Methyl-isoprenaline
NMDA receptor		Dizocilpine		Dizocilpine		Dizocilpine
Ion channel and transporter blockers						
Ca^{2+} channel		Verapamil		Verapamil		Verapamil
Na^{+} channel		r-(-)-Diso-pyramide s-(+)-Diso-pyramide		Procain-amide		Procain-amide

		Procain-amide Quinidine				
Noradrenaline transporter		Cocaine		Cocaine		Cocaine
Serotonin transporter		Citalopram		Citalopram		Citalopram
Anaesthetic		Midazolam				
Antiasthmatic				Beclo-metasone Budesonide		
Antidepressant		Desipra-mine		Desipra-mine		Desipra-mine Imipramine
Antidiabetic	Metformin	Metformin Phenformin	Metformin	Metformin Phenformin		
Antiemetic		Granisetron Odansetron Tropisetron		Granisetron Odansetron Tropisetron		Granisetron Odansetron Tropisetron
Anti-hypertensive				Debriso-quine		
Antimalarial		Quinine		Quinine		Quinine
Antiviral	Aciclovir Ganciclovir					
Antiviral (HIV)		Aquinavir Indinavir Nelfinavir Ritonavir				
Cytostatic		Cisplatin Mito-xantrone		Cisplatin Mitox-antrone		
Muscle relaxant		Vecuro-nium				
Psycho-stimulant		3,4-Methylene-dioxymet-amphetamin D-Amphet-amine		3,4-Methylene-dioxymet-amphetamin D-Amphet-amine		3,4-Methylene-dioxymet-amphetamin D-Amphet-amine
Serine protease inhibitor				Nafamostat mesilate		
Other	MPP TEA	TEA N1-methyl-nicotinamid Tetramethyl ammonium Tetrapropyl ammonium Tetrapentyl ammonium Decynium 22	MPP TEA N1-methyl-nicotinamid	MPP TEA N1-methyl-nicotinamid Tetramethyl ammonium Tetrapropyl ammonium Tetrapentyl ammonium Decynium 22	MPP Tetrapentyl ammonium	MPP TEA N1-methyl-nicotinamid Decynium 22 Dispro-cynium 24

Table 1.8 Selected substrates and inhibitors of OCT1, OCT 2 and OCT3

OCTN1 and OCTN2

OCTN1 and OCTN2 are expressed in epithelial and muscle cells of various tissues. Strongest expression was found in kidney, skeletal muscle, bone marrow, and trachea; for OCTN2 additionally in liver, heart and placenta. Weaker expression of both transporters was observed in many other organs, (brain, prostate, intestine and mammary glands) [Koepsell et al. 2007].

In human lung, expression of OCTN1 and OCTN2 was observed on luminal membrane of the respiratory epithelium of trachea, bronchi and in alveolar epithelial cells [Horvath et al. 2007; Lips et al. 2007].

Substrate specificities for OCTN1 and OCTN2 are narrower than for the other organic cation transporters. Substrates for both are TEA, L-carnitine, quinidine, pyrilamine and verapamil (table 1.9) [Koepsell et al. 2007].

	OCTN1		**OCTN2**	
Class	**Substrate**	**Inhibitor**	**Substrate**	**Inhibitor**
Metabolites		Choline D-Carnitine L-Carnitine	Acetyl-L-carnitine D-Carnitine L-Carnitine	Betaine Choline
Hormones				Aldosterone Corticosterone
Miscellaneous	Agmatine Ergothioneine Stachydrine			
Histamine H_1 receptor		Pyrilamine		Pyrilamine
Histamine H_2 receptor		Cimetidine		Cimetidine
Acetylcholine receptor (nicotinic)		Nicotine		Nicotine
α -Adrenoceptor		Clonidine		Clonidine
Ion channel and transporter blockers				
Ca^{2+} channel		Verapamil		Verapamil
Na^{+} channel		Procainamide Quinidine		Procainamide Quinidine
Anesthetic		Lidocaine		
Antibiotic		Cephaloridine Levofloxacine Ofloxacine	Cephaloridine	Cefepine Cefoselis Cefsulodine

Antiemetic			Emetine	Emetine
Antimalarial		Quinine		Quinine
Antioxidant			Ergothioneine	
Cytostatic				Actinomycin D
Other	TEA	N1-methyl-nicotinamide Tetrabutyl-ammonium Tetrapentyl-ammonium	TEA	MPP

Table 1.9 Substrates and inhibitors of organic cation transporters [Koepsell 2007]

Organic anion transporters (OAT1, OAT2, OAT3 and OAT4)

Human OAT1 (figure 1.14), OAT3 and OAT are strongly expressed in kidney, whereas OAT2 is mainly localised in liver, but only moderate levels in kidney were reported [Anzai, Kanai et al. 2006]. Additionally, OAT1 and OAT3 are found in brain, OAT3 and OAT4 in placenta and OAT3 in skeletal muscle [Koepsell and Endou 2004]. By immunohistochemistry, OAT1, OAT2 and OAT3 were localised to the basolateral membrane of the renal proximal tubule, whereas OAT4 protein was located to the apical side. To date, reports confirm absence of OATs in lung tissue of any species [Koepsell and Endou 2004].

OATs participate in renal excretion and reabsorption of anionic drugs. OAT1 and OAT3 transport a wide spectrum of substrates including PAH, prostaglandins, estrone sulfate, ochratoxin A, and various drugs, including antibiotics, anti-inflammatory drugs and diuretics [Anzai et al. 2006]. The substrate spectrum of OAT2 and OAT4 is narrower. OAT2 transports salicylate, acetylsalicylate, prostaglandin E_2 (PGE_2), dicarboxylates, tetracycline and PAH; the spectrum of OAT4 includes estrone sulphate, dehydroepiandrosterone sulfate, ochratoxin A, and prostaglandins E_2 and F_{2a} [Anzai et al. 2006] (table 1.10).

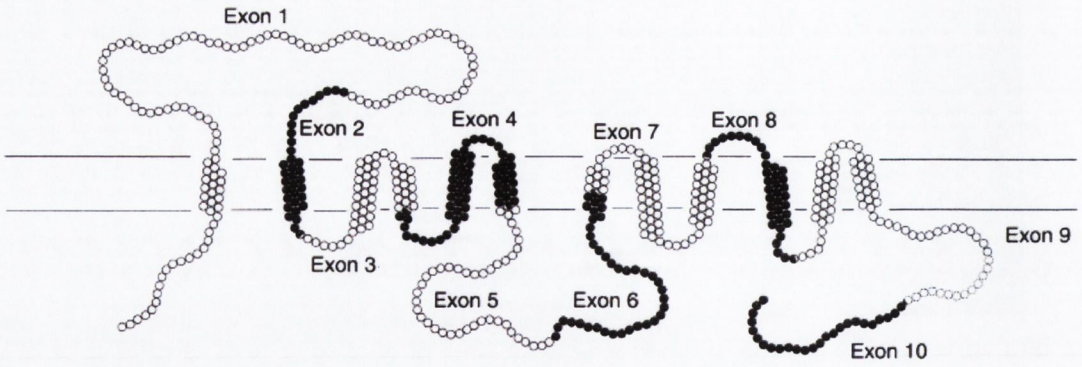

Figure 1.14 Predicted secondary structure of OAT1. Each circle represents one amino acid [Ichida et al 2003].

Class	OAT1	OAT2	OAT3	OAT4
Antibiotics	Benzylpenicillin Cefadroxil Cefamandole Cefazolin Cefoperazone Cefotaxime Ceftriaxone Cephaloridine Cephalotin Cephradine Cinoxacin Doxycyclin Minocycline Nalidixate Oxytetracycline Tetracycline	Cefadroxil Cefamandole Cefazolin Cefoperazone Cefotaxime Ceftriaxone Cephaloridine Cephalotin Chloramphenicol Doxicycline Erythromycinc Minocycline Oxytetracycline Tetracycline	Benzylpenicillin Cefadroxil Cefamandole Cefazolin Cefoperazon Cefotaxim Ceftriaxone Cephalexin Cephaloridine Cephalotin Tetracycline	Benzylpenicillin Cefadroxil Cefamandol Cefazolin Cefoperazone Cefotaxim Ceftriaxon Cephaloridine Cephalotin Tetracycline
Antivirals	Acyclovir Adefovir Cidofovir Ganciclovir PMEDAP PMEG Tenofovir Zalcitabine Zidovudine Azidothymidine Acyclovir Amantadine	Zidovudine Ganciclovir	Acyclovir Ganciclovir Valacyclovir Zidovudine	Zidovudine
H2 antagonists	Cimetidine Ranitidine	Cimetidine Anitidine	Cimetidine Famotidine Ranitidine	
Antiepileptic			Valproate	
Antihyper-tensives	Captopril Losartan			Captopril
Cytostatics	Methotrexate	5-Fluorouracil Methotrexate Taxol	Azathiopurine Methotrexate	Methotrexate

Diuretics	Acetazolamide Bumetanide Chlorothiazide Cyclothiazide Ethacrynate Furosemide Hydrochloro-thiazide Methazolamide Trichlor-methiazide	Bumetanide Chlorothiazide Cyclothiazide Ethacrynate Furosemide Hydrochloro-hiazide Trichlor-methiazide	Acetazolamide Bumetanide Chlorothiazide Cyclothiazide Ethacrynate Furosemide Hydrochloro-thiazide Methazolamide Trichlor-methiazide	Acetazolamide Bumetanide Chlorothiazide Ethacrynate Furosemide Trichlor-methiazide
NSAIDs	Acetaminophen Acetylsalicylate Diclofenac Diflusinal Etodolac Flufenamate Flurbiprofen Ibuprofen Indomethacin Ketoprofen Loxoprofen Mefenamate Naproxen Phenacetin Phenylbutazon Piroxicam Salicylate Sulindac	Acetaminophen Diclofenac Ibuprofen Indomethacin Ketoprofen Mefenamate Naproxen Phenacetin Piroxicam Salicylate Sulindac	Acetylsalicylate Diclofenac Flufenamate Ibuprofen Indomethacin Ketoprofen Loxoprofen Mefenamate Naproxen Phenacetin Phenylbutazone Piroxicam Salicylateb Sulindac	Diclofenac Diflusinal Ibuprofen Indomethacin Ketoprofen Mefenamate Naproxen Phenylbutazone Piroxicam Salicylate Sulindac
Statins	Fluvastatin Pravastatin Simvastatin	Pravastatin	Pravastatin Simvastatin	Pravastatin
Uricosurics; purine metabolism	Allopurinol Benzbromarone Probenecid	Allopurinol Probenecid	Probenecid	Probenecid

Table 1.10 Substrates and inhibitors of organic anion transporters [Rizwan and Burckhardt 2007]

1.3.3 OATP/SLCO family

In 2004, Hagenbuch and Meier introduced a new classification of the organic anion transporting polypeptides (OATPs), formerly known as the SLC21 family. The SLCO family represents a phylogenetically based species-independent and open-ended nomenclature and classification system. These transporters are present in a variety of biological barriers and have a marked impact on xenobiotic absorption.

Among 52 members of the OATP/SLCO superfamily, 36 members have been identified so far in humans, rat and mouse OATPs are capable of transporting various xenobiotics and drugs and, therefore, play an important role in drug absorption, disposition and excretion [Hagenbuch and Gui 2008] (table 1.11).

Protein name	Aliases
OATP1A2	OATP; OATP-A; SLCO1A2; SLC21A3
OATP1B1	OATP-C; LST-1; OATP2; SLCO1B1; SLC21A6; MGC133282
OATP1B3	SLCO1B3; LST3; OATP8; SLC21A8; LST-3TM13
OATP1C1	SLCO1C1; OATP1; OATP-F; SLC21A14
OATP2A1	SLCO2A1; PGT; SLC21A2
OATP2B1	OATP-B; OATPB; SLCO2B1; SLC21A9; KIAA0880; DKFZp686E0517
OATP3A1	OATP-D; SLCO3A1; FLJ40478; SLC21A11
OATP4A1	OATP-E; POAT; OATP1; SLCO4A1; OATPRP1; SLC21A12
OATP5A1	SLCO5A1; OATP-J; OATPRP4; FLJ39560; SLC21A15

Table 1.11 Clinically relevant OATP/SLCO transporters

OATP1A2 was described in 1995. It shows highest expression in brain [Kullak-Ublick et al. 1995], but is also expressed in liver and colon cancer cells as well as in the apical membrane of enterocytes [Lee et al. 2005; Glaeser et al. 2007]. OATP1A2 can transport a wide range of organic anions, summarised by Hagenbuch and Gui [2008], including bile salts, hormones and their conjugates, as well various drugs and toxins. Lee and Boyer suggested OATP1A2 to play an important role for drug delivery and uptake of neuroactive peptides to the brain as well as for elimination of organic metabolites from this organ [Lee and Boyer 2000].

OATP1B1 and OATP1B3 are highly expressed in human liver where OATP1B1 (figure 1.15) has been localised to the basolateral membrane of human hepatocytes and OATP1B3 around the central vein [Hsiang et al. 1999; Konig et al. 2000]. It is involved in the uptake of endogenous substances and of xenobiotics into hepatocytes. The wide spectrum of transport substrates includes bile salts, bilirubin, steroid conjugates, hormones, eicosanoids, cyclic peptides, toxins as well as numerous drugs such as benzylpenicillin, methotrexate, pravastatin and rifampicin [Hagenbuch and Gui 2008] (table 1.12).

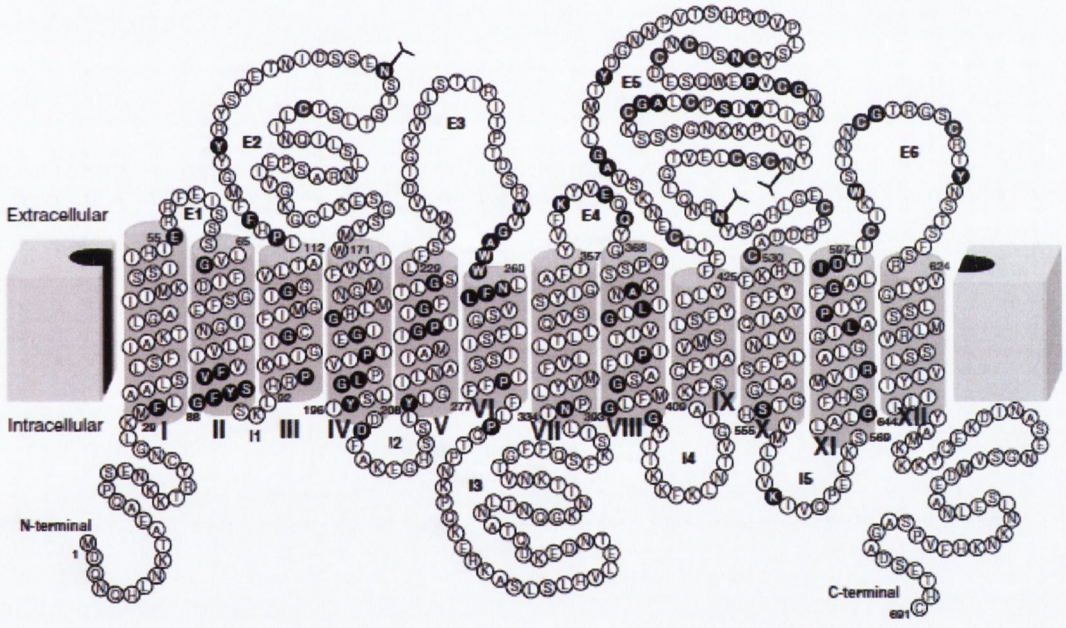

Figure 1.15 Predicted topological model of human OATP1B1 with twelve transmembrane domains [Hagenbuch and Gui 2008].

Expression of OATP1C1 has been shown in the basolateral plasma membrane of the non-pigmented human ciliary body epithelium [Gao et al. 2005]. This subfamily contains human OATP1C1 was isolated from a human brain library and its mRNA has been detected in brain and testis (Leydig cells) [Pizzagalli et al.

2002]. OATP1C1 shows a narrower specificity to its substrates. Highest affinity has been reported for T_4 (thyroxine) and rT_3 (reverse tri-iodothyronine). Furthermore, estradiol-17b-glucuronide, estrone-3-sulfate and the thyroid hormone T_3 are transported. OATP1C1 might play an important role in the delivery and disposition of thyroid hormones in brain and testis, and thus during brain development [Pizzagalli et al. 2002].

OATP2A1 had been first cloned from a kidney library [Lu et al. 1996]. Expression of mRNA for OATP2A1 has been detected ubiquitously with highest levels in heart, skeletal muscle and pancreas [Hagenbuch and Meier 2003]. Neither the protein expression nor its transcriptional and/or post-transcriptional regulations have been studied in any detail. Functional studies have been reported on transiently transfected HeLa cells, where it transported different prostaglandins and thromboxane B_2.

OATP2B1, OATP3A1 and OATP4A1 are expressed in various tissues. Based on RT-PCR highest concentrations of mRNA were localised in liver, colon, lung, pancreas, ovary and testis [Tamai et al. 2000].

Functionally, these transporters have been studied in *Xenopus laevis* oocytes and in transiently transfected HEK293 cells [Tamai, Nezu et al. 2000; Kullak-Ublick, Ismair et al. 2001]. The relative narrow substrate range includes hormones, prostaglandin E_2 and drugs like benzylpenicillin [Tamai et al. 2000; Tamai et al. 2001], but further investigations are required (table 1.12).

OATP5A1 has been isolated and deposited in the database. To date, its transport properties are unknown, yet.

OATP1A2	OATP1B1	OATP1B3
APD-ajmalinium	ACU154	Amanitin
Atrasentan	Arsenic (arsenite, arsenate)	Atrasentan
Bamet-R2	Atorvastatin	Bilirubin
Bamet-UD2	Atrasentan	Bosentan
Bilirubin Briz	Bamet-R2	BQ-123
BQ-123	Bamet-UD2	Bromosulfophthalein (BSP)
Bromosulfophthalein (BSP)	Benzylpenicillin	CDCA-NBD
Chlorambuciltaurocholate	Bilirubin	Cholate (CA)
Cholate (CA)	Bisglucuronosyl bilirubin	Cholecystokinin octapeptide (CCK-8)
Ciprofloxacin	Bosentan	Dehydroepiandrosterone-3-sulfate (DHEAS)
CRC220	BQ-123	Deltorphin II
Dehydroepiandrosterone-3-sulfate (DHEAS)	Bromosulfophthalein (BSP)	Demethylphalloin
Deltorphin II	Caspofungin	Digoxin
[D-penicillamine-2,5]enkephalin (DPDPE)	Cerivastatin	Docetaxel
Enoxacin	CDCA-NBD	[D-penicillamine-2,5]-enkephalin (DPDPE)
Oestradiol-17-glucuronide	Cholate (CA)	Enalapril
Oestrone-3-sulfate	[D-Ala2, D-Leu5]-enkephalin (DADLE)	Oestradiol-17-glucuronide
Fexofenadine	Dehydroepiandrosterone-3-sulfate (DHEAS)	Oestrone-3-sulfate
Gatifloxacin	Demethylphalloin	Fexofenadine
Gd-B20790	[D-penicillamine2,5]-enkephalin (DPDPE)	Fluvastatin
Glycocholate (GCA)	Enalapril	Fluo-3
Levofloxacin	Oestradiol-17-glucuronide	Glutathione (GSH)
Lomefloxacin	Oestrone-3-sulfate	Glycocholate (GCA)
Methotrexate	Fluvastatin	Glycoursodeoxycholate (GUDCA)
Microcystin	Glycocholate (GCA)	Leukotriene C_4 (LTC_4)
N-methylquinidine	Glycoursodeoxycholate (GUDCA)	Methotrexate
N-methylquinine	Leukotriene C_4 (LTC_4)	Microcystin
Norfloxacin	Leukotriene E_4 (LTE_4)	Monoglyucuronosyl bilirubin
Ouabain	Methotrexate	Olmesartan
Pitavastatin	Microcystein	Ouabain
Prostaglandin E_2 (PGE_2)	Monoglyucuronosyl bilirubin	Paclitaxel
Reverse triiodothyronine (rT_3)	Olmesartan	Phalloidin
Rocuronium	Phalloidin	Pitavastatin
Rosuvastatin	Pitavastatin	Rifampicin
Saquinavir	Pravastatin	Ro 48-5033 (Bosentan metabolite)
Taurocholate (TCA)	Prostaglandin E_2 (PGE_2)	Rosuvastatin
Taurochenodeoxycholate (TCDCA)	Rifampicin	Taurocholate (TCA)
Tauroursodeoxycholate (TUDCA)	Ro 48-5033 (Bosentan metabolite)	Taurochenodeoxycholate (TCDCA)
Thyroxine (T_4)	Rosuvastatin	Taurodeoxycholate (TDCA)
TR-14035	SN-38	Tauroursodeoxycholate (TUDCA)
Triiodothyronine (T_3)	Taurocholate (TCA)	Telmisartan
Unoprostone metabolite	Tauroursodeoxycholate (TUDCA)	Thyroxine (T_4)
	Thromboxane B_2 (TXB_2)	TR-14035
	Thyroxine (T_4)	Triiodothyronine (T_3)
	TR-14035	Valsartan
	Triiodothyronine (T_3)	Bromosulfophthalein (BSP)
	Troglitazone sulfate	Oestradiol-17-glucuronide
	Valsartan	Oestrone-3-sulfate
		Reverse triiodothyronine (rT_3)

OATP2B1	OATP3A1_v1	OATP3A1_v2	OATP4A1
Atorvastatin Benzylpenicillin Bosentan Bromosulfophthalein (BSP) CP-671,305 Dehydroepiandrosterone-3-sulfate (DHEAS) Oestrone-3-sulfate Fexofenadine Fluvastatin Glibenclamide M17055 Pravastatin Pitavastatin Pregnenolone sulfate Prostaglandin E_2 (PGE_2) Rosuvastatin Taurocholate (TCA) Unoprostone metabolite	Benzylpenicillin BQ-123 Deltorphin Oestrone-3-sulfate Prostaglandin E_1 (PGE_1) Prostaglandin E_2 (PGE_2) Prostaglandin F_2 (PGF_2) Thyroxine (T_4) Vasopressin	Arachidonic acid BQ-123 Prostaglandin E_1 (PGE_1) Prostaglandin E_2 (PGE_2) Thyroxine (T_4) Vasopressin	Benzylpenicillin Oestradiol-17-glucuronide Oestrone-3-sulfate Prostaglandin E_2 (PGE_2) Reverse triiodothyronine (rT_3) Taurocholate (TCA) Thyroxine (T_4) Triiodothyronine (T_3) Unoprostone metabolite
			OATP4C1
			cAMP Digoxin Methotrexate Ouabain Sitagliptin Thyroxine (T_4) Triiodothyronine (T_3)

Table 1.12 substrates of OATP transporters [Hagenbuch and Gui 2008]

MDR/MRPs	PEPT	OCT	OAT	OATP
Paclitaxel 9-Nitro-camptothecin Cyclosporin A Pentamidine Budesonide Rifampicin Tetracycline(s) Erythromycin	Valacyclovir Cephalosporins	Salbutamol Formoterol (?) Prostaglandins Adrenoceptor (ant)agonists Beclomethasone Budesonide Nicotine Cephalosporins	Methotrexate Tetracycline(s) β-lactam antibiotics	Rifampicin Fexofenadine β-lactam antibiotics

Table 1.13 Transporter substrates with pulmonary relevance

1.4 Overall aim and specific objectives of research

The overall aim of the work undertaken was to contribute toward knowledge on the subject of functional transporter expression within lung epithelial cells models. While significant literature is now available on drug transporter expression within the gastro-intestinal tract, the blood brain barrier and renal epithelium, relatively little is known about the functional expression of clinically relevant transporters in the lung. These transporters can impact upon the disposition of drugs administered both by the inhalation route and also for drugs administered via other routes such as the gastrointestinal tract, where the latter may result in lung accumulation and toxicity. To investigate the impact of transporters in systemic drug delivery, isolation of certain areas of the lung is beneficial for targeting their mechanisms, such as efflux and active uptake. Initial studies prove the effect on increased uptake of idarubicin by inhibiting the efflux pump MDR1 [Kuhlmann et al. 2003]. To date, there is limited knowledge, whether the existing cell lines or primary model reflect the expression pattern of transporters *in vivo*. Identifying the optimal cell model for studies on selected transporters can accelerate initial steps and minimise costs for further investigation in drug delivery.

2 RT-PCR analysis of ABC-, SLC- and SLCO-drug transporters in human lung epithelial cell models

Parts of this chapter have been published. Endter, S., Francombe, D., Ehrhardt, C., Gumbleton, M. (2009). RT-PCR analysis of ABC, SLC and SLCO drug transporters in human lung epithelial cell models. Journal of Pharmacy and Pharmacology **61**(5): 583-91.

2.1 Abstract

Carrier-mediated transport mechanisms play crucial roles in drug absorption and elimination processes, as well as in the transport of endogenous molecules in which they impact upon cellular regulation and function. In this study we have sought, using RT-PCR analysis, to investigate mRNA transcript expression of a wide range of membrane carrier transporters in several *in vitro* lung epithelial cell models. Transporters studied included: 11 ABC transporters, 11 SLC transporters, and 9 SLCO transporters. Employed cell culture models include both established cell lines (A549, Calu-3, 16HBE14o-, BEAS-2B) and freshly isolated cells in primary culture (human bronchial and alveolar epithelial cells). Through RT-PCR analysis, we have documented an expression profile of several clinically relevant drug transporters. Our results have revealed differential transporter expression throughout cell culture models from different regions of the lung and also highlighted disparities when comparing cell lines with primary cell culture models. Moreover, a number of variations regarding transporter expression in cell models of pulmonary compared to gastrointestinal origin were discovered. However, further investigation should be conducted before final conclusions can be drawn.

2.2 *Introduction*

Membrane transporters relevant to xenobiotic transport comprise three main groups: the ATP-binding cassette (ABC) transporters of which there are approximately 50 members, the solute carrier (SLC) transporters of which there are approximately 300 members and organic anion transporting polypeptides, classified within the OATP/SLCO family, of which thirty six members have been identified so far in human, rat and mouse.

ABC transporters are transmembrane proteins that utilise the energy of ATP hydrolysis to actively transport a wide variety of substrates across extra- and intracellular membranes [Schinkel and Jonker, 2003]; substrates include physiologic metabolic products, lipids, sterols, and a wide range of drugs [Dean et al., 2001]. Abnormalities in ABC transporter function have been implicated in inherited human diseases and in tumour and bacterial multidrug resistance. ABC transporter family members that are of particular significance with respect to regarding drug absorption and disposition include: MDR1, the multidrug resistance-related proteins (MRP1-9) and breast cancer-related protein (BCRP) [Cordon-Cardo et al., 1990, Thomas et al., 1994, Ejendal et al., 2002].

The SLC superfamily of transporters is organised into 47 families:

- http://ghr.nlm.nih.gov/geneFamily=slc
- http://www.bioparadigms.org/slc/menu.asp

[Sai and Tsuji, 2004]. Solutes transported by the various SLC group members are extraordinarily diverse and include charged and uncharged organic molecules, inorganic ions, di- and tri-peptides as well as a variety of structurally related drugs and pro-drugs [Sai and Tsuji, 2004]. Both uptake and efflux SLCs influence

physiologic and pathophysiologic function as well as the absorption and disposition of xenobiotics [Sai and Tsuji, 2004]. The SLC superfamily includes among others, the organic cation transporters and organic anion transporters (OAT) (SLC22 family), which play critical roles in renal and hepatic transport and the detoxification of a wide variety of compounds including drugs, toxins, hormones and neurotransmitter metabolites [Koepsell and Endou, 2004].

In 2004, Hagenbuch and Meier [2004] reclassified the organic anion transporting polypeptides (OATP), formerly known as the SLC21 family. The SLCO family represents a phylogenetically based, species independent and open-ended nomenclature and classification system. This group of transporters are present in a variety of biological barriers and exhibit a noted impact upon xenobiotic absorption.

In this study we have examined the expression of mRNA transcripts in several lung epithelial cell types, including cells of bronchial epithelial and alveolar epithelial origin, primary cells and cell lines. The selection of transporters investigated in our study was based on their reported relevance in affecting drug disposition. Transporter proteins examined included: the ABC transporters MDR1, MRP1-8, WHITE1 and BCRP; the SLC transporters OCT1-3, OCTN1 and -2, PEPT1 and -2 and OAT1-4; and the SLCO transporters OATP1A2, 1B1, 1B3, 1C1 2A1, 2B1, 3A1, 4A1 and 5A1.

2.3 Materials and Methods

2.3.1 Cell culture

Human A549

(American Type Culture Collection, ATCC CL-185 LGC Promochem, Teddington Middlesex, UK). A549 cells are derived from a human pulmonary adenocarcinoma [Giard, Aaronson et al. 1973]. Due to phenotype similarity to type II alveolar epithelial cells this cell line has been widely utilised in analysis of alveolar epithelium function [Forbes and Ehrhardt 2005]. Cells were cultured on 6-well plates (Corning, Schiphol, The Netherlands) using a seeding density of 40,000/cm^2 with Dulbecco's modified Eagle's medium (DMEM, 10% FBS, 100 U/ml penicillin and 100 µg/ml streptomycin) exchanged every 48 h. Monolayers reached confluence by day 5 of culture at which time cells were harvested for RNA extraction.

Human Calu-3 (ATCC HTB-55)

Cells of the human bronchial epithelial cell line derived from an adenocarcinoma of the lung were seeded at a density of 75,000 cells/cm^2 on 6-well plates (Corning) and cultured in DMEM (10% FBS, 100 U/ml penicillin and 100 µg/ml streptomycin) and was exchanged every 48 h. Cells reached confluence by day 8 of culture at which time cells were either harvested and RNA extracted or cultured for a further 7 days to allow for further differentiation [Sporty et al., 2008] and respective RNA extraction for traditional PCR. For quantitative PCR, cells were cultured for 12 days on 6-well plates (Corning) for liquid covered conditions and

on Transwell inserts (0.4μm pore size 12mm membrane diameter, Corning) under air-interphase conditions.

Human 16HBE14o-

This cell line was obtained from Dr. Dieter C. Gruenert (California Pacific Medical Center, San Francisco, CA). The cell line was generated by transformation of normal bronchial epithelial cells obtained from a one-year-old male heart-lung transplant patient. Transformation was accomplished with SV40 large T antigen [Cozens et al., 1994]. Cells were cultured at 100,000 cells/cm^2 in Eagle's minimum essential medium (MEM, 10% FBS, 100 U/ml penicillin and 100 μg/ml streptomycin, 1 mM sodium pyruvate and non essential amino acids) exchanged every 48 h. Cell monolayer confluence was reached at 3 days. RNA was isolated after 8 and 15 days, respectively. For quantitative PCR cells were culture for 8 days.

Human BEAS-2B (ATCC CRL-9609)

Cells of the normal human epithelial cell line immortalised using a hybrid virus of adenovirus 12 and SV40 [Reddel et al. 1988] were seeded at a density of 100,000 cells/cm^2 were maintained in culture for 8 days, before RNA was harvested. The cells were grown in DMEM supplemented with 10% FBS, 100 U/ml penicillin and 100 μg/ml streptomycin, which was exchanged every 48 h.

Human alveolar epithelial cells (hAEpC)

Fresh human type II alveolar epithelial cells (hAEpC) were isolated from non-tumour lung tissue obtained from patients undergoing lung resection. The use of human material for isolation of primary cells was reviewed and approved by the local ethical committees (Saarland State Medical Board, Germany). Isolation of primary human type II pneumocytes was performed according to a protocol modified from those of Ehrhardt et al. [2005]. Briefly, finely minced lung tissue was digested for 40 min at 37°C using a combination of 150 mg trypsin type I (Sigma, Seelze, Germany) and 0.641 mg elastase (CellSystems, St. Katharinen, Germany) in 30 ml HEPES-buffered balanced salt solution (BSS; 137 mM NaCl, 5.0 mM KCl, 0.7 mM $Na_2HPO_4 \times 7\ H_2O$, 10 mM HEPES, 5.5 mM glucose, and antibiotics (penicillin (100 units/ml) and streptomycin (100 µg/ml)), pH 7.4). The human alveolar epithelial type II cell (ATII) population was purified from the crude cell mixture using a combination of differential cell attachment, centrifugation with a percoll density gradient, and cell sorting with magnetic beads (anti-HEA (EpCAM) MicroBeads, Miltenyi Biotec, Bergisch Gladbach, Germany). The average yield of ATII cells was 0.8×10^6 cells/g tissue (n = 19) with a purity of >90% determined by staining cells for alkaline phosphatase. Purified ATII cells were either used directly for RNA isolation or seeded at a density of 600,000 cells/cm^2 on collagen/fibronectin coated Transwell inserts (Corning) using small airways growth medium (Lonza, Verviers, Belgium) supplemented with penicillin (100 units/ml), streptomycin (100 µg/ml), and 1% foetal calf serum. Under the chosen culture conditions, the type II pneumocytes transdifferentiated into monolayers of type I-like phenotype [Fuchs et al. 2003; Dehmling et al. 2005] at

approximately day 8 in culture. RNA was extracted from freshly isolated ATII cells and from type I-like phenotypes on day 8 of culture.

Human bronchial epithelial cells (hBEpC)

These primary/first-passage normal human bronchial epithelial cells were obtained from TCS CellWorks (ZHC-1101; Buckingham, UK) and cultured 6-well plates (Corning) at an initial density of 10,000 cells/cm^2 for 10 days in TCS bronchial epithelial growth medium. The medium was exchanged every 48 h with RNA extraction on day 10 of culture.

For quantitative PCR, Clonetics human bronchial/tracheal epithelial cells (NHBE) CC-2541 were supplied by Lonza (Walkersville, MD, USA) and cultured on 6-well plates (Corning) in bronchial epithelial cell growth medium (BEGM, Lonza) for 7 days until confluence.

Human colonic adenocarcinoma cells (Caco-2)

Caco-2 were obtained from the European Collection of Animal Cell Cultures (ECACC, Salisbury, UK) and used as a reference cell line for expression studies [Sun et al., 2008]. The cells were cultured on 6-well plates with exchange of media (DMEM, 10% FBS, 100 U/ml penicillin and 100 μg/ml streptomycin) every 48 h prior to harvesting for RNA at day 21 post seeding.

2.3.2 Bioelectric measurements

The time of the cellular layers reaching confluence was determined by measuring transepithelial electrical resistance (TEER) as a function of days in culture. TEER was measured daily with an epithelial volt-ohm-meter equipped with STX-2 "chopstick" electrodes (WPI, Berlin, Germany) and corrected for the background value contributed by the Transwell Clear filter and medium.

2.3.3 Gene Expression

For comparison of mRNA levels β-actin was selected as a housekeeping gene. Due to the dimension of this study, it was impossible to find a gene which showes the exact same expression levels in all cells tested. The chosen β-actin is a well established and widely used standart.

Total RNA isolation

Total mRNA was isolated using RNeasy Mini Kit (Qiagen, Crawley, UK) animal cells spin protocol. Cells were lysated with 350 µl RLT-Buffer (incl. 10 µl β-Mercaptoethanol per ml, Sigma) per well and collected with a cell scraper. For homogenisation the lysate was passed 10 times through a 20-gauge needle and frozen down at -80°C. After addition of 350 µl ethanol (70%, Sigma) the harvest was pipetted onto an RNeasy column and spun down for 20 s at 10,000 × g (22°C). The column was washed with 700 µl RWE-Buffer and twice with 500 µl RPE-Buffer.

For qPCR, genomic DNA was digested on column using the RNase-free DNase Set (Qiagen, Crawley, UK):

After a first wash with 350 µl RWE-Buffer a mix of 10 µl DNase I stock solution with 70 µl Buffer RDD was pipetted onto each column. After an incubation time of 30 min, the column was washed with 350 µl RWE-Buffer and twice with 500 µl RPE-Buffer.

RNA was eluted with 30 µl diethylpyrocarbonate-treated water (Bioline). Quantification was performed using Gene Quant pro RNA/DNA calculator (Biochrom, Cambidge, UK) or the NanoDrop ND 1000 (NanoDrop Technologies, Wilmington, DE) (The 260/280 nm and 260/230 nm ratios were generally between 1.8 and 2.1 confirming high purity.)

For digestion of genomic DNA after isolation, RNA-solution was diluted to a final concentration of 200 ng/µl. 5.6 µl 10 × TURBO DNase Buffer and 1 µl TURBO DNase (Ambion Ltd, Huntingdon, UK) were added to 50 µl RNA-solution and incubated at 37°C for 30 min on Primus 96 advanced Thermal Cycler (Peqlab, Erlangen, Germany). 6 µl of DNase Inactivation Reagent were added and after 2 min incubation at room temperature under occasional mixing the tubes were placed into 1.5 ml microcentrifuge tubes and particles of Inactivation Reagent were spun down for 2 min at 10,000 × g (4°C). 40 µl supernatant were transferred to microcentrifuge tube.

Reverse transcription

2 µg RNA (total RNA) was reversed transcribed by using Bioscript (M-MLV Reverse Transcriptase, Bioline Ltd, London, UK). For hAEpC, reverse transcription was carried out using Omniscript kit (Qiagen). $Pd(N)_6$ random hexamers (-sodium salt, Amersham, Giles, UK) were used as primers. The reaction mixture contained 2 µg RNA, 200 ng random hexamers, 4 µl 40 mM dNTP Mix,

4µl dithiotreitol (DTT), 8 µl 5 × strand buffer and DEPC treated water to a final volume of 37 µl. RNA was denaturised by incubation for 5 min at 95°C and quenched for 2 min on ice. An enzyme mixture of 1 µl RNasin (Ribonuclease inhibitor; Promega Ltd, Southampton, UK) and 2 µl Bioscript was then added. For each RNA harvest isolated an additional tube was prepared lacking Bioscript to verify the absence of genomic DNA. The followed program was started: 10 min at 25°C followed by 42 min at 42°C, 5 min at 95°C and finally 10 min at 4°C. cDNA harvests were stored at -80°C until use.

2.3.4 Polymerase chain reaction

Semi quantitative PCR with self designed primers

Polymerase Chain Reaction (PCR) was performed using cells from three to five different isolations. Harvests of 40 ng RNA, reverse transcribed to cDNA, were used for each polymerase chain reaction (PCR) run with BIOTAQ Core Kit (Bioline) including 0.75 µl 25 mM $MgCl_2$, 1 µl 2.5 mM dNTP Mix, 1.25 µl Taq buffer, 0.1 µl Taq polymerase, 0.5 µl 10 pM primer forward and reverse (Invitrogen Ltd, Paisly, UK and Eurofins MWG Operon, Ebersberg, Germany) and DEPC treated water up to a volume of 12.5 µl and run the following program: 5 min at 94°C for an initial denaturing of secondary structure allowing access to nucleotide sequences followed by 35 cycles of 30 s at 94°C for denaturing, 45 s at 54-60°C for annealing primers to sequences and 45 s at 72°C to allow Taq polymerase to copy desired sequences. After the last cycle in additional 10 min at 72°C Taq polymerase completed any unfinished regions.

Agarose gel electrophoresis

Three µl loading buffer were added to each PCR sample and 10 µl of this mixture loaded into the wells of a 2% agarose (Bioline) gel. To determinant the band sizes of the PCR products HyperLadder IV (Bioline) was used. For preparation of a gel 2 g agarose was suspended in 100 ml 0.5 × TBE buffer (0.54% TRIS, 0.275 % boric acid and 0.0372% $Na_2EDTA \times 2\ H_2O$, all Sigma), covered with cling film and heated for 1 min in a microwave oven until the suspension came to a running boil. The resultant solution was cooled down on a stirrer to 60°C. 2 µl of Ethidium bromide solution (10 mg/ml; Sigma) were added and the mixture was poured into a gel tray where it was allowed to stand for 1 h. Samples were loaded using HyperLadder IV (Bioline). Electrophoresis was run at 100 Volt for 90 min in a horizontal gel tank (Peqlab). Alternatively, the FlashGel System (Cambrex/Lonza, Rockland, USA) was used. 2.2% double tier cassettes were loaded and run according manufacturers protocol. The bands were visualised using Bio-Rad Gel Doc 1000.

Primer design

To find the suitable region for designing a pair of primers which detect all transcription variants, the sequence of an exon was found which is expressed in all variants and which was long enough to design primers for a product size of 150-250 bp. Design within an exon was necessary since genomic DNA can be utilised for optimisation. The following online programs were used:

Existing transcription variants were identified via "PubMed" and the gene database of NCBI:

- http://www.ncbi.nlm.nih.gov/entrez/query.fcgi?CMD=search&DB=gene

Different mRNA sequences were aligned with a tool from the nucleotide database

- http://www.ncbi.nlm.nih.gov/blast/bl2seq/wblast2.cgi

To identify exons within genes SNPper was used:

- http://snpper.chip.org

The suitable regions were input into Primer3

- http://frodo.wi.mit.edu/cgi-bin/primer3/primer3_www.cgi

Tables 2.1 to 2.3 show characteristics of primers used in this study.

After design, primer sequences were copied into the Blast program "Nucleotide-nucleotide BLAST (blastn)" of nucleotide database of NCBI to confirm their selectivity.

- http://www.ncbi.nlm.nih.gov/BLAST/

Primer	Gene		Sequence	Size (bp)	Gen Bank Accession No
MDR1	ABCB2	Forw	CAC CTG CAT TGT GAT TGC TC	174	NM_000593
		Rev	AGA GTT CAC TGG CGC TTT GT		
MRP1	ABCC1	Forw	GCT GTG AAG ACC CAG GAG AG	230	NM_004996
		Rev	ACA GAC TTC GGC TGG AGA GA		
MRP2	ABCC2	Forw	CTA TCC AAC TTG GCC AGG AA	166	NM_000392
		Rev	AGG GTC CCA ACT CTC TCC AT		
MRP3	ABCC3	Forw	GCA CTG CTG CAC AAC AAG AT	157	NM_003786
		Rev	GGC GTT GAA GAA GGA ATT GA		
MRP4	ABCC4	Forw	GAG GGA TGA ATT TGG CTT CA	180	NM_005845
		Rev	ACA CCC TCT CAA TGG CTG AG		
MRP5	ABCC5	Forw	AAC CAG CCA GTC CTC ACA TC	247	NM_005688
		Rev	CCT TCT TCC TCT TCG GGA CT		
MRP6	ABCC6	Forw	CAC CTG CTA AAC CGC TTC TC	180	NG_007558
		Rev	CTG AAA CCC AGC GTA GAG GA		
MRP7	ABCC10	Forw	CTG CCC TTC ATC CTC AAC AT	211	NM_033450.2
		Rev	CGG CCA GAT GGC TAT ACA GT		
MRP8	ABCC11	Forw	GCC ACA GCC ACT TCT TCA CT	197	NM_145186.2
		Rev	GCC TAT TCC AGG GTT TCC AT		
WHITE1	ABCG1	Forw	ATG GCT TAG ACC GGG AAG AT	218	NM_016818
		Rev	GTT TCC TGG CAT TCA GGT GT		
BCRP	ABCG2	Forw	GTG GCC TTG GCT TGT ATG AT	180	NM_004827
		Rev	GAT GGC AAG GGA ACA GAA AA		

Table 2.1 Specific primer sequences for RT-PCR analysis. All primers were derived from GenBank, using the displayed accession numbers. Where more than one transcript variant exists, accession number for variant 1 is displayed. Other variants can be accessed through this record.

Primer	Gene		Sequence	Size (bp)	Gen Bank Accession No
PEPT1	SLC15A1	Forw	CCA TCA TGG CTC GGT TCT AT	219	NM_005073
		Rev	ATC CAA TGG AGT GTC CTG CT		
PEPT2	SLC15A2	Forw	TTC TGT CCT GAC CCC AAT TC	222	NM_021082
		Rev	CCA GCA ACA CTG CAC AAG TT		
OCT1	SLC22A1	Forw	CTG AGG GAG ACA TTG CAC CT	161	NM_003057
		Rev	CGA CAG CAG GCA TAA GAT GA		
OCT2	SLC22A2	Forw	ATC TAC GTG GGC ATC GTC TT	186	NM_003058
		Rev	GTT CCA GTC CAC CTC GTA GC		
OCT3	SLC22A3	Forw	GTC ACC TTC GCC TTC CTC TT	242	NM_021977
		Rev	CAG CTG AGA GCG CTA GTG G		
OCTN1	SLC22A4	Forw	CTG AGA ACG CTG TCA TCA CC	182	NM_003059
		Rev	GCC AGG AAC ACG ACT GAC AT		
OCTN2	SLC22A5	Forw	CTG TCC TCC GTG TTC CTG AT	233	NM_003060
		Rev	AGA CAG CTC TCC TGC TCC AG		
OAT1	SLC22A6	Forw	CAG CAA CAA GAG CAC CAG AA	166	NM_004790
		Rev	TGG GTC ACC ATT TCC TCT TC		
OAT2	SLC22A7	Forw	TGC TGC TAC CAC TGC ACT TC	247	NM_006672
		Rev	ACT GTG GCA GGT TCA TCC TC		
OAT3	SLC22A8	Forw	TGA CCT TCT CGG AGA TCC TG	216	NM_004254
		Rev	ACC TCT CAG GCT TCC CAT TT		
OAT4	SLC22A9	Forw	AGC TCT GTT CAT GGC GTT CT	206	NM_080866
		Rev	GGG TCA TGT TTG TGG AAA CC		

Table 2.2 Specific primer sequences for RT-PCR analysis. All primers were derived from GenBank, using the displayed accession numbers. Where more than one transcript variant exists, accession number for variant 1 is displayed. Other variants can be accessed through this record.

Primer	Gene		Sequence	Size (bp)	Gen Bank Accession No
OATP1A2	SLCO1A2	Forw	TGG CTT TCT GAT TTG TGC AG	150	NM_134431
		Rev	TCC TTC TTG ACC TCT TCT TTT TG		
OATP1B1	SLCO1B1	Forw	AGG GTC TAC TTG GGC TTG TCT	186	NM_006446
		Rev	CCA GCA GAA GGG ACA AAA TG		
OATP1B3	SLCO1B3	Forw	AGA TAC CAA GGC ATC GGA CA	154	NM_019844
		Rev	GCA ATG TTA GTT GGC AGC AG		
OATP1C1	SLCO1C1	Forw	TGG GCA CAG TGT CAA TTC TC	173	NM_017435
		Rev	TGG CCA GTA GTT GGG TTG TA		
OATP2A1	SLCO2A1	Forw	AGG GGT GAA AGG AAG AAG GA	244	NM_005630
		Rev	TTC TCA GTC CCT GCT CTG GT		
OATP2B1	SLCO2B1	Forw	GGT AGG GAG GGA GAC TCA GG	183	NM_007256
		Rev	CAG GCA CCC AGG AGA AAA TA		
OATP3A1	SLCO3A1	Forw	AAA TCC TTC GCC TTC ATC CT	207	NM_013272
		Rev	CCA CTC ATG GTC TTC CAG GT		
OATP4A1	SLCO4A1	Forw	GGC ATC CTG TTC TTC CTG TG	184	NM_016354
		Rev	CCG AAG TAG CTG ACG AAG GT		
OATP5A1	SLCO5A1	Forw	TGG ACC TCA GCA AAA CCT TC	233	NM_030958
		Rev	GGG CGA GAT GAA GTG AGG TA		
β-actin	ACTB	Forw	AAA CTG GAA CGG TGA AGG TG	171	NM_001101
		Rev	AGA GAA GTG GGG TGG CTT TT		

Table 2.3 Specific primer sequences for RT-PCR analysis. All primers were derived from GenBank, using the displayed accession numbers. Where more than one transcript variant exists, accession number for variant 1 is displayed. Other variants can be accessed through this record.

Real time/quantitative PCR

The RT^2 Profiler PCR Array (SABiosciences Frederick, MD, USA) provides 96-well plates loaded with primers for 84 human drug transporters and 12 control targets including GAPDH, β-actin, human genomic DNA contamination, and triplets of reverse transcription control and positive PCR control. For normalisation, β-actin was selected for easier comparison to traditional PCR.

Total RNA was isolated using the RNeasy Kit, as described, and diluted to a final concentration of 31.25 ng/µl. RNA was reverse transcribed using RT^2 First Strand Kit: 8 µl (250 ng) were incubated with 2 µl of GE (5 × gDNA Elimination Buffer) for five minutes at 42°C. The reaction was stopped by chilling on ice for two minutes. 10 µl of an RT Cocktail consisting of 4 µl BC3 (5 × RT Buffer 3), P2 (Primer & external Control Mix), RE3 (RT Enzyme Mix 3) and 3 µl RNase free water were added to the purified RNA. This mix was incubated at 42°C for 15 minutes followed by 95°C for five minutes to degrade the RNA and to inactivate the reverse transcriptase. 91 µl of RNase-/ DNase-free water was added to the each cDNA mix and samples were stored at -20°C until further use.

For each plate of the RT^2 Profiler PCR Arrays 102 µl of cDNA was added to 1275 µl of RT2 SYBR Green qPCR Master Mix and filled up with 1173 µl RNase-/ DNase-free water to a final volume of 2550 µl. 25 µl of the final mix were pipetted into each well. The plate was sealed with cap strips and spun down briefly to remove bubbles.

The following program was run with an Eppendorf Mastercycler ep realplex (Eppendorf, Hamburg, Germany): 10 minutes at 95°C for an initial denaturing of secondary structure allowing access to nucleotide sequences followed by 40 cycles

of 15 seconds at 94°C for denaturing and one minute at 60°C for annealing primers to sequences and amplification of DNA. During this minute, SYBR Green fluorescence was detected and recorded (figure 2.1).

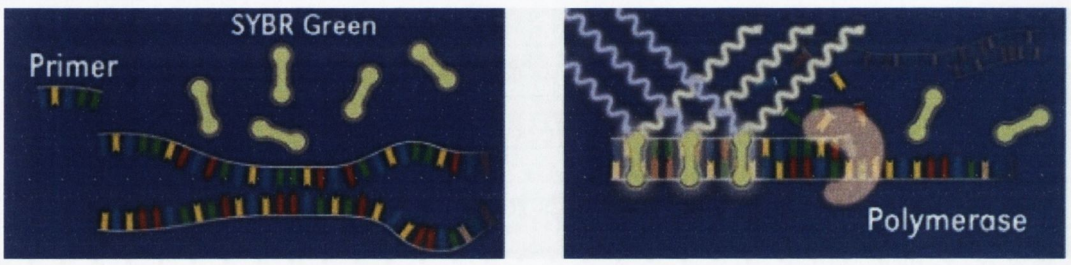

Figure 2.1 Schematic of quantification with SYBR Green. SYBR Green is an asymmetrical cyanine dye that binds to Minor Groove of double-stranded DNA. The resulting DNA-dye-complex absorbs blue light and emits green light. As more double stranded amplicons are produced, SYBR Green dye signal will increase. (Image source: http://www.dkfz.de/gpcf/lightcycler480.html)

Threshold cycles were calculated by instrument's software and normalised to β-actin [Livak and Schmittgen 2001]:

$$\Delta C_t = C_{t\ \text{target gene}} - C_{t\ \beta\text{-actin}}$$

Relative gene expression levels were calculated as followed:

$$R = 2^{-\Delta Ct}$$

For the transporters OCTN1 and OCTN2 TaqMan Expression Assay Hs00268200_m1 and Hs00929869_m1 (Applied Biosystems, Foster City,

California, USA) were used. For a calibration curve Hs00375701_m1 (MRP7) was used. The concentration of mRNA was chosen which result in the same threshold cycle as detected with the RT^2 Profiler PCR Array.

For each run, with a total volume of 25 µl, 11.25 µl cDNA were mixed with 1.25 µl TaqMan Expression Assay and 12.5 µl TaqMan Universal PCR Master Mix (Applied Biosystems). The following program was run with an Eppendorf Mastercycler ep realplex (Eppendorf, Hamburg, Germany): 10 minutes at 95°C for an initial denaturing of secondary structure allowing access to nucleotide sequences followed by 40 cycles of 15 seconds at 94°C for denaturing and one minute at 60°C for annealing primers to sequences and amplification of DNA (figure 2.2). During this minute, FAM (6-carboxyfluorescein) fluorescence was detected and recorded. Threshold cycles were calculated by instrument's software and adjusted to MRP7.

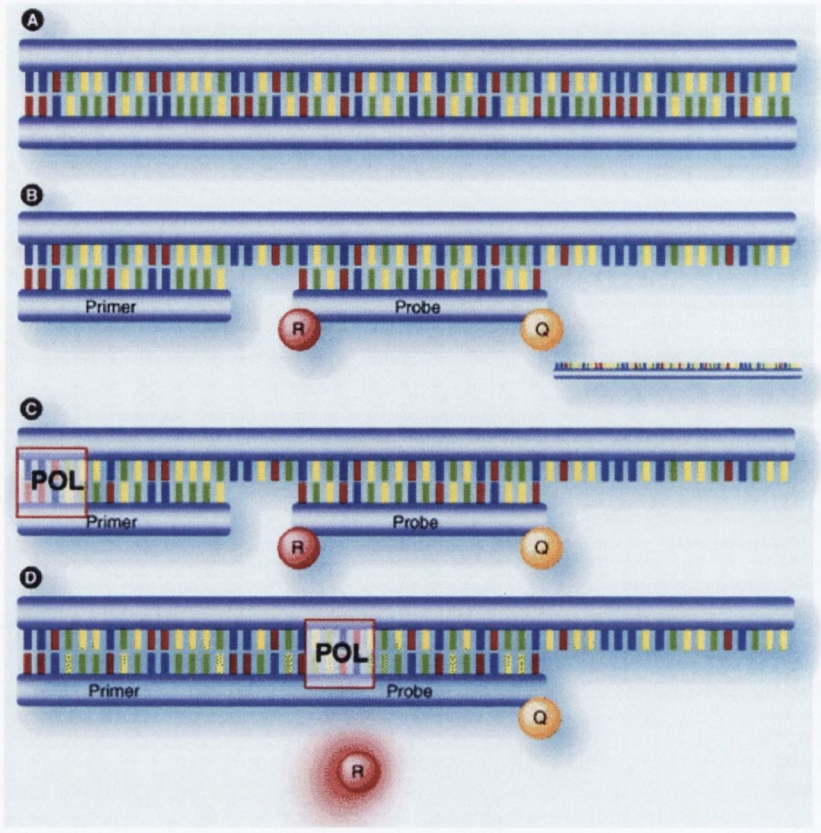

Figure 2.2 Schematic of TaqMan PCR using an internal probe labelled with a reporter (R) and a quencher (Q). Following denaturation of template DNA (A), TaqMan primers and probe anneal to the denatured template (B). Polymerisation is catalysed by the DNA polymerase (POL) (C), and the 5′-nuclease activity of the polymerase results in the fluorescent reporter of the probe being cleaved (D). The release of the reporter dye from close proximity to the quencher moiety results in increased fluorescent signal that is proportional to the amount of PCR product accumulated. [Logan and O'Sullivan 2008]

2.4 Results and Discussion

In recent years, interest has greatly increased into the contribution of drug transporters to the distribution of clinically relevant drugs. Improved knowledge of transporter localisation throughout organ systems would allow greater understanding and prediction of both the likelihood of transporter-mediated drug

resistance and also impact upon disposition of drugs delivered to, or targeted at specific organs. Many transporters have already been localised to several organs, for example liver, kidney and intestine [Sai and Tsuji 2004]. However, there is comparatively less data regarding transporter localisation in the lung.

In this study, we have sought to generate a comprehensive mRNA expression profile of several prevalent drug transporters in human lung epithelial cell types. Beta-actin served as a positive control in all the RT-PCR reactions with the negative controls comprising cDNA negative, RT-negative wells. Semi-quantitative RT-PCR-derived expression profiles for selected transporters in human respiratory epithelial cell models are shown in Tables 2.4, 2.6 and 2.8. Expression was quantified and the following symbols used to indicate signal intensity: – representing no expression; + representing low expression; ++ representing moderate expression and +++ representing high expression. Figure 2.3 illustrates the typical signal intensities corresponding to the assigned mRNA expression index. In Tables 2.4, 2.6 and 2.8 can also be seen the expression we determined within the human colonic adenocarcinoma cells, Caco-2. The Bleasby et al. [2006] data refers to a microarray study of gene expression intensity in human whole lung tissue based on a reference set of 19,000 genes. With the symbols used in the Tables to define the following Bleasby et al. data: -, corresponding to an intensity of gene expression within the 0-25% quartile of genes examined; +, within the 25-50% quartile; ++, within the 50-75% quartile; +++, within the 75-100% quartile.

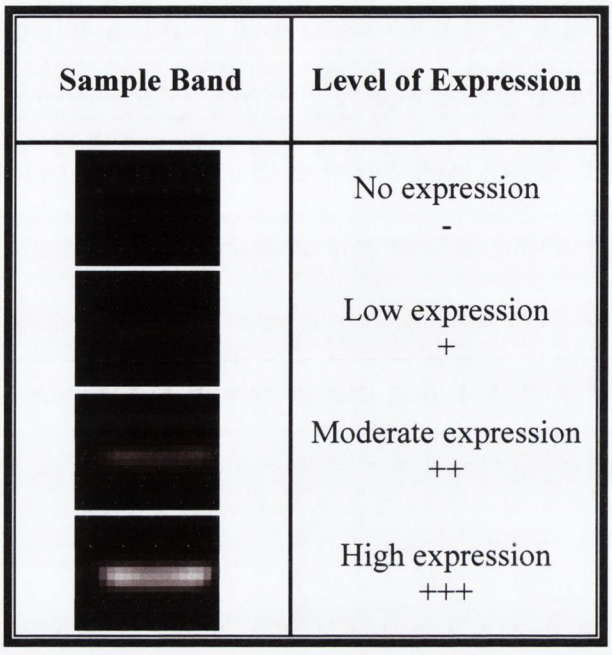

Figure 2.3 Representative samples of RT-PCR signal strengths. Data were grouped according to the intensity of the obtained signals of the product bands on agarose gels.

The RT^2 Profiler PCR Array allows a parallel analysis of 84 human drug transporters. Twenty-five of these were of interest for this project: MDR1, MRP1, MRP2, MRP3, MRP4, MRP5, MRP6, MRP7, MRP8, BCRP, PEPT1, PEPT2, OCT1, OCT2, OCT3, OAT1, OAT2, OAT3, OATP1A2, OATP1B1, OATP1B3, OATP2A1, OATP2B1, OATP3A1 and OATP4A1. Further transporters are summarised in Figure 2.7, but will not be discussed in this work.

Relative expression levels were calculated using threshold cycles [Livak and Schmittgen 2001], determined by instrument's software: $2^{-\Delta Ct}$ for the cell lines 16HBE14o-, Calu-3 (under liquid-covered culture and air-interphased culture), A549 and primary bronchial epithelium cells (hBEpC). Expression was classified as: $2^{-\Delta Ct}$ lower than 0.001 representing no expression; 0.001-0.005 representing low

expression; 0.005-0.019 representing moderate expression, and 0.02-0.1 representing high expression and higher than 0.1 representing highest expressions.

2.4.1 Expression analysis of ABC transporters in human respiratory cell models

The expression of 10 ABC transporter genes in human respiratory epithelial cell models is summarised in Table 2.4. MDR1 is the probably most commonly investigated ABC transporter with regards to drug disposition and is recognised to be expressed in a variety of biological barriers and organs of elimination including the blood-brain barrier, intestine, kidney and the liver [Loo et al., 2005]. Within the lung, previous works have localised MDR1 to the bronchial and alveolar epithelial cells [van der Deen, 2005] with, in addition, MDR1 functionality demonstrated in lung epithelial cell lines [Hamilton et al., 2001; Ehrhardt et al., 2003] as well as rat and human pneumocytes [Campbell et al., 2003]. Our results for MDR1 confirm and complement these reported findings and extend the findings with MDR1 to include a range of respiratory cell models commonly utilised in various in vitro model assays. The primary bronchial epithelial model, hBEpC, arguably closer to the *in vivo* cell type, showed a low MDR1 signal; it was lower than the detection limit of the RT^2 Profiler PCR Array. The 16HBE14o- cell line displayed also low levels of MDR1 expression independent of time in culture. Likewise in hBEpC, none were detectable by the RT^2 Profiler PCR Array. Higher MDR1 levels in Calu-3 were detected which showed a temporal dependence increasing with time in culture. Samples, analysed by the RT^2 Profiler PCR Array, showed relatively high expression under liquid-covered culture ($2^{-\Delta Ct} = 0.09 \pm 0.031$), but not under air-

interphased culture. Little to no expression in the BEAS-2B cells was found. The ATII were studied freshly isolated from human lung and also cultivated for 8 days at which point they have adopted many of the characteristics of the type-I alveolar epithelial cell (ATI-like) [Fuchs et al., 2003; Demling et al., 2006]. The ATII cells showed moderate expression for MDR1 with the ATI-like phenotype showing a lower MDR1 signal similar to that for the adenocarcinoma cell line, A549. In A549, surprisingly high expression of transcripts for MDR1 was detected with the RT^2 Profiler PCR Array ($2^{-\Delta Ct} = 0.048 \pm 0.008$).

Another family of ABC transporters is represented by the ABCC group to which MRP transporters belong. The different family members are variously expressed throughout the tissues of the body [Schinkel and Jonker, 2003]. In particular MRP1 has been quite extensively investigated for its role in drug resistance [Cascorbi, 2003]. The transporter shares many similarities, including substrate specificity and localisation, with MDR1 and has 15% sequence homology with this protein [Kruh et al., 2003]. Perhaps predictably, MRP1 has previously been shown to be expressed in the lung with positive transporter localisation in both whole lung samples and cell culture reported [Scheffer et al., 2002; Torky et al., 2005]. In our studies extending the characterisation of MRP expression in respiratory models we noted that the primary bronchial epithelial model, hBEpC showed strong MRP1 and MRP5 transcript signals with both methods ($2^{-\Delta Ct}$ = MRP1 0.145 ± 0.016, MRP5 0.076 ± 0.009) moderate MRP2, MRP3, MRP4 and MRP7 signals and weak MRP6 and MRP8 signals with traditional PCR, whereas the RT^2 Profiler PCR Array revealed relatively strong expression of MRP7 ($2^{-\Delta Ct}$ = MRP7 0.073 ± 0.020), moderate for MRP4 ($2^{-\Delta Ct}$ = MRP4 0.012 ± 0.001), low of MRP2 and MRP3 ($2^{-\Delta Ct}$ = MRP2, 0.001 ± 0.000, MRP3 0.004 ± 0.002) and no detectable expression of MRP6

and MRP8. In comparison to hBEpC, some notable differences in the immortalised (16HBE14o- or BEAS-2B) or bronchial adenocarcinoma (Calu-3) cells included for:

	hBEpC	Calu-3 day 8	Calu-3 day 15	16HBE14o- day 11	16HBE14o- day 18	BEAS-2B	ATII	ATI-like	A549	Caco-2	Bleasby et al. 2006
MDR1	+	++	+++	+	+	-	++	+	+	+++	-
MRP1	+++	+++	+++	++	+++	+++	+++	+++	+++	++	++
MRP2	++	++	++	++	++	++	++	+	+++	+++	-
MRP3	++	+++	+++	++	++	++	+++	+++	+++	+++	++
MRP4	++	+	-	-	+	-	++	++	+	+	+
MRP5	+++	++	+++	+	++	+++	++	++	++	++	++
MRP6	+	+	++	+	++	++	+++	+++	+	+++	+
MRP7	++	++	+++	++	+++	+++	++	+++	++	++	+++
MRP8	+	-	+	-	-	-	++	++	-	-	++
WHITE1	+++	+	++	+++	+++	++	+++	+++	+	++	N/A
BCRP	++	+	+	+++	+++	+++	++	++	+++	+++	++
β-actin	+++	+++	+++	+++	+++	+++	+++	+++	+++	+++	+++

Table 2.4 RT-PCR expression profile of selected ABC transporters. Transcript expression was examined in a variety of cell culture models including both primary and immortalised cell lines. The Bleasby et al. [2006] column refers to the gene expression intensity in human whole lung tissue based on a reference set of 19,000 genes. n = 3 – 5 isolations

MRP1: Highest concentrations of mRNA were observed in Calu-3 (AIC) ($2^{-\Delta Ct}$ = 0.122±0.002) and 16HBE14o- ($2^{-\Delta Ct}$ = 0.092±0.031) and on a slightly lower level, but still in the high expression range, in Calu-3 (LCC) ($2^{-\Delta Ct}$ = 0.039±0.015).

MRP2 revealed similar constancy on a low level: 16HBE14o- ($2^{-\Delta Ct}$ = 0.002±0.000), Calu-3 (LCC) ($2^{-\Delta Ct}$ = MRP2 0.003±0.002), Calu-3 (AIC), ($2^{-\Delta Ct}$ = MRP2 0.005±0.001).

For MRP3, highest levels of mRNA was detected in Calu-3 (LCC) ($2^{-\Delta Ct}$ = 0.170±0.098) and Calu-3 (AIC), ($2^{-\Delta Ct}$ = 0.106±0.005), whereas concentrations in 16HBE14o- were in the lower part of this classification ($2^{-\Delta Ct}$ =0.053±0.012).

MRP4 transcript – a lower to a complete absence of expression in BEAS-2B, Calu-3 and 16HBE14o- cells with traditional PCR; with the RT^2 Profiler PCR Array, moderate expression on the same level as hBEpC was detected in Calu-3 (LCC) ($2^{-\Delta Ct}$ = 0.010±0.004), Calu-3 (AIC), ($2^{-\Delta Ct}$ = 0.011±0.000) and 16HBE14o- ($2^{-\Delta Ct}$ = 0.019±0.008).

MRP5 transcript – lower levels evident in the day 11 16HBE14o- cells with levels increasing to moderate expression by day 18; Calu-3 (LCC) ($2^{-\Delta Ct}$ = 0.076±0.026), Calu-3 (AIC), ($2^{-\Delta Ct}$ = 0.042±0.006) 16HBE14o- ($2^{-\Delta Ct}$ = 0.034±0.016).

MRP8 transcript – lower expression signified by little to no transcript in the BEAS-2B cells, Calu-3 and 16HBE14o- cells with both methods. The RT^2 Profiler PCR Array revealed low expression in Calu-3 under LCC condition ($2^{-\Delta Ct}$ = 0.001±0.000), but no detectable under AIC condition and for 16HBE14o-.

Transcript quantities for MRP7 were relatively similar on a moderate to high level 16HBE14o- ($2^{-\Delta Ct}$ = 0.038±0.018), Calu-3 (LCC) ($2^{-\Delta Ct}$ = 0.053±0.017), Calu-3 (AIC) ($2^{-\Delta Ct}$ = 0.029±0.004).

MRP6 levels of mRNA were on a low level for 16HBE14o- ($2^{-\Delta Ct}$ = 0.001±0.0000), Calu-3 (LCC) ($2^{-\Delta Ct}$ = 0.003±0.002) and Calu-3 (AIC) ($2^{-\Delta Ct}$ = 0.001±0.000).

The ATII cells showed strong signals for MRP1, MRP3, and MRP6 with the remaining MRP transcripts showing moderate expression in the ATII model. The ATI-like phenotype showed a similar result to the ATII cells except a lower MRP2 transcript and a higher MRP7 level. Compared to both the ATII and ATI-like cells the adenocarcinoma cell line, A549, displayed higher MRP2 and lower MRP4, MRP6, MRP8 levels. The RT^2 Profiler PCR Array revealed high levels of mRNA for MRP1, MRP2 and MRP3. These were the highest observed in these experiments ($2^{-\Delta Ct}$ = MRP1 0.378±0.024, MRP2 0.547±0.056, MRP3 1.358±0.238, MRP4 0.115±0.017). Moderate levels for MRP5, MRP7 and MRP6 were comparable to detections in hBEpC: ($2^{-\Delta Ct}$ = MRP5 0.028±0.005, MRP7 0.032±0.001), ($2^{-\Delta Ct}$ = MRP6 0.006±0.001). MRP8 was nor detectable (figure 2.4, table 2.5).

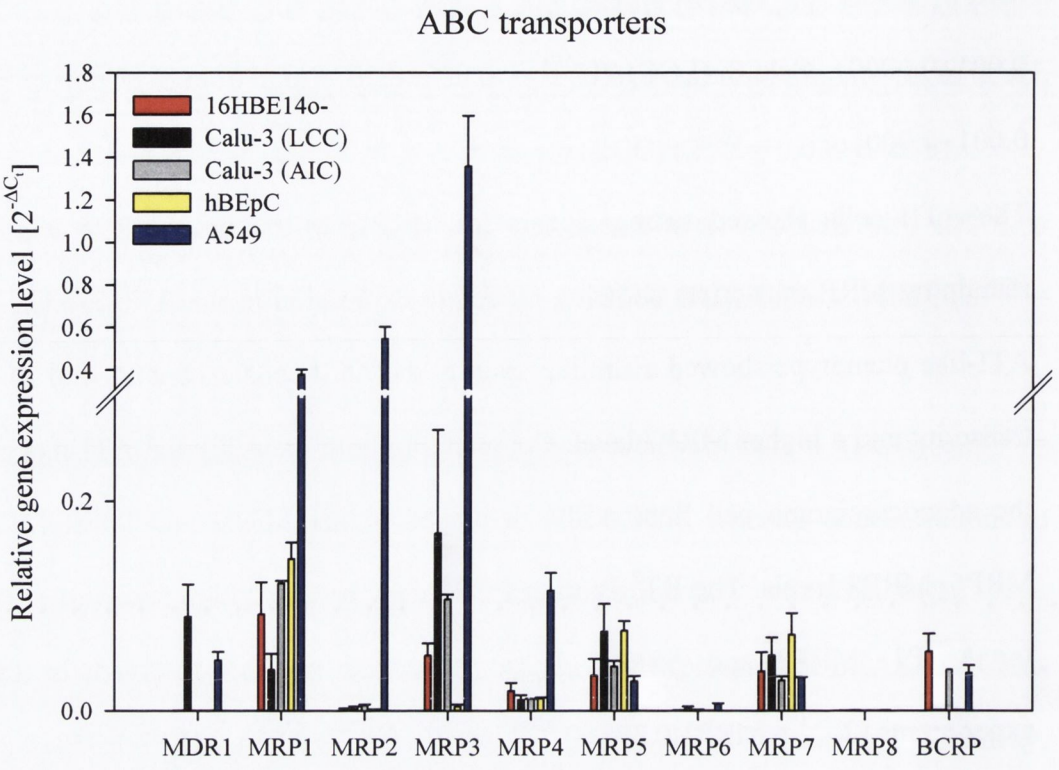

Figure 2.4 Relative gene expression profiles of selected ATP-binding cassette (ABC) transporters of relevance to drug disposition expression. Threshold cycles were calculated by instrument's software and normalised to β-actin. Data shown represents mean±SD from n = 3 experiments.

The G family of ABC transporters consists of half-transporters oligomerising for function. Here we studied the expression of ABCG1 (WHITE1) involved in steroid and lipid transport. The primary hBEpC showed a strong WHITE1 signal which was similar to that seen in the 16HBE14o- cells with the Calu-3 and BEAS-2B cells showing lower levels. In addition, we examined for expression of ABCG2 (BCRP) a multidrug transporter which like MDR1 and MRP family members appears to be able to confer resistance in cancer cells [Bakos and Homolya, 2007]. The hBEpC showed moderate BCRP levels with the Calu-3 being somewhat lower in expression and the 16HBE14o- and BEAS-2B cells higher. The ATII cells and the ATI-like phenotype showed strong signals for WHITE1 and moderate signals

for BCRP. In comparison the adenocarcinoma A549 cells showed low WHITE1 expression and high BCRP expression. The RT^2 Profiler PCR Array showed a different expression pattern for BCRP: highest mRNA readings were observed for 16HBE14o- ($2^{-\Delta Ct} = 0.056 \pm 0.017$), Calu-3 (AIC) ($2^{-\Delta Ct} = 0.039 \pm 0$) and A549 ($2^{-\Delta Ct} = 0.036 \pm 0.007$), but hardly detectable for hBEpC ($2^{-\Delta Ct} = 0.001 \pm 0.000$) and not in Calu-3 (LCC) (figure 2.4, table 2.5).

MDR1	Calu-3 (LCC)	>	A549	>	Calu-3 (AIC)	=	hBEpC	= 16HBE14o-
MRP1	A549	>	hBEpC	>	Calu-3 (AIC)	>	16HBE14o-	> Calu-3 (LCC)
MRP2	A549	>	Calu-3 (AIC)	>	Calu-3 (LCC)	>	16HBE14o-	> hBEpC
MRP3	A549	>	Calu-3 (LCC)	>	Calu-3 (AIC)	>	16HBE14o-	> hBEpC
MRP4	A549	>	16HBE14o-	>	hBEpC	>	Calu-3 (AIC)	> Calu-3 (LCC)
MRP5	hBEpC	>	Calu-3 (LCC)	>	Calu-3 (AIC)	>	16HBE14o-	> A549
MRP6	Calu-3 (LCC)	>	A549	>	Calu-3 (AIC)	>	16HBE14o-	> hBEpC
MRP7	hBEpC	>	Calu-3 (LCC)	>	16HBE14o-	>	A549	> Calu-3 (AIC)
MRP8	Calu-3 (LCC)	>	16HBE14o-	=	hBEpC	=	Calu-3 (AIC)	= A549
BCRP	16HBE14o-	>	Calu-3 (AIC)	>	A549	>	hBEpC	> Calu-3 (LCC)

Table 2.5 Relative expression of ABC transporters. Transporters in blue are absent.

2.4.2 Expression analysis of SLC transporters in human respiratory cell models

The expression of 11 SLC transporter genes in human respiratory epithelial cell models is summarised in table 2.6, 2.7 and figure 2.5. We have chosen a selection

of those transporters that are most relevant to drug disposition. The organic cation and anion transporters are known to be expressed in organs of elimination notably the kidney, but also the liver and in barriers such as the blood brain barrier and intestine [Zhang et al., 1998; Mikkaichi et al., 2004]. Our results show the transcripts for the organic anion transporters represented by OAT1, OAT2 and OAT3 showed little to no expression in all of the bronchial cell models, and indeed were also negligible in the A549 cells. Apart from developmental studies in embryonic lung tissue [Pavlova et al. 2002] quite limited information is available on OAT expression within the adult lung. In the microarray experiments of Bleasby et al. [2006] the OAT family members showed comparatively low levels of expression intensity in whole human lung tissue with only OAT2 within the 50-75 quartile of gene expression intensity. With regard to the organic cation transporters, our *in vitro* model study showed OCT1 to be moderately expressed in BEAS-2B, but in all other bronchial models, as well as A549, its expression was low.

The RT^2 Profiler PCR Array showed low levels of mRNA for OCT1 in Calu-3 (LCC) ($2^{-\Delta Ct} = 0.001 \pm 0.000$) and hBEpC ($2^{-\Delta Ct} = 0.002 \pm 0.001$), but no transcripts were detectable in 16HBE14o-, Calu-3 (AIC) and A549.

OCT2 showed little to no expression in any of the bronchial cell models, and indeed was also negligible in the A549 cells.

	hBEpC	Calu-3 day 8	Calu-3 day 15	16HBE14o- day 11	16HBE14o- day 18	BEAS-2B	A549	Caco-2	Bleasby et al. 2006
PEPT1	-	+	++	+	++	+	+	+++	-
PEPT2	++	+	++	+	++	++	+	+++	++
OCT1	+	+	+	+	+	++	+	+	+
OCT2	-	-	-	-	-	-	-	+	-
OCT3	++	+++	++	-	-	-	+++	+	+
OCTN1	-	++	++	+	++	+++	++	++	++
OCTN2	+	+	+	+	++	+	+	++	++
OAT1	-	-	-	-	-	-	-	+	-
OAT2	-	-	-	-	-	-	-	+++	++
OAT3	-	-	-	-	-	-	-	++	-
OAT4	-	+	++	++	++	++	++	++	-
β-actin	+++	+++	+++	+++	+++	+++	+++	+++	+++

Table 2.6 RT-PCR expression profile of selected SLC transporters of interest to drug disposition. Transcript expression was examined in a variety of cell culture models including both primary and immortalised cell lines. The Bleasby et al. [2006] column refers to the gene expression intensity in human whole lung tissue based on a reference set of 19,000 genes. n = 3 – 5 isolations

Expression of OCT3 showed a variable pattern across the bronchial cells with moderate to high expression in the hBEpC and Calu-3 cells, and negligible expression in the 16HBE14o- and BEAS-2B models using traditional PCR, but

detection by the RT^2 Profiler PCR Array showed moderate expression in Calu-3 (LCC) ($2^{-\Delta Ct}$ = 0.016±0.004), hBEpC ($2^{-\Delta Ct}$ = 0.009±0.002) and low levels of mRNA in Calu-3 (AIC) ($2^{-\Delta Ct}$ = 0.002±0.000) and 16HBE14o- ($2^{-\Delta Ct}$ = 0.001±0.001). In the alveolar A549 cell line, OCT3 expression was pronounced ($2^{-\Delta Ct}$ = 0.222±0.004).

While OCTN1 was negligible in hBEpC the expression of this transporter was evident at low to high levels in the other bronchial cells with traditional PCR. Surprisingly, using the TaqMan Expression Assay, transcripts for OCTN1 were only detected in A549 on a low level ($2^{-\Delta Ct}$ = 0.001±0.000) and seemed to be absent in 16HBE14o-, Calu-3 (LCC), Calu-3 (AIC) and hBEpC.

Finally, except for the day 18 16HBE14o- cells, the expression of OCTN2 was consistently low in all the respiratory cultures studied with traditional PCR. However, the TaqMan Expression Assay detected high to moderate expression in all cell models tested: 16HBE14o- ($2^{-\Delta Ct}$ = 0.024±0.011), Calu-3 (LCC) ($2^{-\Delta Ct}$ = 0.026±0.004), Calu-3 (AIC) ($2^{-\Delta Ct}$ = 0.025±0.010), A549 ($2^{-\Delta Ct}$ = 0.102±0.058), hBEpC ($2^{-\Delta Ct}$ = 0.005±0.001). The OCT family members have been previously found to varying degrees in several lung tissue specimens or cell culture models. Ishiguro et al. [2008] has identified OCT3 protein expression within A549 cells and primary rat alveolar type II cells. Wang et al. [2007] have reported OCT3, OCTN1 and OCTN2 protein expression in the A549 cell line and Miakotina et al. [2005] also showing robust expression of OCT2 protein in isolated rat pneumocytes. Lips et al. [2005] utilising immunohistochemistry demonstrated expression of OCT1, OCT2 and OCT3 in both human and rat lung ciliated airway epithelial cells within intact lung tissue. Similarly, Horvath et al. [2007] have used immunocytochemistry to show OCTN1 and OCTN2 protein expression within airway epithelial cells

within intact human lung. However, in the same study expression of OCT1-3 was not confirmed. In the microarray work of Bleasby et al. [2006] it is OCTN1 and OCTN2 that appeared to be the more strongly expressed transcripts at the 50-75% quartile of gene expression intensity, whereas OCT1 and OCT3 were in the 25-50% quartile and OCT2 even lower at 0-25%.

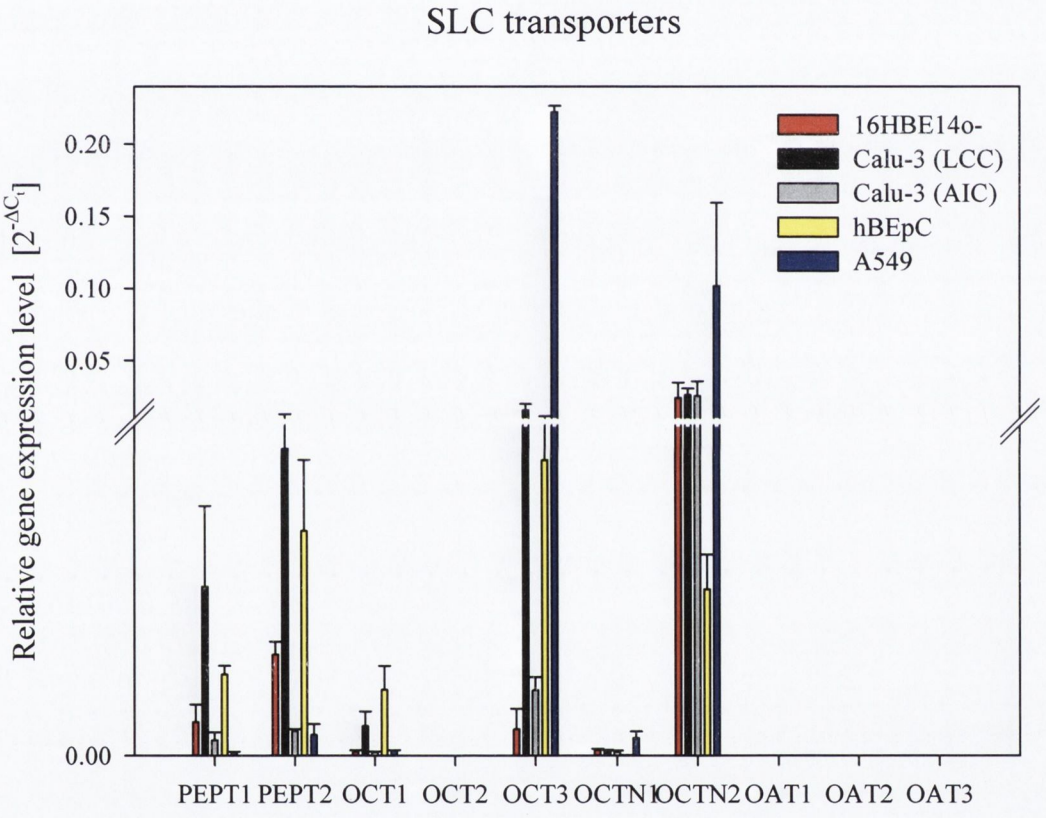

Figure 2.5 Relative gene expression profile of selected solute carrier (SLC) transporters of relevance to drug disposition. Threshold cycles were calculated by instrument's software and normalised to β-actin. Data shown represents mean±SD from n = 3 experiments. Break: 0.01-0.01001

The proton-dependent peptide transporters (PEPT) are well characterised in their expression in the kidney and intestine [Daniel and Kottra, 2004]. PEPT1 expression within the intestine is well recognised although its expression in the lung is less

established. Bleasby et al. showed PEPT1 presence at the mRNA transcript level in whole human lung to be represented within the 25-50% quartile of gene expression intensity. In our studies PEPT1 showed low to moderate expression in all of the bronchial cell lines, Calu-3 (LCC) ($2^{-\Delta Ct}$ = 0.005±0.002), 16HBE14o- ($2^{-\Delta Ct}$ = 0.001±0.001, Calu-3 (AIC) ($2^{-\Delta Ct}$ = 0.001±0.000) and with the RT^2 Profiler PCR Array in hBEpC ($2^{-\Delta Ct}$ = 0.002±0.000), but negligible expression in the primary human model with traditional RT-PCR. The importance of PEPT2 expression in kidney is recognised as is its presence in lung. The protein has been localised in bronchial epithelial cells and ATII by a number of research groups [Bahadduri et al., 2005; Groneberg et al., 2005; Lu and Klaassen, 2006], and we have illustrated expression in all the examined culture models. In our studies PEPT2, similar to PEPT1, showed low to moderate expression in all of the bronchial cells with some evidence of a temporal dependence in both Calu-3 and 16HBE14o- cells: Calu-3 (LCC) ($2^{-\Delta Ct}$ = 0.009±0.003), 16HBE14o- ($2^{-\Delta Ct}$ = 0.003±0.000), Calu-3 (AIC) ($2^{-\Delta Ct}$ = 0.001±0.000), hBEpC ($2^{-\Delta Ct}$ = 0.007±0.002) and A549 ($2^{-\Delta Ct}$ = 0.001±0.000). Of note the hBEpC and BEAS-2B cells showed a greater intensity of signal for PEPT2 than PEPT1.

OCT1	hBEpC	>	Calu-3 (LCC)	>	16HBE14o-	=	Calu-3 (AIC)	=	A549
OCT2	16HBE14o-	=	Calu-3 (LCC)	=	Calu-3 (AIC)	=	hBEpC	=	A549
OCT3	A549	>	Calu-3 (LCC)	>	hBEpC	>	Calu-3 (AIC)	>	16HBE14o-
OCTN1	A549	>	16HBE14o-	=	Calu-3 (LCC)	=	Calu-3 (AIC)	=	hBEpC
OCTN2	A549	>	Calu-3 (LCC)	>	Calu-3 (AIC)	>	16HBE14o-	>	hBEpC
OAT1	16HBE14o-	=	Calu-3 (LCC)	=	Calu-3 (AIC)	=	hBEpC	=	A549
OAT2	16HBE14o-	=	Calu-3 (LCC)	=	Calu-3 (AIC)	=	hBEpC	=	A549
OAT3	16HBE14o-	=	Calu-3 (LCC)	=	Calu-3 (AIC)	=	hBEpC	=	A549
PEPT1	Calu-3 (LCC)	>	hBEpC	>	16HBE14o-	>	Calu-3 (AIC)	>	A549
PEPT2	Calu-3 (LCC)	>	hBEpC	>	16HBE14o-	>	Calu-3 (AIC)	>	A549

Table 2.7 Relative expression of SLC transporters. Transporters in blue are absent.

2.4.3 Expression analysis of SLCO transporters in human respiratory cell models

The organic anion-transporting polypeptides (OATP) are responsible for transport of a considerable number of endogenous solutes and xenobiotic compounds of diverse chemical nature. The expression of 9 OATP transporter genes in human respiratory epithelial cell models are summarised in table 2.8, 2.9 and figure 2.6. OATP1A2 (OATP-A) transcript we observed to be expressed only in the hBEpC, Calu-3 (day 15) and A549 cells using traditional PCR, but the RT^2 Profiler PCR Array revealed low expression in A549 ($2^{-\Delta Ct}$ = 0.002±0.001) and no detectable mRNA in 16HBE14o-, Calu-3 (LCC), Calu-3 (AIC) and hBEpC. Kullak-Ublick et al. [1995] have reported the RNA transcript for OATP1A2 in whole human lung.

	hBEpC	Calu-3 day 8	Calu-3 day 15	16HBE14o- day 11	16HBE14o- day 18	BEAS-2B	A549	Caco-2	Bleasby et al. 2006
OATP1A2	++	-	++	-	-	+	++	+++	-
OATP1B1	-	+++	+++	-	-	-	+	-	-
OATP1B3	-	++	+++	-	-	+	+	-	-
OATP1C1	-	++	++	-	-	-	+	-	-
OATP2A1	-	-	-	-	-	-	-	+++	+++
OATP2B1	-	+++	+++	-	-	-	+++	+++	++
OATP3A1	+++	+++	+++	++	++	++	+++	-	++
OATP4A1	++	++	++	++	++	+++	++	++	++
OATP5A1	-	+	-	-	-	+	+	-	-
β-actin	+++	+++	+++	+++	+++	+++	+++	+++	+++

Table 2.8 RT-PCR expression profile of selected SLCO transporters. SLCO transporter expression was examined in 8 cell culture models to examine relative pulmonary expression. mRNA signals were quantified according to gel electrophoresis band intensity. The Bleasby et al. [2006] column refers to the gene expression intensity in human whole lung tissue based on a reference set of 19,000 genes. n = 3 – 5 isolations

We found OATP3A1 and OATP4A1 transcripts to be expressed at moderate to high levels in all of the bronchial epithelial cell models OATP3A1: Calu-3 (LCC) ($2^{-\Delta Ct}$ = 0.037±0.023), Calu-3 (AIC) ($2^{-\Delta Ct}$ = 0.021±0.006) and hBEpC ($2^{-\Delta Ct}$ = OATP3A1 0.052±0.007), 16HBE14o- ($2^{-\Delta Ct}$ = 0.019±0.003); OATP4A1:

16HBE14o- ($2^{-\Delta Ct}$ = 0.068±0.023), Calu-3 (LCC) ($2^{-\Delta Ct}$ = 0.071±0.031) and Calu-3 (AIC) ($2^{-\Delta Ct}$ = 0.092±0.005) hBEpC ($2^{-\Delta Ct}$ = 0.004±0.000), as well as in the A549 cell line OATP3A1 ($2^{-\Delta Ct}$ = 0.020±0.003), OATP4A1 ($2^{-\Delta Ct}$ = 0.010±0.000). Both Adachi et al. (2003) and Tamai et al. (2001) reported RNA transcript for OATP3A1 (OATP-D) in whole human lung, and Tamai et al. (2001) the presence also of OATP4A1 (OATP-E). For OATP1B1, OATP1B3, OATP1C1, OATP2B1 transcripts a divergent pattern of expression was noted with Calu-3 cells expressing moderate to high levels of the above transcripts while all other bronchial cells displayed negligible expression; OATP1B1 A549 low ($2^{-\Delta Ct}$ = OATP1B1 0.001±0.000), 16HBE14o-, Calu-3 (LCC), Calu-3 (AIC) and hBEpC negative. OATP2B1 A549 Moderate ($2^{-\Delta Ct}$ = 0.011±0.000), 16HBE14o-, Calu-3 (LCC), Calu-3 (AIC) OATP2B1 and hBEpC negative, except in the case of OATP1B3, where a low level of this transcript in BEAS-2B was observed OATP1B3 low Calu-3 (LCC) ($2^{-\Delta Ct}$ = 0.001±0.001) and A549 ($2^{-\Delta Ct}$ = 0.004±0.001), 16HBE14o-, Calu-3 (AIC) and hBEpC negative. Both Kullak-Ublick et al. [2001] and Tamai et al. [2001] previously identified the presence of RNA transcript in whole human lung for OATP2B1 (OATP-B). We noted OATP5A1 was absent in the bronchial cell models except Calu-3 at day 8 and BEAS-2B where low levels of expression were evident.

OATP2A1 Moderate 16HBE14o- ($2^{-\Delta Ct}$ =0.015 0.008) and Calu-3 (AIC) ($2^{-\Delta Ct}$ = 0.011±0.004), hBEpC low ($2^{-\Delta Ct}$ = OATP2A1 0.001±0.000), Calu-3 (LCC) and A549 negative.

OATP1A2	A549	>	16HBE14o-	=	Calu-3 (LCC)	=	Calu-3 (AIC)	=	hBEpC
OATP1B1	A549	>	16HBE14o-	=	Calu-3 (LCC)	=	Calu-3 (AIC)	=	hBEpC
OATP1B3	A549	>	16HBE14o-	=	Calu-3 (LCC)	=	Calu-3 (AIC)	=	hBEpC
OATP2A1	16HBE14o-	>	Calu-3 (AIC)	>	hBEpC	>	A549	=	Calu-3 (LCC)
OATP2B1	A549	>	16HBE14o-	=	Calu-3 (LCC)	=	Calu-3 (AIC)	=	hBEpC
OATP3A1	hBEpC	>	Calu-3 (LCC)	>	Calu-3 (AIC)	>	A549	>	16HBE14o-
OATP4A1	Calu-3 (AIC)	>	Calu-3 (LCC)	>	16HBE14o-	>	A549	>	hBEpC

Table 2.9 Relative expression of SLCO transporters. Transporters in blue are absent.

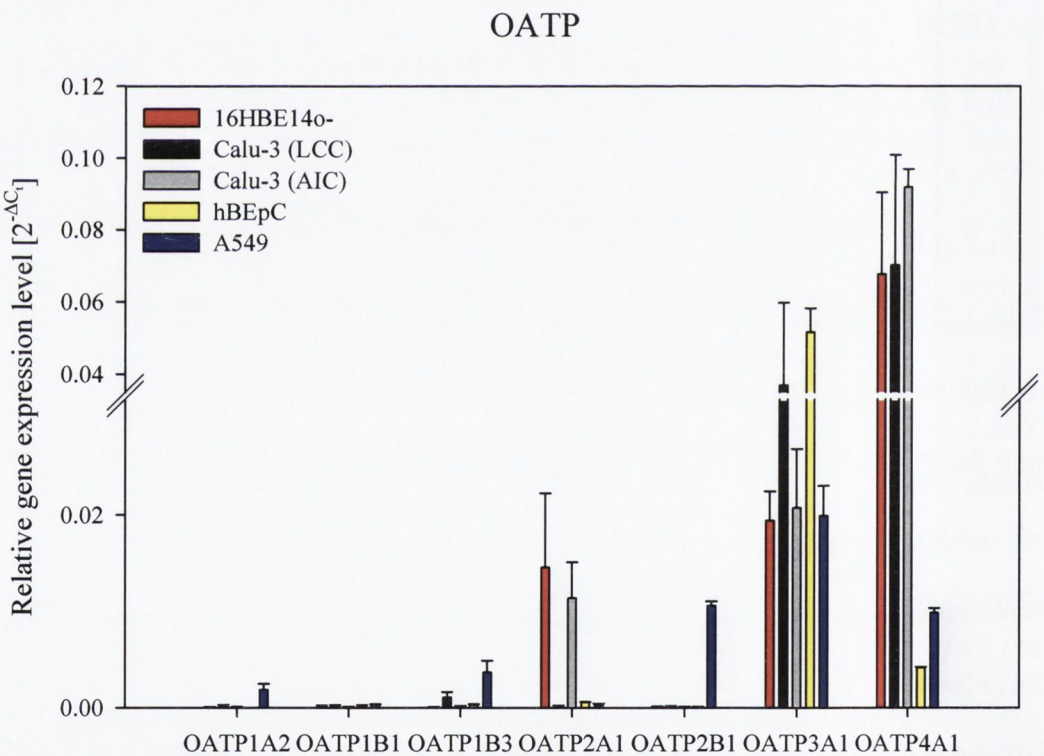

Figure 2.6 Relative gene expression levels of OATP transporters. Threshold cycles were calculated by instrument's software and normalised to β-actin. Data shown represents mean±SD from n = 3 experiments

2.4.4 Comparison to expression in Caco-2 cells

Several drug transporters have recently been investigated in Caco-2 cells on q-PCR level by others [Hilgendorf et al., 2007; Maubon et al., 2007]. When comparing the transporter expression between the intestinal Caco-2 cell line and the respiratory models characterised in this study, some pronounced differences were noted. While transcript expression and signal intensity of all investigated ABC transporters was generally comparable (with the exception of MRP8 which was absent in Caco-2, but present in the primary models as well as Calu-3 cells), earlier reports have found a significantly higher activity of the MDR1/P-gp efflux pump in Caco-2 cells, as measured by rhodamine 123 transport [Ehrhardt et al., 2003; Hamilton et al., 2001] (see also chapter 3). When looking at the SLC transporter data, Caco-2 showed comparatively stronger signals for PEPT1 and -2. Moreover, OCT2 and OAT1-3 transcripts were positively identified in Caco-2 cells, whereas they were absent in any of the respiratory models. The situation with regards to SLCO transporters is even more complex. OATP4A1 was the only transporter whose mRNA could be positively identified across all investigates specimens. OATP1A2 transcripts were strongly expressed in Caco-2 and at lower levels in hBEpC, Calu-3 (day 15), BEAS-2B and A549 with traditional PCR, but with the RT^2 Profiler PCR Array, this transporter was detectable only in A549. Signals for OATP1B1, 1B3, 1C1 and 5A1 were found in Calu-3, A549 and BEAS-2B (1C1 and 5A1 only), while none could be detected in Caco-2. The RT^2 Profiler PCR Array revealed absence of OATP1B1 in any cell model tested. We noted OATP2A1 transcript was completely absent in all the bronchial cell models as well as the A549 cell line, although positive expression was observed in the reference intestinal cell line Caco-2, whereas the situation was the absolute reverse for OATP3A1. OATP2B1

was strongly expressed in all adenocarcinoma-derived cell lines (i.e., Calu-3, A549 and Caco-2) but absent in all other models with traditional PCR, whereas with the RT^2 Profiler PCR Array OATP3A1 was detectable in all cells tested, but OATP2B1 only in A549.

2.5 Conclusions

The impact of active carrier mechanisms on the absorption and disposition of xenobiotics is now clearly recognised. Beyond this, of course, is an increasing awareness of the functional role that such carriers possess in the transport of endogenous molecules that serve as key modulators of cellular function. The value of *in vitro* cell-based models clearly has a role to fulfil in the study of mechanistic aspects of molecule membrane transport and indeed in the biopharmaceutical screening of candidates drug molecules [Ehrhardt and Kim, 2008]. In this study we sought to provide an analysis of key carrier transporters within a wide range of respiratory cell culture models commonly used in biopharmaceutics and indeed pharmacological research. Our results have revealed differential transporter expression throughout cell culture models from different regions of the lung and also highlighted disparities when comparing cell lines with primary cell culture models. Moreover, a number of variations regarding transporter expression in cell models of pulmonary compared to gastrointestinal origin were discovered. The data provided will help guide the use of particular respiratory cell models and also explain potential differences in results outcome. While our investigation provides an mRNA expression profile of many prevalent drug transporters in several

pulmonary cell models, a more extensive study of functional impact awaits examination.

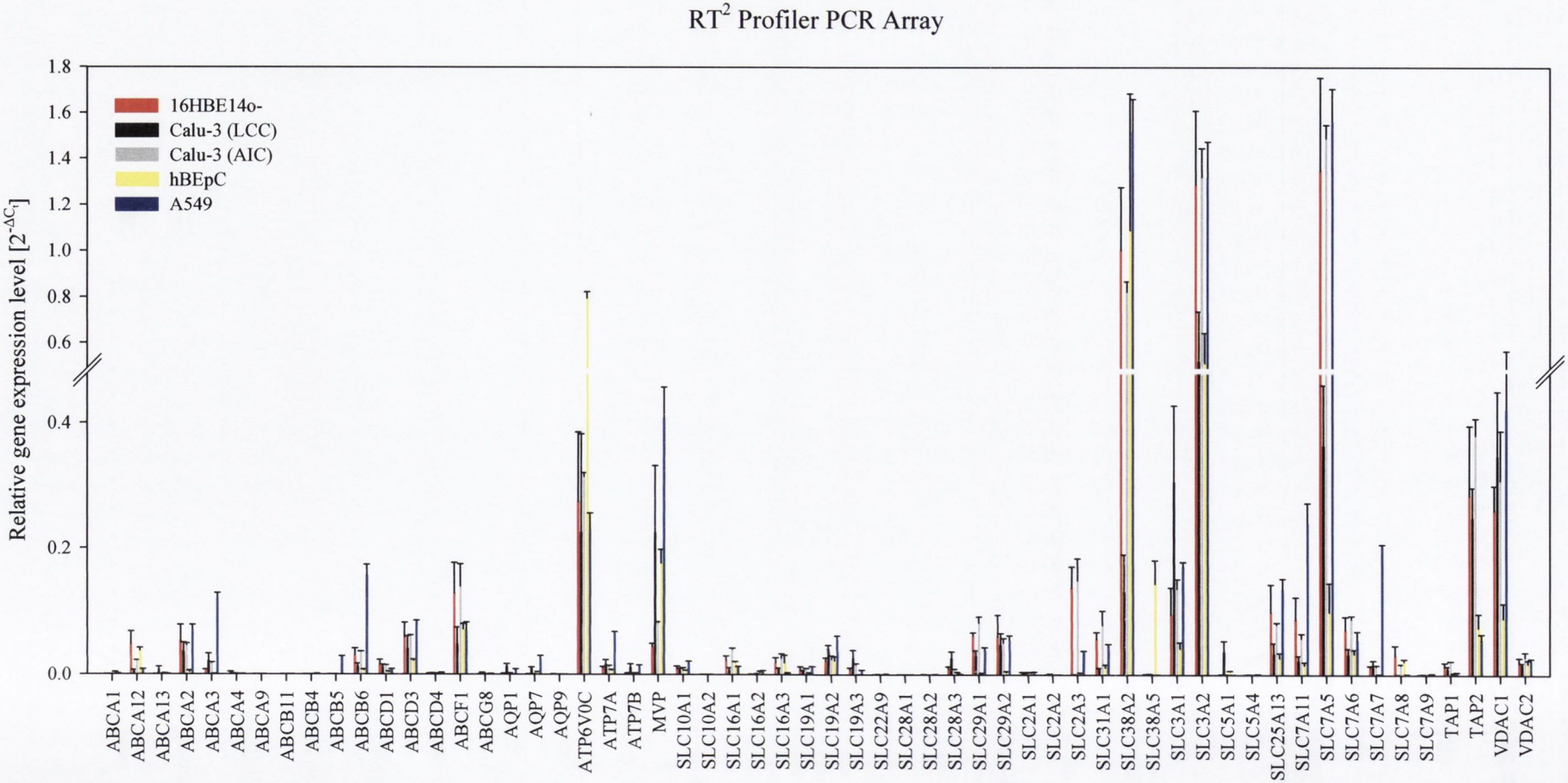

Figure 2.7 Relative gene expression levels of drug transporters. Threshold cycles were calculated by instrument's software and normalised to β-actin. Data shown represents mean±SD from n = 3 experiments.

3 P-glycoprotein (MDR1) functional activity in human alveolar epithelial cell monolayers

Parts of this chapter have been published. Endter, S., Becker, U., Daum, N,. Huwer, H., Lehr, C. M., Gumbleton, M., Ehrhardt, C. (2007). P-glycoprotein (MDR1) functional activity in human alveolar epithelial cell monolayers. Cell and Tissue Research **328**(1): 77-84

3.1 Abstract

The distribution of the MDR1 efflux transporter at mucosal barriers has defined it as a functionally important element in limiting drug absorption into the systemic circulation. However, little is known about the distribution and functionality of MDR1 in the human lung. Here, the presence of MDR1 was investigated immunohistochemically in distal human lung tissue and at mRNA and protein levels in human alveolar epithelial cells (hAEpC) in primary culture. We studied the presence and activity of MDR1 in hAEpC monolayers by Western blotting, by immunofluorescence microscopy and by conducting bi-directional transport studies employing a MDR1 substrate (rhodamine 123) with and without a MDR1 inhibitor (verapamil). The flux of fluorescein sodium was also examined as a paracellular transport marker. Alveolar tissue specimens showed MDR1 localised at the luminal membranes of type I pneumocytes. Reverse transcription-polymerase chain reaction revealed the presence of mRNA encoding for MDR1 in freshly isolated (i.e. type II) hAEpC and in monolayers of hAEpC cultured for 8 days (i.e. type I-like morphology). At the protein level, MDR1 could be detected in hAEpC monolayers after 8 days in culture but not in freshly isolated type II pneumocytes. The flux of rhodamine 123 across hAEpC monolayers on day 8 in culture exhibited net secretion, which disappeared in the presence of verapamil. Fluorescein sodium fluxes showed no distinct directionality. Our findings indicate that MDR1 is functionally active in the human alveolar airspace and that hAEpC monolayers might provide a suitable in vitro model for studying MDR1 function mechanistically in the distal human lung.

3.2 Introduction

Technical advances in inhaler device design and intrinsic barrier properties have made the lung an attractive route for the systemic delivery of drugs [Patton et al. 2004]. This is true not only for proteins and peptides whose bioavailability across other mucosal surfaces is often severely compromised, but potentially also for low molecular weight molecules, such as opiate analgesics, requiring the rapid onset of action [von Wichert and Seifart 2005].

As with other absorption barriers, the use of valid in vitro cell culture models of lung epithelium can impact significantly upon our understanding of the mechanisms of drug transport and absorption. In this context, cell lines have been screened for their suitability to serve as in vitro respiratory cell models [Florea et al. 2003; Foster et al. 1998] and, with the aim of preserving the differentiated phenotype of the original tissue, airway epithelial cell lines have been obtained by immortalisation [Ehrhardt et al. 2002, 2006; Manford et al. 2005]. Furthermore, protocols have been established for the isolation and primary cultivation of respiratory epithelial cells, from various lung zones across several species [Gruenert et al. 1995; Wise and Lechner 2002; Dobbs and Gonzales 2002]. The differing properties of respiratory cell cultures used within the pharmaceutical sciences have recently been reviewed [Forbes and Ehrhardt 2005; Steimer et al. 2005].

Of the surface area of the distal airspaces (i.e. alveoli), 95% comprises the alveolar epithelial type I pneumocyte, which not only serves as the tissue pathway for gaseous exchange, but is also the effective limiting barrier to solute movement between alveolar airspace and capillary blood. This epithelial barrier has to be capable of a wide range of functions including solute and ion transport, fluid

homeostasis and macromolecule uptake. With the lack of suitable continuous cell line models, primary alveolar cultures have dominated the study of alveolar epithelial biology and of solute and drug transport with significant progress in our understanding being gained through the use of primary cultures of rat alveolar epithelium [Kim et al. 2001; Chen et al. 2004].

Paralleling the approach used for primary rodent alveolar cultures, human alveolar epithelial type II cells can be isolated and, in culture, undergo transdifferentiation leading to the loss of the type II phenotype and the acquisition of the morphology and biochemical marker characteristics of type I cells. Elbert and co-workers [Elbert et al. 1999] have reported the optimal conditions for the primary culture of human alveolar epithelial cells (hAEpC) leading to the formation of an electrically tight monolayer displaying a highly restrictive paracellular pathway. Such a culture system represents a model suitable for examining aspects of drug absorption.

MDR1 is a member of the ATP binding cassette superfamily of membrane transport proteins mediating the efflux, across cell membranes, of a wide range of physico-chemically diverse solutes, including low molecular weight organic molecules and peptides [Stouch and Gudmundsson 2002]. MDR1 is constitutively present at a number of anatomic barriers and thus fulfils a critical role in limiting the absorption of pharmaceuticals. Previous immunohistochemical investigations of intact human tissue have shown MDR1 to be present in the epithelium of the conducting airways in lung [Cordon-Cardo et al. 1990; Lechapt-Zalcman et al. 1997] and one report provides evidence for the presence of MDR1 within intact alveolar epithelium [Campbell et al. 2003].

In order to characterise primary cultures of hAEpC further as a model system for pharmaceutical investigations, we have explored the presence of functionally active

MDR1 along human alveolar epithelial membranes and in primary cultures of human alveolar epithelial pneumocytes at various stages of transdifferentiation.

3.3 Materials and methods

3.3.1 Cell culture

Primary type II alveolar cells (ATII) were isolated from human non-tumour lung tissue obtained from patients undergoing lung resection. The use of human material for the isolation of primary cells was reviewed and approved by the local ethical committee (State Medical Board of Registration, Saarland, Germany). The isolation, purification and culture of hAEpC were carried out as published elsewhere [Elbert et al. 1999; Ehrhardt et al. 2005]. Briefly, the chopped tissue was digested with a combination of trypsin (Sigma, Deisenhofen, Germany) and elastase (Cell-Systems, St. Katharinen, Germany) for 40 min at 37°C. The ATII cell population was purified by a combination of differential cell attachment, Percoll density gradient centrifugation and magnetic cell sorting with CD326-MicroBeads (Miltenyi Biotec, Bergisch-Gladbach, Germany). The isolated ATII cells were seeded at a cell density of 6×10^5 cells/cm^2 on collagen/fibronectin-coated polyester filter inserts (Transwell Clear, 6.5 mm in diameter, 0.4 µm pore size; Costar, Bodenheim, Germany) by using small airways growth medium (SAGM, CellSystems) containing penicillin (100 U/ml, Sigma), streptomycin (100 µg/ml, Sigma) and 1% foetal bovine serum (FBS; Greiner, Frickenhausen, Germany). Under these culture conditions, generally more than 90% of the cultures grew to confluent monolayers with type I-like morphology by 8 days in culture [Fuchs et al. 2003; Demling et al. 2006].

3.3.2 Bioelectric measurements

The time of the cellular layers reaching confluence was determined by measuring transepithelial electrical resistance (TEER) as a function of days in culture. TEER was measured daily with an epithelial volt-ohm-meter equipped with STX-2 "chopstick" electrodes (WPI, Berlin, Germany) and corrected for the background value contributed by the Transwell Clear filter and medium.

3.3.3 Immunohistochemical localisation of MDR1 in intact normal lung tissue

Human lung tissue for immunohistochemistry comprised archival formalin-fixed human lung specimens exhibiting normal morphology and embedded in paraffin wax (obtained from the Department of Histopathology, Cardiff, UK). The paraffin wax sections (5 μm) were mounted on Superfrost microscope slides (Shandon, Cheshire, UK). Following removal of the paraffin from the mounted sections, endogenous peroxidase activity within the rehydrated sections was blocked with 0.6% hydrogen peroxide in methanol for 15 min at room temperature. The slides were then briefly washed in tap water before each section was equilibrated in Optimax wash buffer (pH 7.4; Menerium Diagnostics, Oxford, UK) at room temperature for an additional 10 min. After drainage of the slides, the P-gp monoclonal antibody (JSB-1; ID Labs, Glasgow, UK), which was diluted 1:10 in 0.6% bovine serum albumin (BSA) in Optimax wash buffer, was applied to each section and incubated overnight (15 h) at 4°C within a humidified slide chamber. The following day, the slides were washed to remove unbound primary antibody and a goat anti-mouse secondary horseradish-peroxidase-conjugated antibody

(diluted 1:100; Dako, High Wycombe, UK) was then applied for 1 h at room temperature. Immunoreactivity was subsequently detected by using the 3,3'-diaminobenzidine system (Sigma, Poole, Dorset, UK). The sections were counterstained with haematoxylin and finally mounted. Images were captured by using an Olympus BX 41 microscope fitted with a Color View 12 camera and equipped with AnalySIS software (Norfolk Analytical, UK).

3.3.4 RNA isolation and reverse transcription/polymerase chain reaction

The mRNA primer sequences were aligned with BLAST 2:

- http://www.ncbi.nlm.nih.gov/blast/bl2seq/wblast2.cgi

To identify exons within genes, SNPper was employed

- http://snpper.chip.org

Exons present in all transcription variants and of suitable size were validated by using Primer3:

- http://frodo.wi.mit.edu/cgi-bin/primer3/primer3_www.cgi

Primer sequences used in this study are given in Table 3.1. The polymerase chain reaction (PCR) was performed with cells from three different isolations. Briefly, total RNA was isolated and purified from cells with an RNeasy mini kit (Qiagen, Hilden, Germany) according to the manufacturer's instructions. Reverse transcription-PCR (RT-PCR) amplification of total RNA was carried out by using first-strand cDNA generated with an Omniscript kit (Qiagen). The cDNA was initially amplified with $Pd(N)_6$ random hexamers (Amersham, Chalfont St. Giles, UK). Samples of 40 ng RNA were used for each PCR run with a BIOTAQ Core kit

(Bioline, London, UK) including 0.75 µl 25mM $MgCl_2$, 1 µl 2.5 mM dNTP Mix, 1.25 µl Taq buffer, 0.1 µl Taq polymerase, 10 pmol primer (forward and reverse) and diethylpyrocarbonate-treated water up to a volume of 12.5 µl. The following program was applied to all samples: 5 min at 94°C followed by 35 cycles of 30 s at 94°C for denaturing, 45 s at 60°C for annealing primers to sequences and 45 s at 72°C to allow the Taq polymerase to copy the desired sequences. After the last cycle, an additional step of 10 min at 72°C with the Taq polymerase completed any unfinished regions. DNA fragments were separated by 2% agarose gel electrophoresis and visualised by ethidium bromide staining. A HyperLadder IV size marker (Bioline) was run in parallel. Electrophoresis was carried out at 90 V for 45 min.

The RT^2 Profiler PCR Array (chapter 2) was not on the market at time of publication of contents in this chapter. Therefore, self designed primers were used.

Primer		Sequence	Amplicon size
MDR1	Forward	5′ CAC CTG CAT TGT GAT TGC TC 3′	174 bp
	Reverse	5′ AGA GTT CAC TGG CGC TTT GT 3′	
β-actin	Forward	5′ AAA CTG GAA CGG TGA AGG TG 3′	171 bp
	Reverse	5′ AGA GAA GTG GGG TGG CTT TT 3′	

Table 3.1 Primer sequences for PCR (identical to primers used in chapter 2)

3.3.5 Immunofluorescence microscopy

The mouse monoclonal anti-MDR1 antibody (clone F4, Sigma) was diluted 1:100 in PBS containing 1% (w/v) BSA (Sigma). Mouse IgG1 (clone MOPC-21; Sigma) was used as an isotypic control. hAEpC monolayers grown on Transwell filters

were stained on day 8 after cell plating. Cells were fixed for 10 min with 2% (w/v) paraformaldehyde and blocked for 10 min in 50 mM NH_4Cl, followed by permeabilisation for 8 min in 0.1% (w/v) Triton X-100. After a 60-min incubation with 100 µl diluted primary antibody, the cell monolayers were washed three times with PBS before incubation with 100 µl Alexa Fluor 488- labelled goat anti-mouse $F(ab)_2$ fragment (Invitrogen, Karlsruhe, Germany) diluted 1:100 in PBS containing 1% (w/v) BSA. Propidium iodide (1 µg/ml) was then added to counterstain cell nuclei. After 30-min incubation, the specimens were washed three times with PBS and embedded in FluorSave anti-fade medium (Calbiochem, Bad Soden, Germany). Images were obtained by means of a confocal laser scanning microscope (MRC 1024, Bio-Rad, Hemel Hempstead, UK) with the instrument settings adjusted so that no positive signal was observed in the channel corresponding to the green fluorescence of the isotypic controls.

Acknowledgement: The corresponding image (figure 3.3) was kindly provided by Dr. Carsten Ehrhardt.

3.3.6 Western blotting

Western blotting was performed on hAEpC directly after isolation or after 8 days in culture on polyester filter inserts; Caco-2 cells served as a positive control. Protein concentrations were determined with a bicinchoninic acid protein assay kit (Sigma) with BSA as a standard. Samples were normalised to equal protein concentrations and loaded (30 µg/lane) onto 6% SDS-gel for MDR1 and 12% SDS-gel for D-glyceraldehyde-3-phosphate dehydrogenase (GAPDH; as an internal control). The SDS-gel was electrophoresed at 100 V for 2 h and then the bands were transferred

onto cellulose nitrate membranes (Protran BA85; Schleicher&Schuell, Dassel, Germany) at 48 V for 2 h. Loading efficiency was tested by Ponceau staining (Sigma, Germany). Blots were blocked for non-specific binding by overnight incubation (4°C) in PBS containing 0.1% Tween 20 and 10% non-fat milk (blocking buffer). The cellulose nitrate membranes were then incubated with mouse monoclonal anti-P-gp antibody (Clone F4, Sigma; diluted 1:1,000 in blocking buffer) or mouse monoclonal anti-GAPDH antibody (Chemicon, Chandlers Ford, UK; diluted 1:1,000 in blocking buffer), respectively, for 90 min at room temperature. The membranes were washed once with PBS and twice with PBS containing 0.1% Tween 20, followed by one wash with PBS, and were then incubated for 90 min at room temperature with alkaline phosphatase (AP)-conjugated goat anti-mouse IgG secondary antibody (Promega, Mannheim, Germany; 1:7,500 in blocking buffer). The membranes were rinsed again in PBS and in PBS containing 0.1% Tween 20 according to the washing procedure after the primary antibody incubation. Stained bands were detected via the nitroblue tetrazolium/5-bromo-4-chloro-3-indolyl-phosphate assay (Roche Diagnostics, Mannheim, Germany).

Note: Change of standart (from β-actin to GAPDH) was due to supply by host lab (Saarland University, Department of Biopharmaceutics and Pharmaceutical Technology, Saarbrücken, Germany) where this study has been performed.

Acknowledgement: The corresponding image (figure 3.4) was kindly provided by Dr. Nicole Daum.

3.3.7 Transport studies

Transport experiments were conducted on hAEpC monolayers cultured for 8 days on Transwell filters. Both sides of the cell layers were washed twice with pre-equilibrated bicarbonated Krebs-Ringer solution (KRB) composed of 15 mM HEPES, 116.4 mM NaCl, 5.4 mM KCl, 0.78 mM NaH_2PO_4, 25 mM $NaHCO_3$, 1.8 mM $CaCl_2$, 0.81 mM $MgSO_4$, and 5.55 mM glucose, pH 7.4. The monolayers were then placed in new cluster plates containing 800 µl pre-warmed KRB (37°C) per well. In MDR1 inhibition experiments, verapamil at 50 µM was present both in donor and receiver solutions to ensure the continued inhibition of the MDR1 efflux pump. After a 60-min equilibration with KRB, transport of either fluorescein sodium (FluNa, MW 376.3, Sigma) or the known MDR1 substrate, rhodamine 123 (Rh123, MW 380.8, Sigma), was initiated by replacing the fluid in the donor chamber with KRB containing 50 µM of the respective fluorophore. The apical and basolateral fluid volumes were 220 µl and 820 µl, respectively. The initial concentration in the donor fluid was assayed by drawing a 20-µl sample immediately after the initiation of the flux studies. The cell layers were agitated by an orbital shaker at a constant stirring rate (100 rpm) at 37°C during transport experiments. Samples (100 µl) were drawn serially from the receiver compartment at 30, 60, 120, 180 and 240 min. After each sampling, fresh transport buffer of an equal volume was returned to the receiver side to maintain a constant volume. At the end of the transport experiment, a 20-µl sample was drawn from the donor fluid and assayed for its activity. Each experiment was performed on a total of 12 cell layers from three different isolations. In order to assess the integrity of cell layers during the transport studies, TEER was measured before and after each experiment.

Flux (J) was determined from steady-state appearance rates of FluNa and Rh123 in receiver fluid. The apparent permeability coefficient, P_{app}, was calculated according to the equation

$$P_{app} = J / (A \times C_i)$$

where C_i was the initial concentration of the drug under investigation in the donor fluid and A the nominal surface area of cell layers (0.33 cm^2) utilised in this study. The fluorescence of the samples was analysed in 96-well plates in a fluorescence plate reader (Cytofluor II, PerSeptive Biosystems, Wiesbaden, Germany) at excitation and emission wavelengths of 485 and 530 nm, respectively. These samples were diluted with KRB, where appropriate.

3.3.8 Statistical analysis

Results are expressed as mean±SD. Significance ($P<0.05$) of differences in the group mean values for TEER and P_{app} were determined by two-way analysis of variances, followed by Student-Newman-Keuls post-hoc tests.

3.4 Results

3.4.1 MDR1 at the mRNA level

mRNA was extracted from both freshly isolated ATII cells and cell monolayers that showed an ATI-like phenotype after 8 days in culture on Transwell filters. Figure 3.1 shows representative gels of PCR amplicons of MDR1 mRNA. Both cell populations showed a clear positive signal that did not appear to change over

time in culture between day 1 and day 8, as far as this could be interpreted from the semi-quantitative approach used in this study.

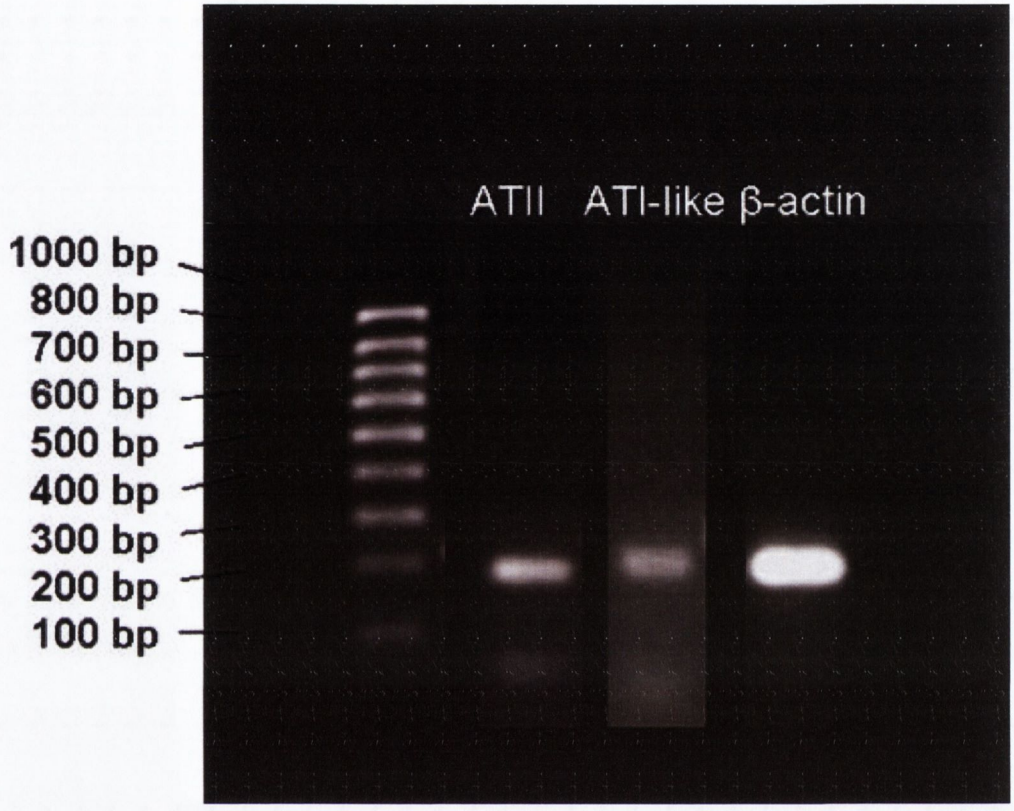

Figure 3.1 Analysis of MDR1 expression in human alveolar epithelial cells (hAEpC) on various days of primary culture by reverse transcription-polymerase chain reaction (RT-PCR). The results of RTPCR for MDR1 (left to right) in freshly isolated cells (lane 2, ATII) and in cells cultured for 8 days (lane 3, ATI-like) are shown (lane 1 molecular weight standards); β-actin (lane 4) was used as an internal standard. The bands for the MDR1 amplicons are located on the gel at a position consistent with the expected size of 174 bp. The time course reveals similar expression levels for MDR1 in freshly isolated cells and cells after 8 days of culture.

3.4.2 MDR1 at the protein level

Immunohistochemical staining for MDR1 was performed in normal human lung tissue (figure 3.2). Immunostaining for MDR1 was observed across the entire alveolar epithelial surface membrane, with staining clearly present at the apical surface of the type I alveolar epithelial cells. Negative control sections were run in parallel (antibody omission or replacement of primary antibody with an isotypic IgG_{2a} antibody); no staining was observed in any of these control sections.

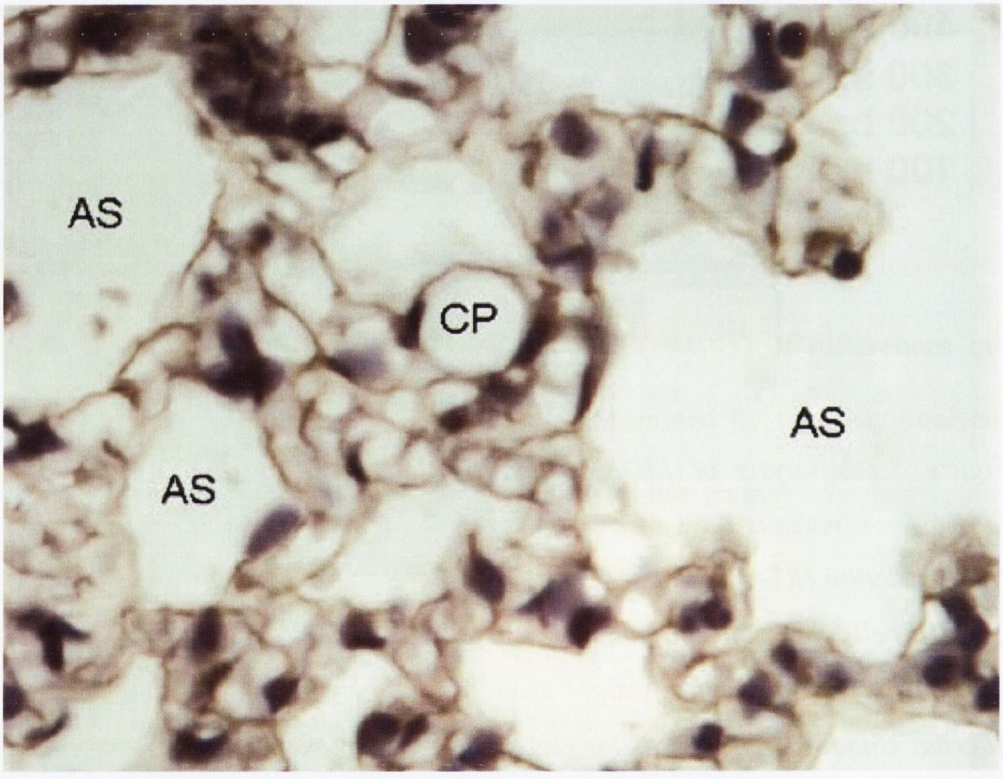

Figure 3.2 Normal human lung tissue; immunohistochemical staining for MDR1 was observed across the entire alveolar epithelial surface membrane, with staining clearly present at the apical surface of the type I alveolar epithelial cells (CP capillary, AS alveolar airspace).

Immunofluorescence confocal laser scanning microscopy was performed to confirm the presence of MDR1 in monolayers of hAEpC after 8 days in culture on Transwell filters. As shown in figure 3.3, the hAEpC monolayers exhibited a strong signal for MDR1, which was located predominantly at the apical plasma membranes.

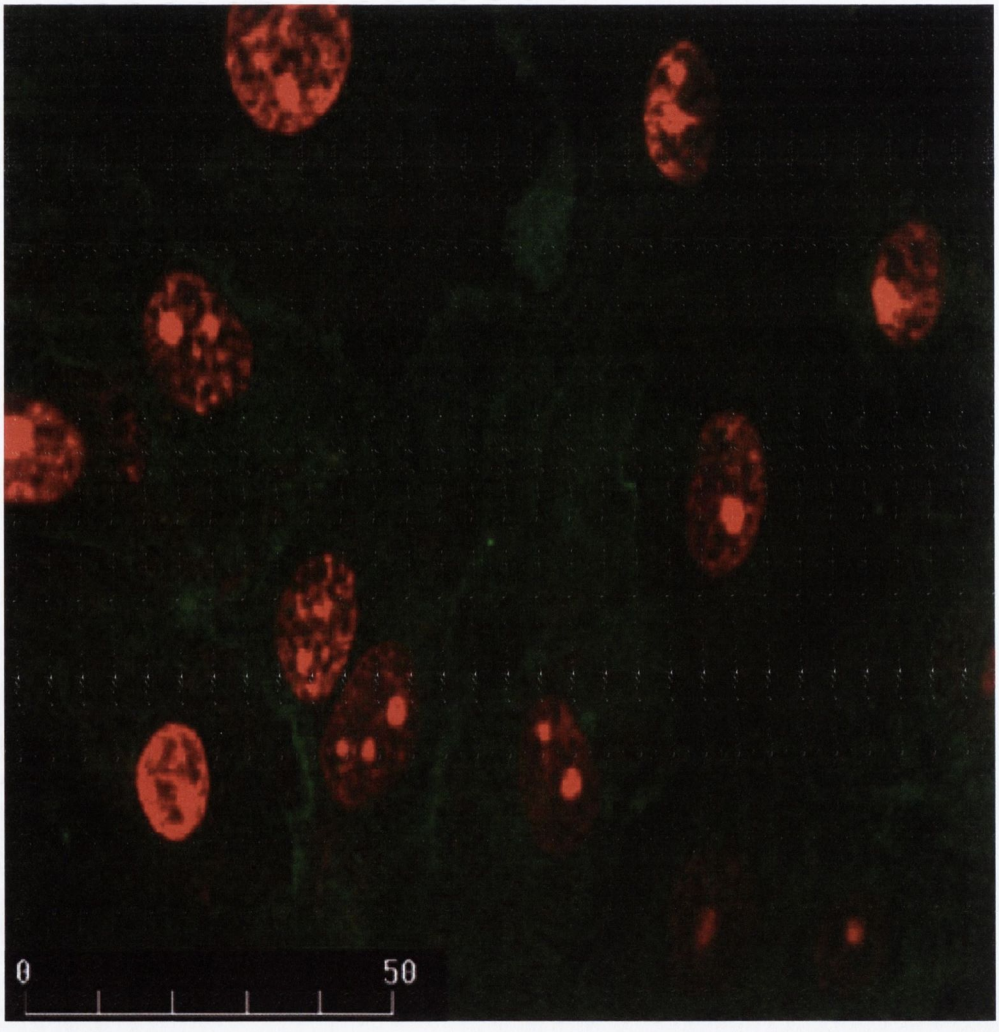

Figure 3.3 Immunolabelling of MDR1 in hAEpC monolayers grown on Transwell filters for 8 days in primary culture. Cells were plated at a density of 6×10^5 cells/cm^2 and cultured under liquid. Staining for MDR1 (green) is shown by confocal laser scanning microscopy. Nuclei were counterstained with propidium iodide (red). Bar 50 μm

By means of immunoblotting, MDR1 was investigated in freshly isolated ATII cells and in hAEpC monolayers after 8 days in culture. Figure 3.4 shows a representative Western blot. Whereas a strong signal at 170 kDa was observed for the positive control (Caco-2 cell line), weaker band(s) that were consistent with the MDR1 weight range were found for the ATI-like cells at day 8. However, only a faint band was seen in freshly isolated ATII cells.

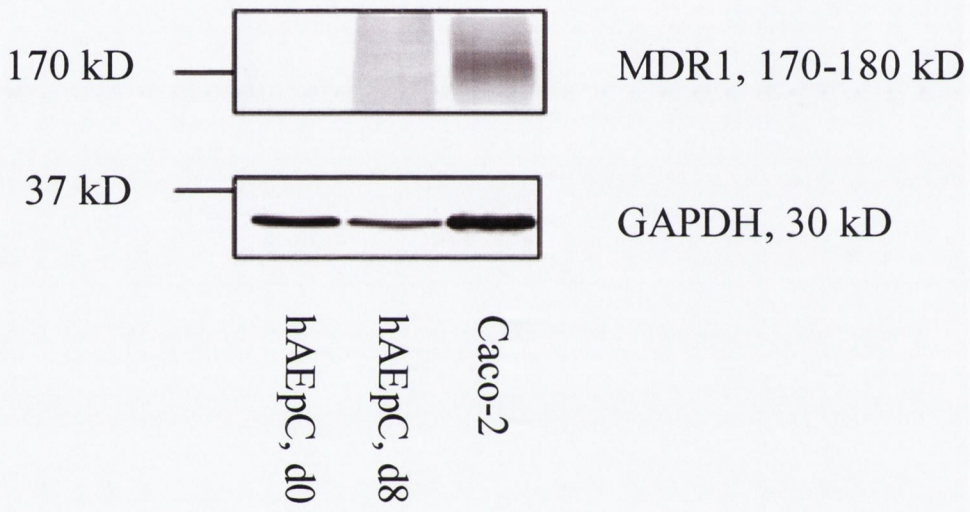

Figure 3.4 Western blot for MDR1 in hAEpCs after various times in culture. Caco-2 cell lysate was used as a positive control; D-glyceraldehyde-3-phosphate dehydrogenase (GAPDH) was employed as an internal control. A band of 170 kDa was detected in Caco-2 cells, whereas the signal was markedly weaker for hAEpC after 8 days in culture (hAEpC, d8; ATI-like phenotype). The signal obtained with lysate from freshly isolated ATII cells was almost undetectable (hAEpC, d0)

3.4.3 Transport studies

A significantly ($P<0.05$) higher P_{app} at $(4.35\pm2.15) \times 10^{-6}$ cm/s (n=12) for Rh123 was observed in the secretory (i.e. basolateral-to-apical) direction (figure 3.5), which was significantly reduced by 55% in the presence of verapamil. The permeability of Rh123 in the apical-to-basolateral direction was $(1.41\pm0.78) \times 10^{-6}$ cm/s (n=12), which was increased by 92% in the presence of verapamil. The secretion/absorption-ratio for Rh123 across hAEpC monolayers was 3.09, comparable to a value of 2.95 calculated for 16HBE14o- human bronchial epithelial cell layers, whereas it was 4.80 in 3-week-old Caco-2 cells under similar experimental conditions (Ehrhardt et al. 2002). The P_{app} value of the paracellularly transported FluNa across hAEpC monolayers showed no significant ($P<0.05$) differences in transport direction (figure 3.5). The respective P_{app} values were $(1.04\pm0.16) \times 10^{-7}$ cm/s (n=12) in the secretory direction and $(1.21\pm0.19) \times 10^{-7}$ cm/s (n=12) in the absorptive direction. These values were approximately eight times higher than those previously reported for the 16HBE14o- cell line, with TEER values of ~4 times higher being found for the hAEpC monolayers ($2493\pm876\ \Omega\times cm^2$, n=60 versus $671\pm133\ \Omega\times cm^2$, n=60; [Ehrhardt et al. 2002]).

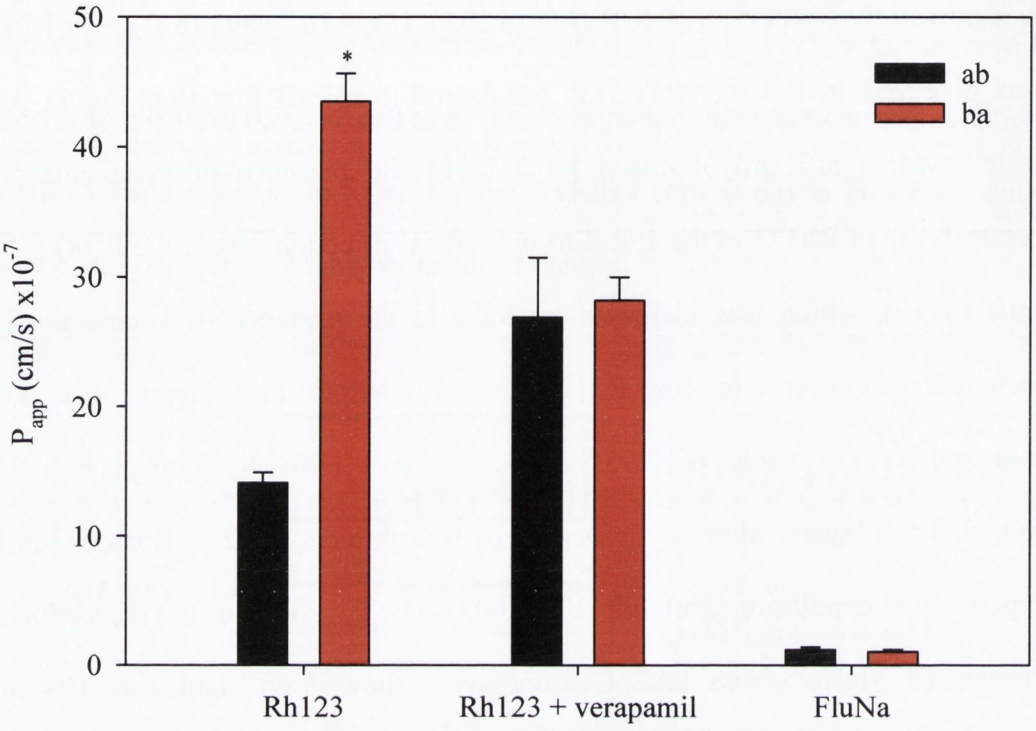

*Figure 3.5 Permeability of rhodamine (Rh123) and fluorescein sodium (FluNa) across monolayers of hAEpC after 8 days of primary culture. Cell layers were cultured on Transwell Clear filters and bi-directional transport studies in apical-to-basolateral (ab, black bars) and basolateral-to-apical (ba, red bars) directions were carried out. Net secretion was found for Rh123, which disappeared in the presence of the MDR1 inhibitor verapamil. FluNa transport showed no significant directionality. Data represent mean±SD (n = 12). *Significantly different from the Rh123 flux measured in the ab direction*

3.5 Discussion

This is the first investigation of functional MDR1 in an in vitro model of primary monolayer cultures of hAEpC. We have confirmed, by RT-PCR, the presence of MDR1 mRNA transcripts in cultured human pneumocytes as they develop into an ATI-cell-like phenotype. By immunofluorescence microscopy, we have also confirmed that MDR1 protein in the cells is localised predominantly at the luminal membranes. These data are in agreement with immunohistochemical staining for MDR1 performed in normal human lung tissue and resulting in a positive signal at luminal membranes of ATI cells. Furthermore, Western blot has revealed the presence, although relatively low, of MDR1 protein in the primary hAEpC at day 8 of culture. For the Western blot, we used a specific monoclonal antibody against MDR1 and demonstrated, as others have found [Kennedy and Mangini 2002; Mi et al. 2001], the presence of multiple bands for MDR1 (especially evident with lower protein quantities). These bands are consistent with the wide and varied reports for MDR1 migration (and hence molecular weight) on Western blots (from 150 to 200 kDa; [Greiner et al. 1999; Demeule et al. 2000, 2001; Hamilton et al. 2001; Axiotis et al. 1995]) and with the observed single or multiple bands that are probably dependent upon the varied glycosylation products of this protein. The antibody recognizes an epitope located at the third extracellular loop of the molecule. Digestion of this domain by trypsin during the isolation process could explain the marginal detection in freshly isolated cells.

In addition, we have found that the transport of rhodamine-123 (a MDR1 substrate) across the confluent hAEpC monolayers is polarised, with the basal-to-apical flux being approximately three to four times greater than the apical-to-basal flux.

Although different MDR1 substrates have been investigated, this polarised flux ratio across the human monolayers is of the same magnitude as that reported by Campbell et al. [2003] who have examined functional MDR1 within primary rat alveolar epithelial cell monolayers by using vinblastine as the transport probe.

This study provides further support for the presence and activity of MDR1 within the alveolar epithelium and for its physiological role at this barrier, not only by serving as an efflux pump available for the extrusion of potentially harmful inhaled xenobiotics and environmental pollutants, but probably also by being involved in other functions, such as the regulation of ion transport [Higgins 1995] or phospholipid homeostasis [Abulrob and Gumbleton 1999; Bosch et al. 1997]. In addition, the establishment of the functional presence of MDR1 in human alveolar monolayer cultures should allow their further characterisation and provides support for their value in addressing pharmaceutical or basic biological questions.

4 Characterisation of organic cation transporters in human lung epithelial cell models

4.1 Abstract

The influence of transporter proteins on uptake of inhaled cationic drugs is hardly understood. To find the suitable model for investigations in this area, selected cell lines and a primary bronchial epithelium model were examined regarding protein expression and activity of organic cation transporters. Immunofluorescence microscopy confirmed the presence of OCT1, OCT3, OCTN1 and OCTN2 in all cell models tested with highest expression of OCTN1 and OCTN2 in Calu-3 (AIC). Uptake of the cationic fluorophore 4-[4-(dimethylamino)-styryl]-N-methylpyridinium (ASP^+) was characterized. A549 revealed the fastest uptake and Caco-2 the highest saturation limit, whereas uptake into Calu-3 and 16HBE14o- appeared to be much slower and earlier saturable. The primary model hBEpC showed relatively fast uptake with early saturation. The uptake of ASP^+ was pH and sodium dependent in A549 and pH dependent in Calu-3. L- and D- carnitine did not reduce uptake in any cell model tested. Inhibition by formoterol, amantadine and verapamil was of significance in A549 only. Additionally tested in A549, salmeterol did inhibit the uptake of ASP^+ significantly, whereas budesonide and beclomethasone did not demonstrate any effect. Bi-directional transport studies revealed net secretion with Calu-3 and net absorption with 16HBE14o-, whereas hBEpC did not show any directed transport.

4.2 Introduction

The majority of inhaled drugs, such as bronchodilators, are positively charged at physiologic pH. The preferred uptake route of larger charged molecules is transporter or vesicle driven rather than by diffusion. During recent years the role of transporters in drug uptake has been studied. Whereas the importance of PEPT1 and PEPT2 to uptake of peptides has been demonstrated in the lung, interests in the high potential of organic cation transporter of the solute carrier family 22 (SLC22) are preferably focused on other organs. The electrogenic cation uniporters OCT1, OCT2 and OCT3 as well as the cation and carnitine transporters OCTN1 and OCTN2, have been shown to play an important role in absorption and secretion of cationic drugs and metabolites in human intestine, liver and kidney [Koepsell 2007] (figure 1.11-1.13). To date, there is no sufficient knowledge of the influence of organic cation transporters on absorption or secretion in the lung. Utilising the potential of these transporters can lead to a higher effectiveness of pulmonary drug transport. Initial studies using cell culture models can provide a first impression on the capability of this route. Recently, the active uptake of salbutamol across airway epithelium [Ehrhardt et al. 2005] and inhibition of uptake by OCTN2 [Horvath et al. 2007] have been reported. Further studies need to show the full potential of these transport proteins.

4.3 Materials and Methods

4.3.1 Cell culture

Human A549

(American Type Culture Collection, ATCC CL-185 LGC Promochem, Teddington Middlesex, UK). Cells were cultured on 24-well plates (Corning, Schiphol, The Netherlands) for uptake studies and on 6-well plates (Corning) for FACS using a seeding density of 40,000/cm^2 with Dulbecco's modified Eagle's medium (DMEM, 10% FBS, 100 U/ml penicillin and 100 µg/ml streptomycin) exchanged every 48 h. Monolayers reached confluence by day 5 of culture at which time cells were used.

Human Calu-3 (ATCC HTB-55)

Cells of the human bronchial epithelial cell line derived from an adenocarcinoma of the lung were seeded at a density of 75,000 cells/cm^2 on 24-well plates (Corning), for uptake studies, on Transwell inserts (0.4µm pore size 12mm membrane diameter, Corning), for immunofluorescence microscopy and transport studies and on Transwell inserts (24mm membrane diameter, Corning) for FACS. Cells were maintained in culture for 12 days using DMEM (10% FBS, 100 U/ml penicillin and 100 µg/ml streptomycin).

Human 16HBE14o-

Cells were seeded at 100,000 cells/cm^2 on 24-well plates (Corning), for uptake studies, on Transwell inserts (12mm membrane diameter, Corning), for immunofluorescence microscopy and transport studies and on Transwell inserts

(24mm membrane diameter, Corning) for FACS. They were cultured in Eagle's minimum essential medium (MEM, 10% FBS, 100 U/ml penicillin and 100 µg/ml streptomycin, 1 mM sodium pyruvate and non essential amino acids) for 8 days.

Human bronchial epithelial cells (hBEpC)

Clonetics human bronchial/tracheal epithelial cells (NHBE) CC-2541 were supplied by Lonza (Walkersville, MD, USA) and cultured in bronchial epithelial cell growth medium (BEGM, Lonza) or a mix of BEGM/DMEM-F12 (50/50) for 7 days until confluence for uptake studies, for 12 days on Transwell inserts (12mm membrane diameter, Corning), for immunofluorescence microscopy and transport studies and on Transwell inserts (24mm membrane diameter, Corning) for FACS.

Human colonic adenocarcinoma cells (Caco-2)

Caco-2 were obtained from the European Collection of Animal Cell Cultures (ECACC, Salisbury, UK) and used as a reference cell line for expression studies [Sun et al., 2008]. The cells were cultured for 21 days on 24-well plates (Corning), for uptake studies, and Transwell inserts (12mm membrane diameter, Corning), for immunofluorescence microscopy, respectively, with exchange of media (DMEM, 10% FBS, 100 U/ml penicillin and 100 µg/ml streptomycin) every 48 h.

4.3.2 Protein Expression

Immunofluorescence microscopy

Cells were fixed for 10 min with 2% (w/v) paraformaldehyde and blocked for 10 min in 50 mM NH_4Cl, followed by permeabilisation for 8 min in 0.1% (w/v) Triton X-100. After a 60-min incubation with 100 µl goat polyclonal anti-OCT1, anti-OCT2, anti-OCT3, anti-OCTN1 and anti-OCTN2 primary antibodies (2 µg/ml, Santa Cruz, Santa Cruz, USA), the cell monolayers were washed three times with PBS before incubation with 100 µl Alexa Fluor 488-labelled $F(ab')_2$ fragment of rabbit anti-goat IgG (H+L) (Invitrogen, Karlsruhe, Germany) 2 µg/ml in PBS containing 1% (w/v) BSA. 4',6-diamidino-2-phenylindole dihydrochloride (DAPI, 1 µg/ml) or propidium iodide (1 µg/ml) were added to counterstain cell nuclei. After 30 min incubation, the specimens were washed three times with PBS and embedded in FluorSave anti-fade medium (Calbiochem, San Diego, CA). Images were obtained on a confocal laser scanning microscope (Zeiss Axiovert 200, Göttingen, Germany).

Propidium iodide was the preferred method to counterstain cell nuclei. Due to a software problem of the microscope, it had to be replaced by 4',6-diamidino-2-phenylindole dihydrochloride (DAPI, 1 µg/ml). Additionally, an inconsistancy in scales of images was observed. After correction of the defects propidium iodide was used and different scales were displayed.

Fluorescence activated cell sorting (FACS)

After washing three times with PBS, cells were transferred into microcentrifuge tubes using Accutase (Sigma). Cells were washed twice and re-suspended in FACS

Buffer (FB: PBS + 0.1% NaN_3 + 5% FBS). An equal amount of Reagent A (100-150 µl) was added to each sample. After incubation in the dark at room temperature for 15 minutes, the samples were washed twice with FB and re-suspended in 50µl of a solution of primary antibody in reagent B (1:300). The samples were incubated in the dark at room temperature for 15 minutes, washed twice with FB and re-suspended in 100 µl of secondary antibody (Alexa Fluor 488-labelled F(ab')2 fragment of rabbit anti-goat IgG (H+L)) in FB (1:200). After incubation in the dark at room temperature for 20 minutes, the samples were washed three times with FB and re-suspended in FB. Samples were analysed using a FACSCalibur (BD, Swindon, UK). Two controls were used – FB and secondary antibody in FB (1:200).

Protein quantification

Cells were washed with PBS and lysated using extraction buffer (40 µl/cm^2) (BioSciences) supplemented with proteinase inhibitors 60 µg/ml aprotinin and 1 µg/ml leupeptin (Sigma) followed by collection of cells with a cell scraper and treatment with ultrasound. Samples were spun down to use the supernatant for further steps. 10 µl of sample were mixed with 200 µl of a filtered 1:5-dilution of dye reagent concentrate (Bio-Rad Protein Assay, Bio-Rad, Hercules, CA). After incubation of 10 min at room temperature, absorbance at 595 nm was measured with a FLUOstar OPTIMA fluorescence plate reader. Concentration was calculated using bovine serum albumin standards for a calibration curve.

4.3.3 Functional studies

Bioelectric measurements

TEER was measured every 48 h with an epithelial Volt-Ohm-meter equipped with STX-2 "chopstick" electrodes (WPI, Berlin, Germany) and corrected for the background value contributed by the Transwell Clear filter and medium.

Uptake studies

Uptake of organic cationic compounds measurements was carried out with the fluorophore 4-[4-(dimethylamino)styryl]-N-methylpyridinium iodide (ASP^+). Cells were grown on 24-well plates (Greiner, Stonehouse, UK). Initially, the time course of ASP^+ uptake during 90 min was assessed. Each well was exposed to 1 ml 10 µM ASP^+ in Krebs Ringer Buffer (KRB) containing 15 mM HEPES, 116.4 mM NaCl, 5.4 mM KCl, 0.78 mM NaH_2PO_4, 25 mM $NaHCO_3$, 1.8 mM $CaCl_2$, 0.81 mM $MgSO_4$, and 5.55 mM glucose with pH 7.4. Active transport was stopped by washes with ice-cold KRB and ASP^+ was released from cells by incubation with 1% Triton X-100 (Sigma). Fluorescence of ASP^+ was quantified with an OPTIMA plate reader (BMG LABTECH, Offenbach, Germany) using an excitation wavelength of 485 nm and emission of 590 nm, respectively.

To assess the contingent of active transport, two 24-well plates were loaded equally with ASP^+ concentrations from 10 µM to 1 mM in KRB with KRB only as negative control. The plates were incubated for 90 min at 4°C and 37°C, respectively. Active uptake of ASP^+ was calculated as the difference in fluorescence signals of the concentrations divided by duration of experiment in minutes. The inhibitory potential of salbutamol (racemic mixture, R- and S-

enantiomers), formoterol (RR- and SS-enantiomers), L- and D-carnitine, amantadine, verapamil, beclomethasone, salmeterol and budesonide was tested. Na^+ dependence of ASP^+ uptake was investigated by changing the incubation solution to 5.4 mM Na^+, in which sodium salts were isotonically replaced with potassium counterparts. Furthermore, the effect of extracellular proton (pH 5.7 – 8.2) and solvents (methanol, ethanol and dimethyl sulfoxide (DMSO)) concentration on ASP^+ uptake was investigated.

Transport studies

Transport experiments were conducted with monolayers cultured on Transwell filters. Both sides of the cell layers were washed twice with pre-equilibrated bicarbonated KRB. After 60 min equilibration with KRB, transport of ASP^+ was initiated by replacing the fluid in the donor chamber with KRB containing 100 or 500 μM of the fluorophore. The apical and basolateral fluid volumes were 520 μl and 1520 μl, respectively. The initial concentration in the donor fluid was assayed by drawing a 20-μl sample immediately after the initiation of the flux studies. The cell layers were incubated at 37°C during transport experiments. Samples (200 μl) were drawn serially from the receiver compartment at 30, 60, 120, 180 and 240 min. After each sampling, an equal volume of fresh transport buffer was returned to the receiver side to maintain a constant volume. At the end of the transport experiment, a 20-μl sample was drawn from the donor fluid and assayed for its activity. Each experiment was performed on a total of 12 cell layers. In order to assess the integrity of cell layers during the transport studies, TEER was measured before and after each experiment. The apparent permeability coefficient, P_{app}, was calculated according to the equation

$$P_{app} = J / (A \times C_i)$$

where Ci was the initial concentration of the drug under investigation in the donor fluid and A the nominal surface area of cell layers (1.12 cm^2) utilised in this study. The fluorescence of the samples was analysed in 96-well plates in a FLUOstar OPTIMA fluorescence plate reader at excitation and emission wavelengths of 485 and 590 nm, respectively. Samples were diluted with KRB, where appropriate.

4.3.4 Statistical analysis

Results are expressed as mean±SD. Significance ($P<0.05$) of differences in the group mean values were determined by two-way analysis of variances, followed by Student-Newman-Keuls post-hoc tests.

4.4 Results

4.4.1 Protein expression

Immunofluorescence microscopy

Immunofluorescence confocal laser scanning microscopy showed very low expression of OCT1 (Figure 4.1) in 16HBE14o- and low expression in Caco-2. In Calu-3 and hBEpC moderate levels were observed. Calu-3 cells under air-interfaced conditions showed slightly higher expression. OCT2 (Figure 4.2) was absent in all lung epithelial cells tested, while expression in Caco-2 was at low levels. Low to very low expression of OCT3 (Figure 4.3) was observed in all cell

types. 16HBE14o- and Calu-3 (AIC) showed expression just above detection limit, whereas Caco-2, Calu-3 (LCC) and hBEpC revealed low but clear signals for OCT3. Relatively high expression of OCTN1 (Figure 4.4) was observed in Calu-3(LCC and AIC). For all other cell models, expression was on a moderate level. Calu-3 (AIC) and hBEpC (LCC) showed high expression of OCTN2 (Figure 4.5), whereas the other models revealed moderate expression.

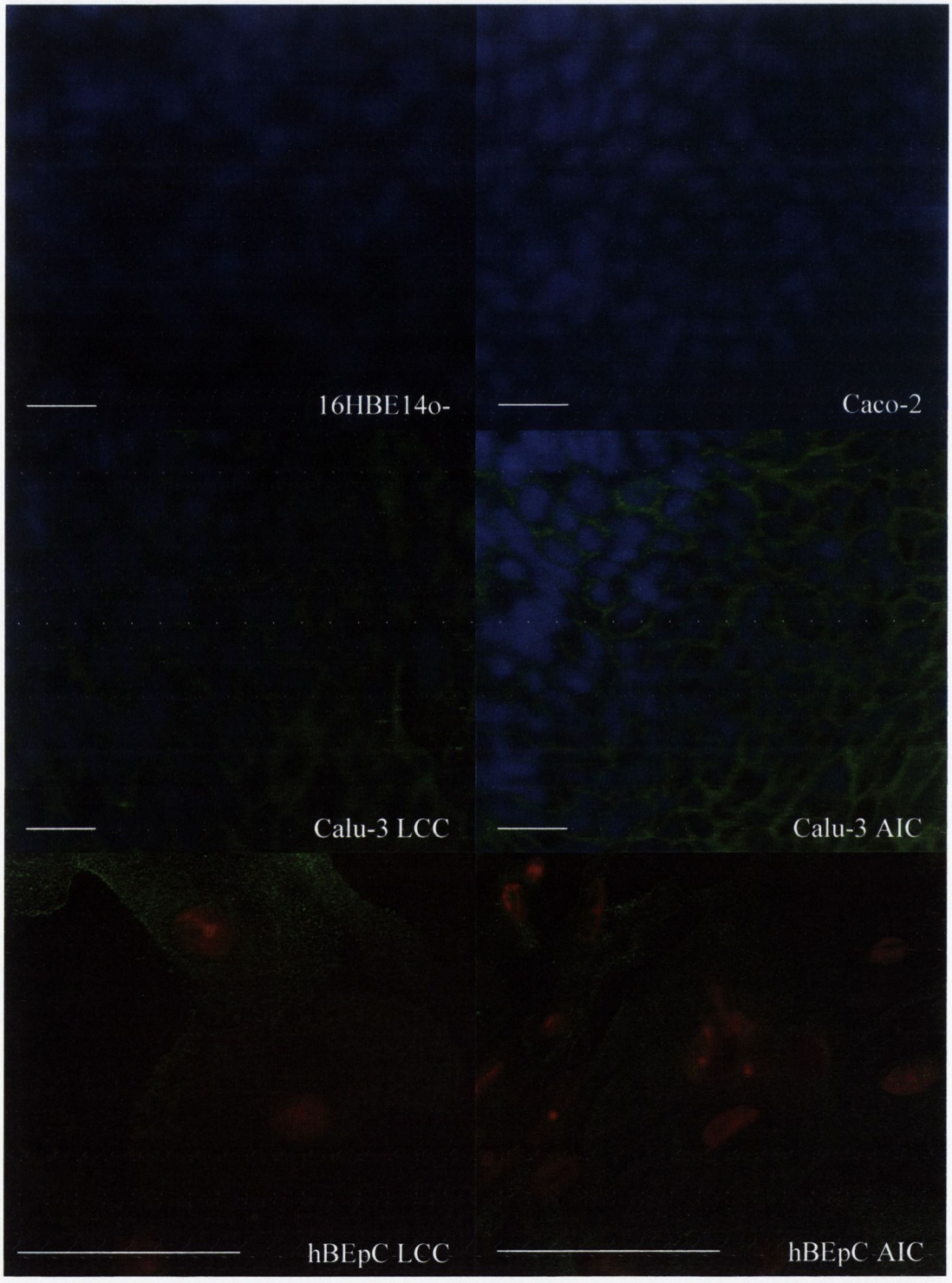

Figure 4.1 Immunolabelling of OCT1. 16HBE14o-, Caco-2, Calu-3 (LCC and AIC), hBEpC (LCC and AIC) monolayers grown on Transwell filters. Staining for OCT1 (green) is shown by confocal laser scanning microscopy. Nuclei were counterstained with DAPI (blue) and propidium iodide (red), respectively. Bar 20 µm

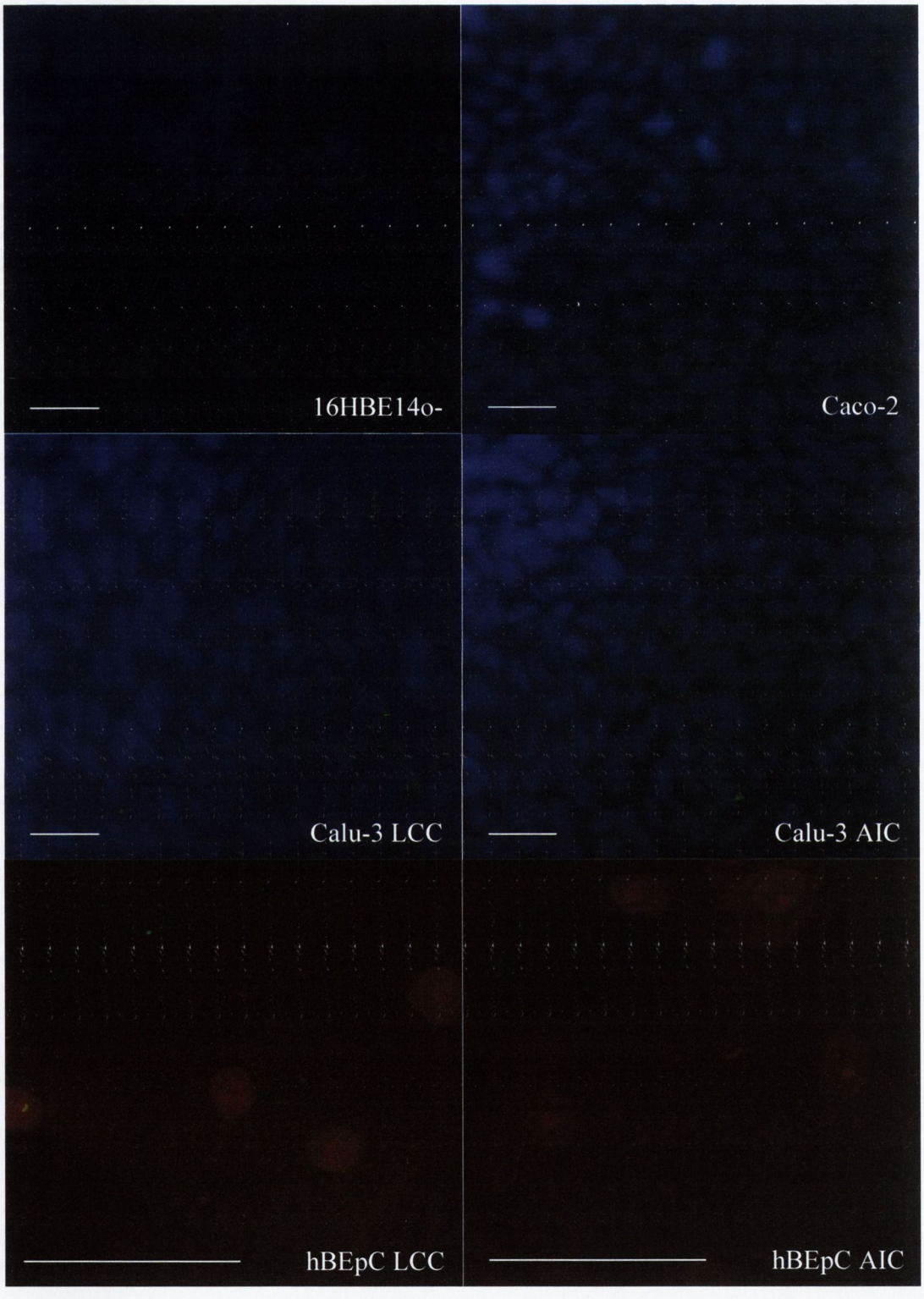

Figure 4.2 Immunolabelling of OCT2 16HBE14o-, Caco-2, Calu-3 (LCC and AIC), hBEpC (LCC and AIC) monolayers grown on Transwell filters. Staining for OCT2 (green) is shown by confocal laser scanning microscopy. Nuclei were counterstained with DAPI (blue) or propidium iodide (red). Bar 20 μm

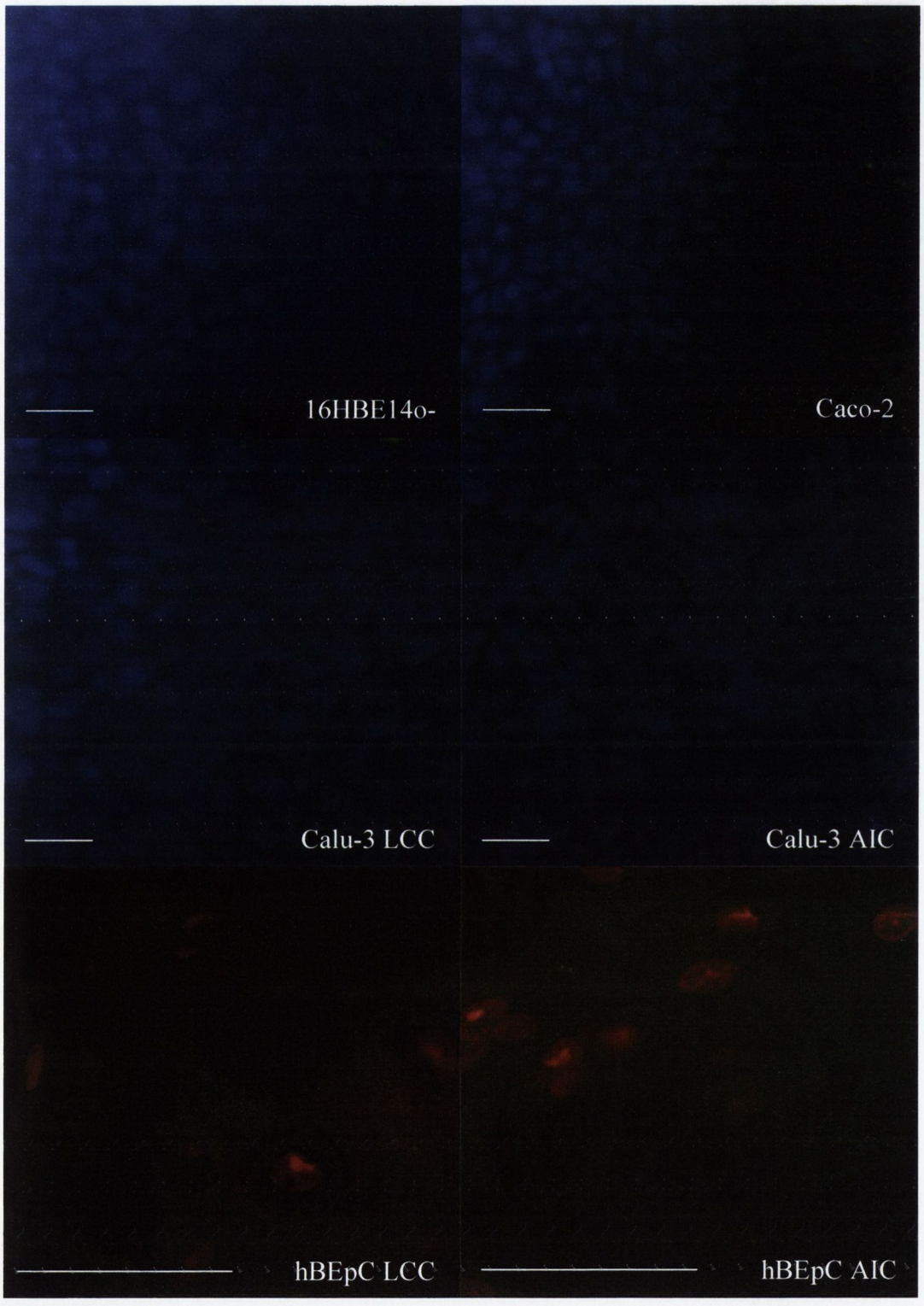

Figure 4.3 Immunolabelling of OCT3 16HBE14o-, Caco-2, Calu-3 (LCC and AIC), hBEpC (LCC and AIC) monolayers grown on Transwell filters. Staining for OCT3 (green) is shown by confocal laser scanning microscopy. Nuclei were counterstained with DAPI (blue) or propidium iodide (red). Bar 20 μm

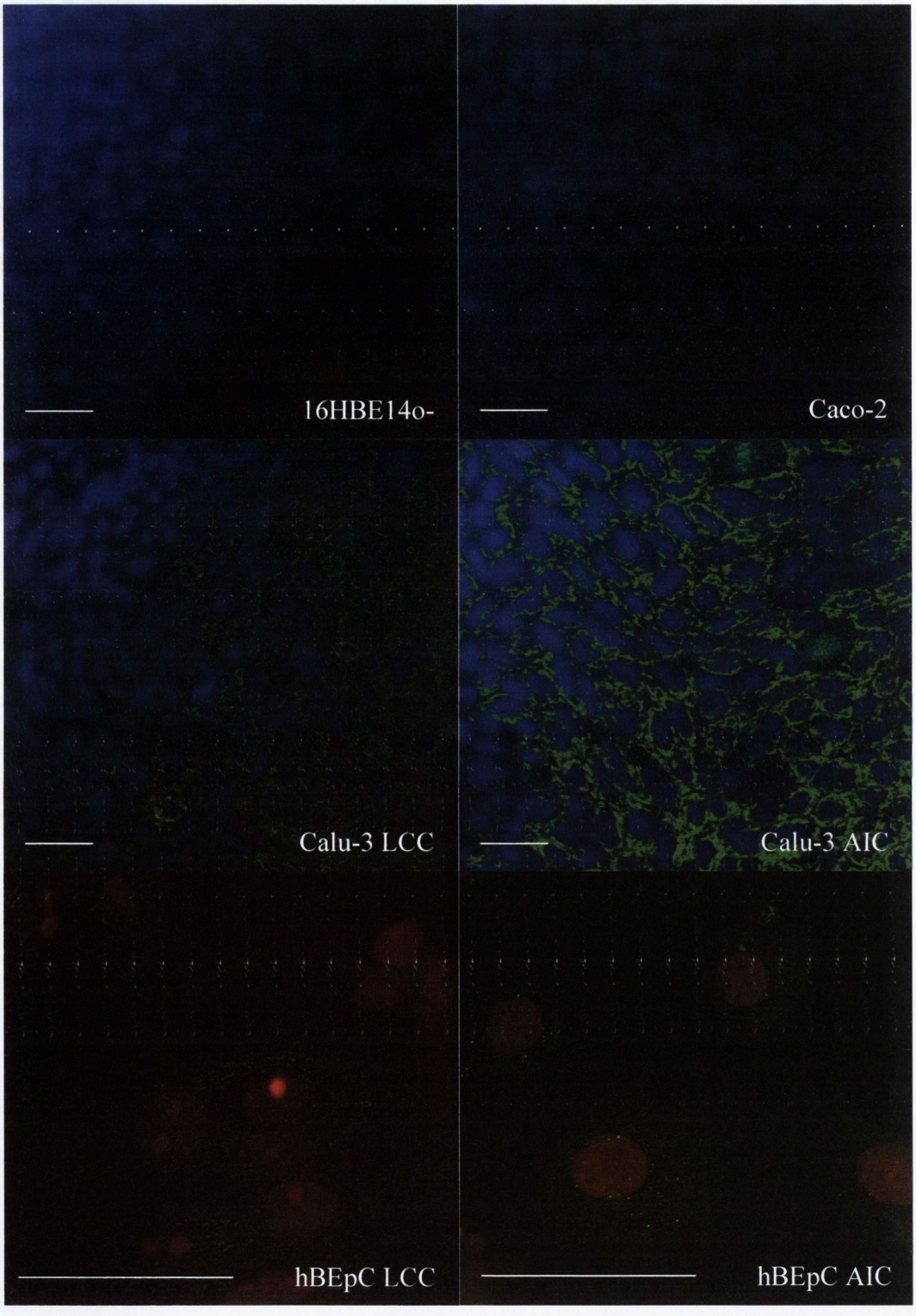

Figure 4.4 Immunolabelling of OCTN1 16HBE14o-, Caco-2, Calu-3 (LCC and AIC), hBEpC (LCC and AIC) monolayers grown on Transwell filters. Staining for OCTN1 (green) is shown by confocal laser scanning microscopy. Nuclei were counterstained with DAPI (blue) or propidium iodide (red). Bar 20 μm

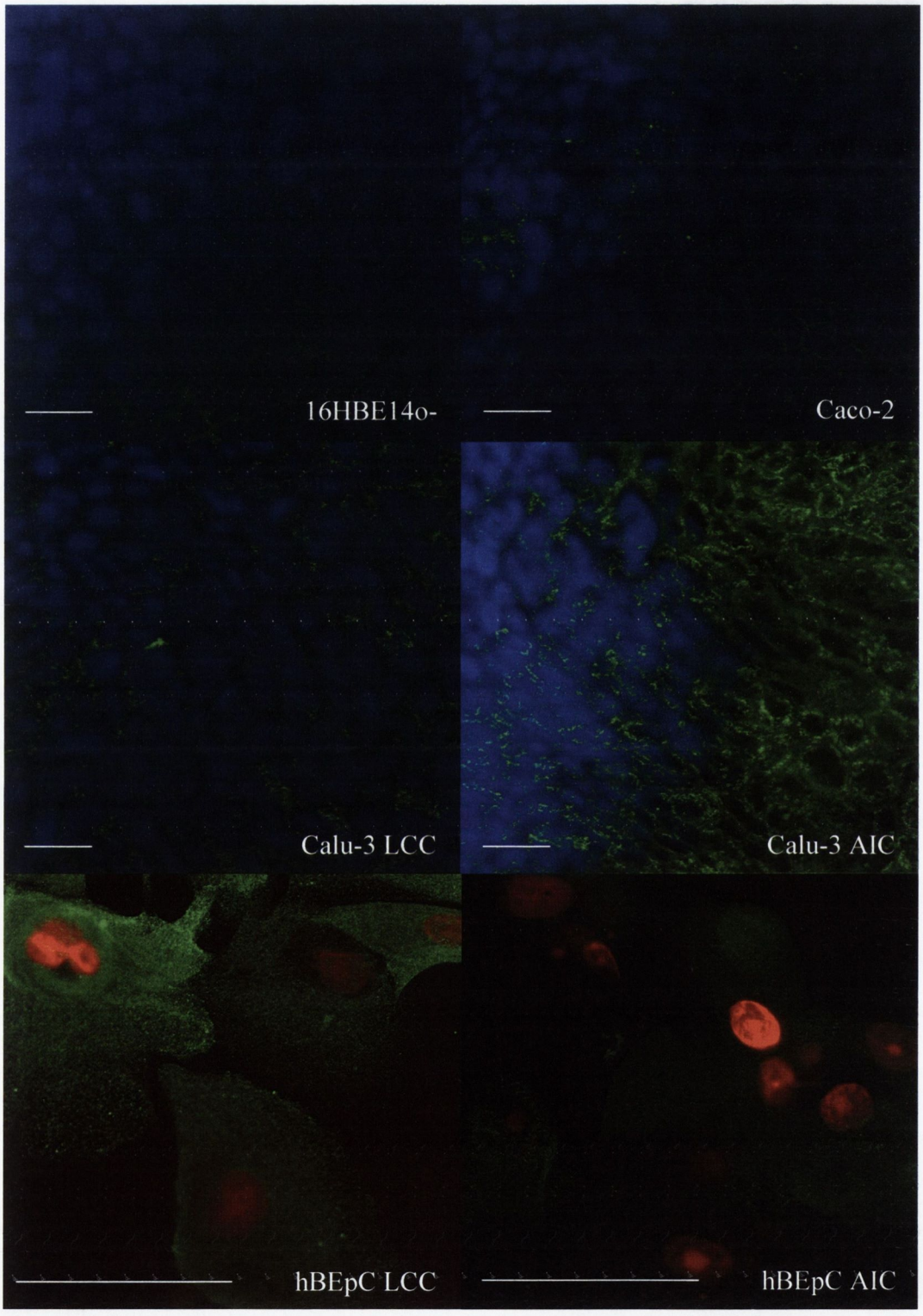

Figure 4.5 Immunolabelling of OCTN2 16HBE14o-, Caco-2, Calu-3 (LCC and AIC), hBEpC (LCC and AIC) monolayers grown on Transwell filters. Staining for OCTN2 (green) is shown by confocal laser scanning microscopy. Nuclei were counterstained with DAPI (blue) or propidium iodide (red). Bar 20 μm

Fluorescence activated cell sorting (FACS)

Figures 4.6 – 4.8 show dot plots of fluorescence activated cell sorting of Calu-3 (LCC), Calu-3 (AIC) and 16HBE14o- for selected transporters. Because the difference between mean and median of labelled transporter compared to control was small, counts of cells with higher fluorescence than control (%) were used for figure 4.9. These counts did show differences between expressions of organic cation transporters (figure 4.9). However, none of the variations were significant. Furthermore, OCT2 appeared to be expressed on moderate levels.

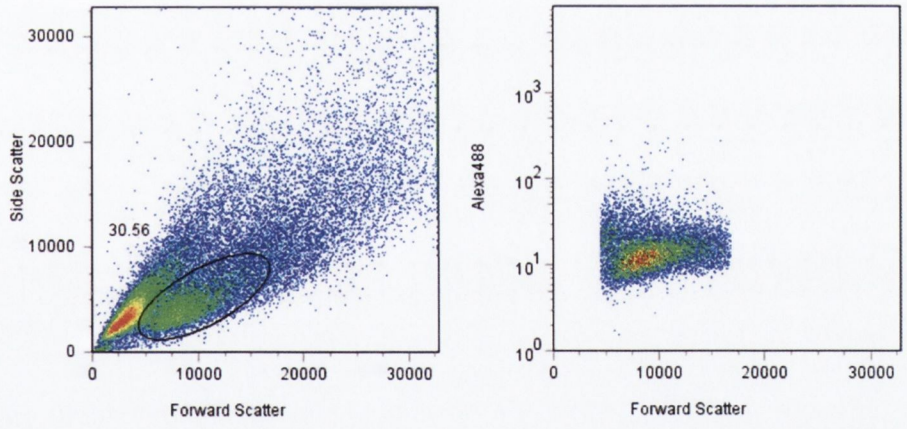

Figure 4.6 Dot plot of Calu-3 (LCC) selected population (single cells, left) and fluorescence for OCTN2 (right)

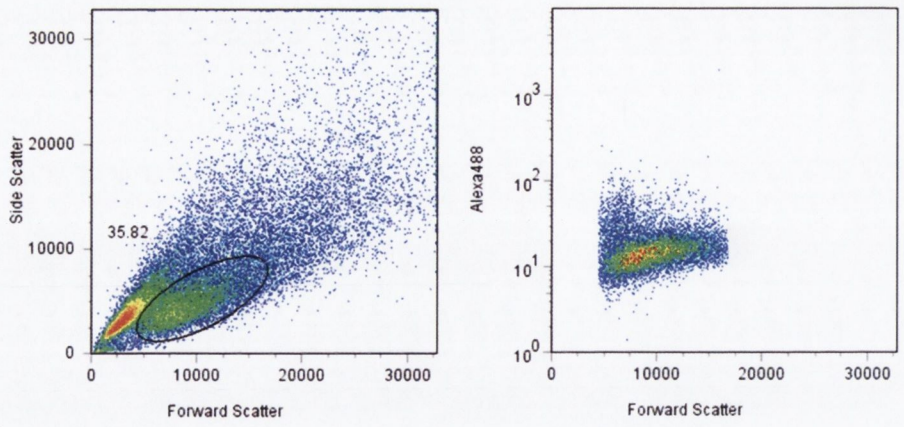

Figure 4.7 Dot plot of Calu-3 (AIC) selected population (single cells, left) and fluorescence for OCT3 (right)

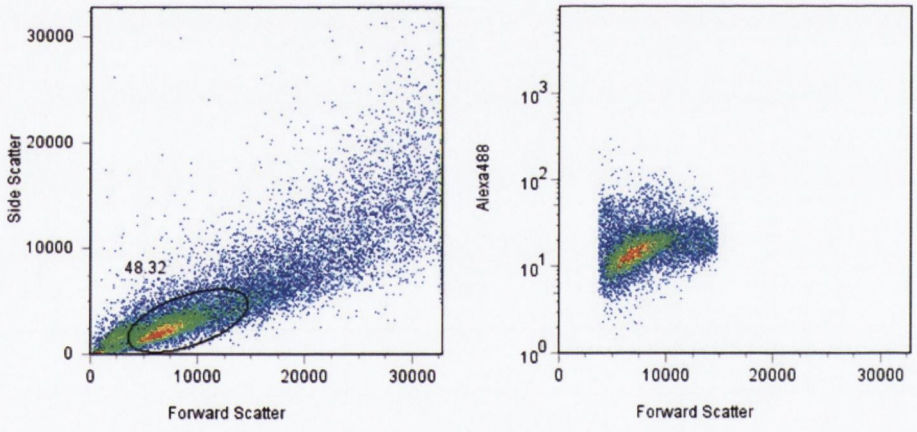

Figure 4.8 Dot plot of 16HBE14o- selected population (single cells, left) and fluorescence for OCT1 (right)

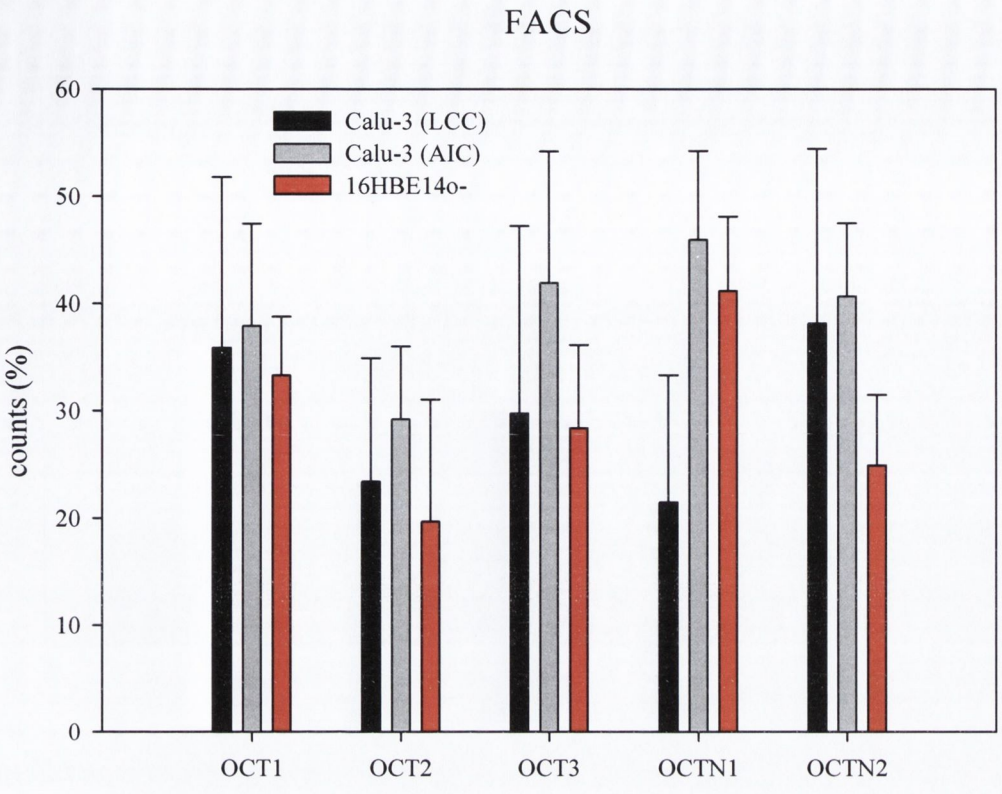

Figure 4.9 Fluorescence activated cell sorting. Counts of positive cells compared to control (%). Data shown represents mean±SD from n = 3 – 5 isolations.

Protein quantification

As fluorescence activated cell sorting was not sufficient to quantify OCT1, OCT2, OCT3, OCTN1 and OCTN2, total protein content was calculated per cm^2 as a guideline. It differed between the various cell types cultured on 6 or 24-well plates. Figure 4.10 shows highest concentrations in Caco-2 with 1289.7±82.52 $\mu g/cm^2$ which is more than twice the concentration detected in Calu-3 with 531.2±27.14 $\mu g/cm^2$, about four times the amount quantified in 16HBE14o- (294.3±16.39 $\mu g/cm^2$) and A549 (16.8±49.83 $\mu g/cm^2$) and nearly 10-times the protein expressed in hBEpC with 133.6±21.41 $\mu g/cm^2$.

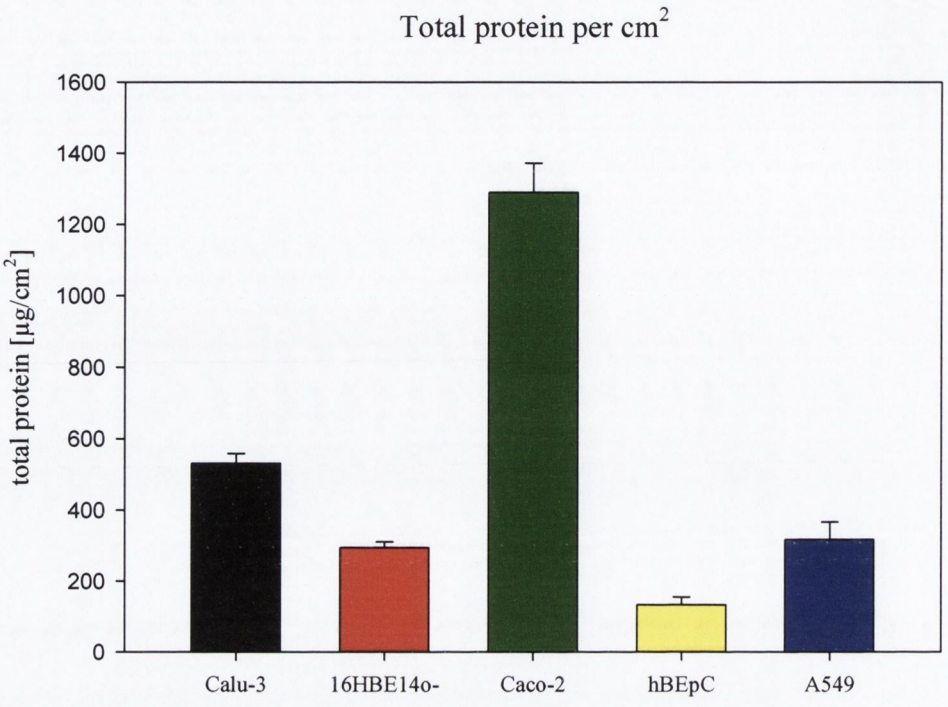

Figure 4.10 Total protein per cm^2. Total protein was isolated from 6 and 24 well plates, respectively, concentrations were determined with a protein assay (Bio-Rad) and expression was calculated as total protein per cm^2. Data shown represents mean±SD from n = 6 isolations.

4.4.2 Uptake studies

When cells were incubated with 10 µM ASP$^+$, characteristic differences could be observed over a period of 90 min (Figure 4.11). A549 showed the highest uptake of all cell models tested. Caco-2 and hBEpC were lower in the middle range at approximate half of A549 readings, whereas Calu-3 and 16HBE14o- revealed a far lower uptake; units detected in A549 were about 10-fold higher than these two cell lines.

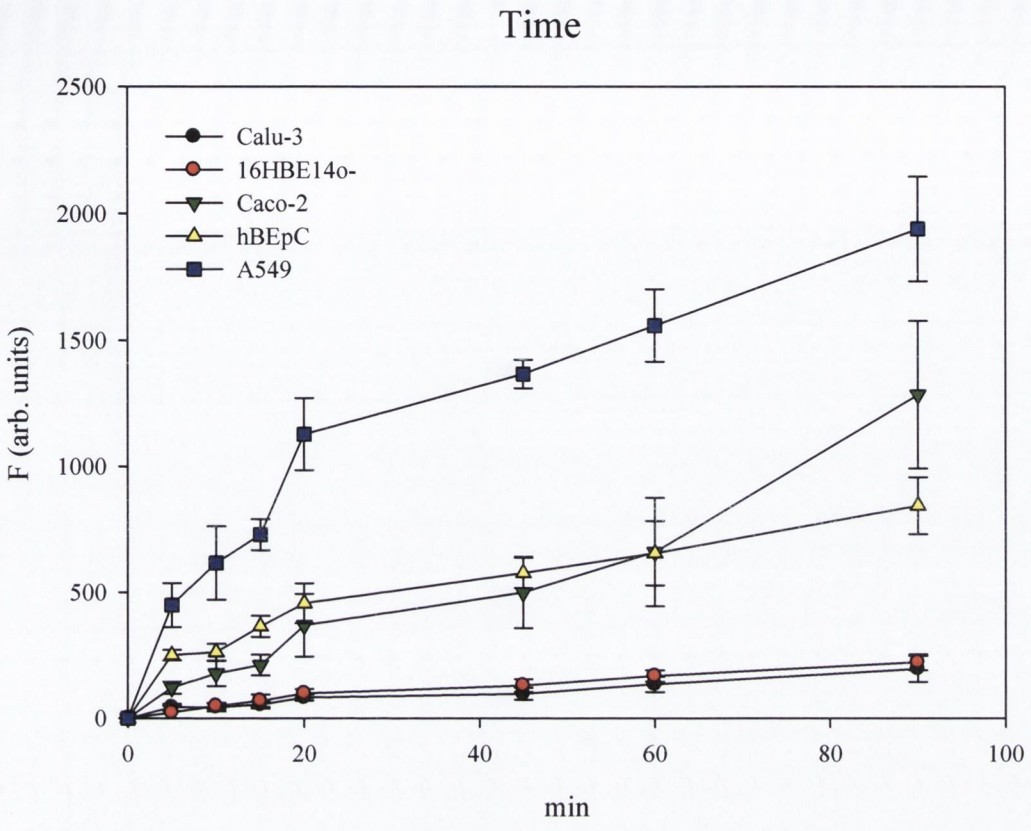

Figure 4.11 Time course of fluorescence (F) after exposing the cells to 10 μM ASP^+ at 37°C. Data shown represents mean±SD from n = 6 – 12 experiments.

Figures 4.12-16 show the effect of temperature on uptake of ASP^+ while exposing the cells for 20/90 min. For all cells tested, there was a noticeable difference between 37°C and 4°C on varying levels. At 37°C Caco-2 showed uptake of ASP^+ within 20 min similar to Calu-3 and 16HBE14o- within 90 min. A549 showed only a quarter of uptake of ASP^+ during 20 min, but the difference between 37°C and 4°C is more distinctive than seen with the other cell models. The lowest uptake was observed with hBEpC, which revealed only one tenth of the units detected with Caco-2. Temperature-sensitive (saturable) uptake of ASP^+ was calculated as the difference between the fluorescence after exposure to ASP^+ at 37°C and 4°C

(Figure 4.17) divided by time of exposure in minutes. Results represent mean from n = 3 – 12 experiments ± SD.

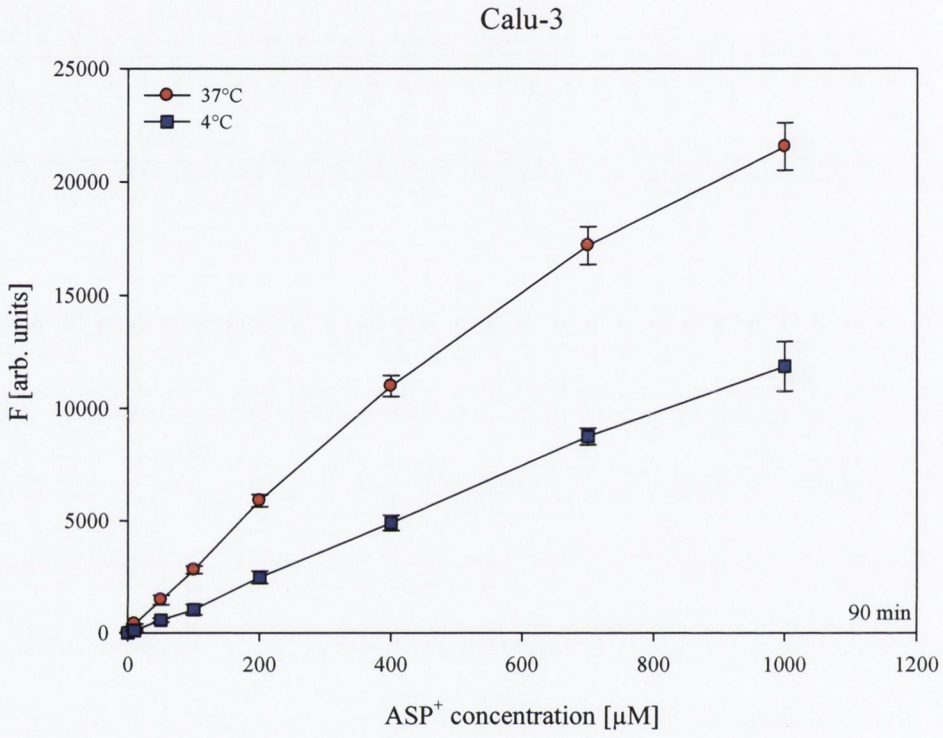

Figure 4.12 Effect of temperature on fluorescence (F) after exposing Calu-3 to ASP^+ for 90 min. Data shown represents mean±SD from n = 3 experiments.

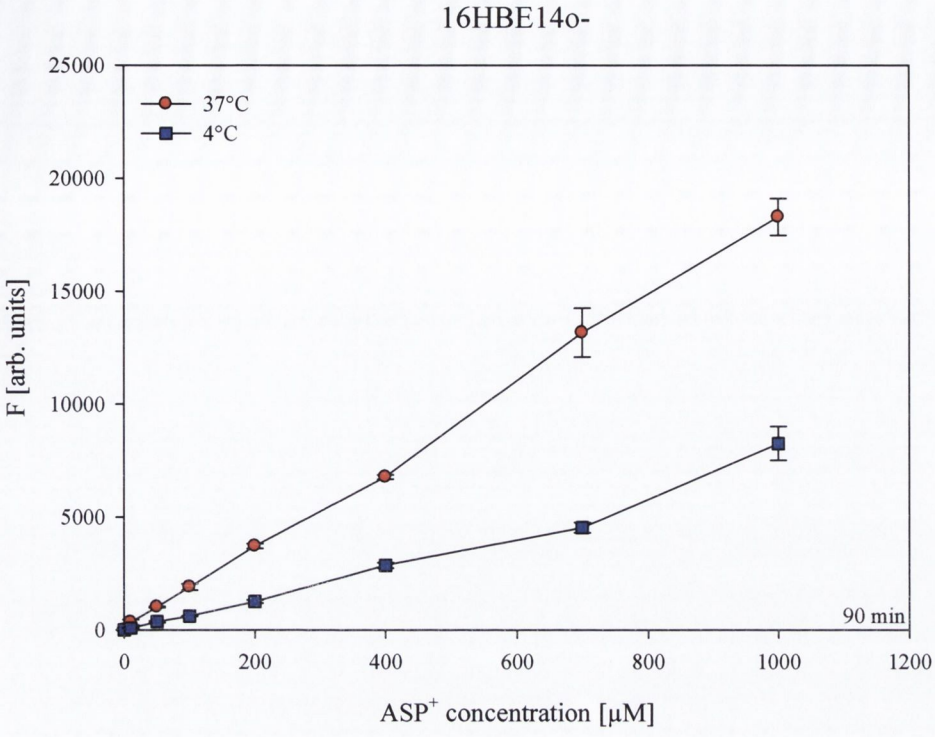

Figure 4.13 Effect of temperature on fluorescence (F) after exposing 16HBE14o- to ASP^+ for 90 min. Data shown represents mean±SD from n = 3 experiments.

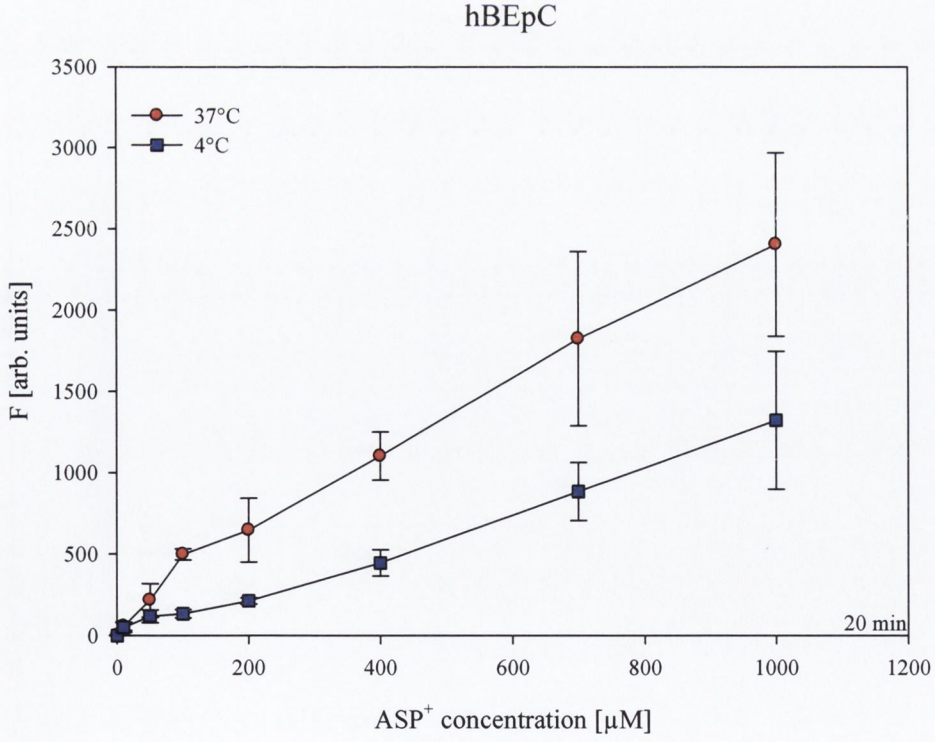

Figure 4.14 Effect of temperature on fluorescence (F) after exposing hBEpC to ASP^+ for 20 min. Data shown represents mean±SD from n = 6 experiments.

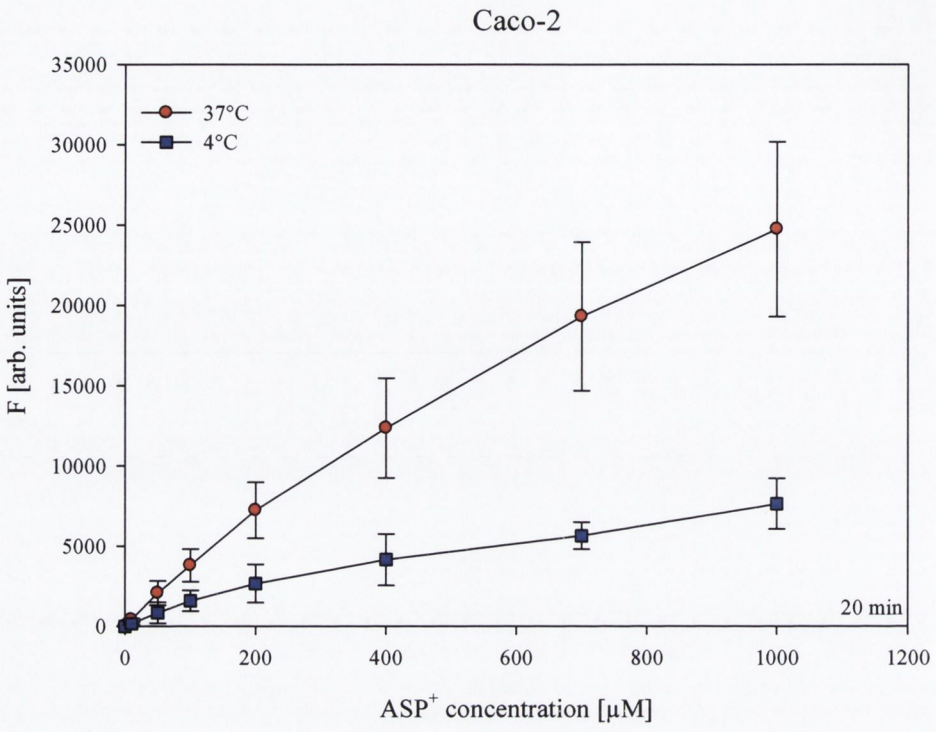

Figure 4.15 Effect of temperature on fluorescence (F) after exposing Caco-2 to ASP^+ for 20 min. Data shown represents mean±SD from n = 3 experiments.

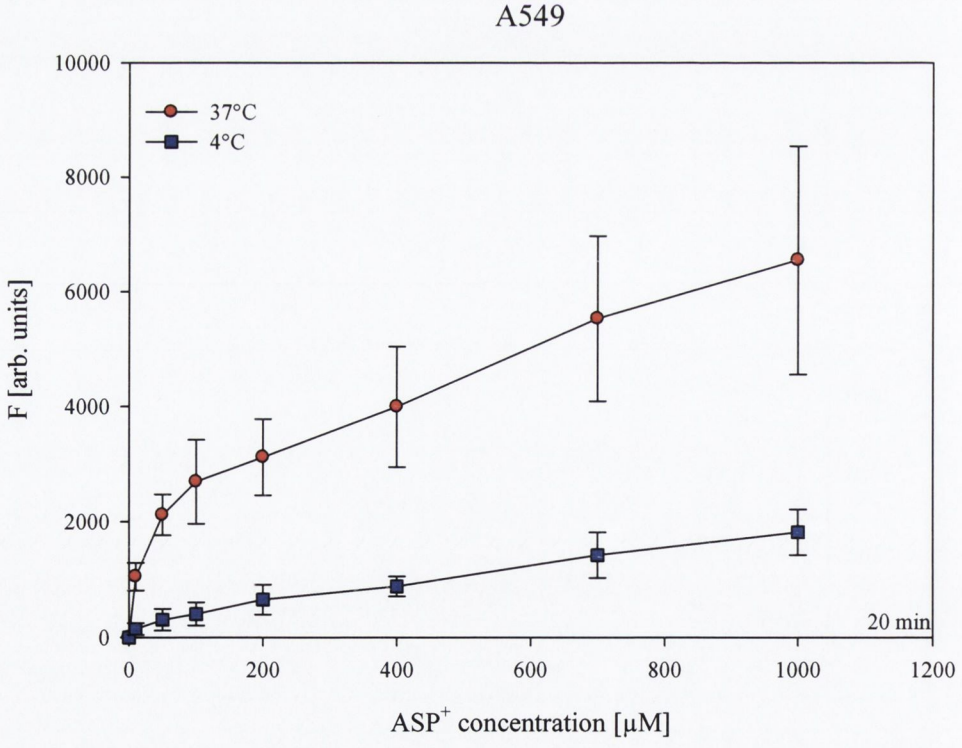

Figure 4.16 Effect of temperature on fluorescence (F) after exposing A549 to ASP^+ for 20 min. Data shown represents mean±SD from n = 12 experiments.

Caco-2 differed most in this parameter. The uptake was 4 to 17-fold higher than observed in other cell models. Second highest were A549. Calu-3 and 16HBE14o- exposed similar data, respectively, whereas uptake by hBEpC stayed far below the other models.

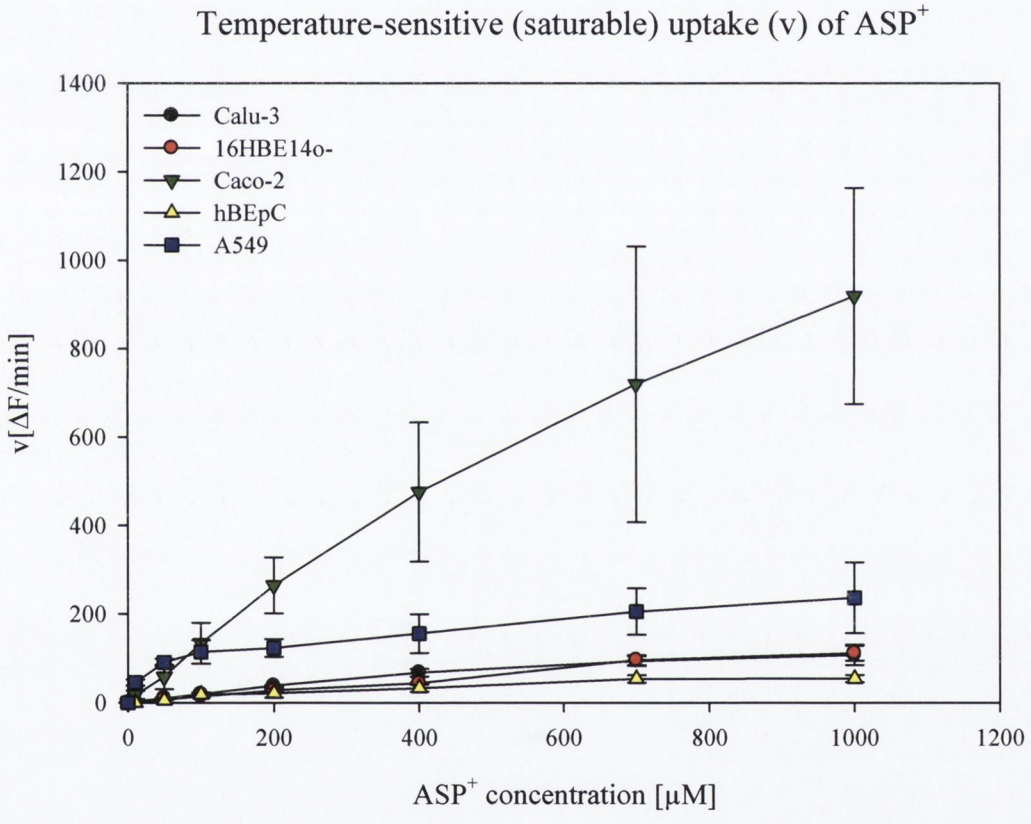

Figure 4.17 Temperature-sensitive (saturable) uptake (v) of ASP^+ was calculated as the difference between the fluorescence (F) after exposure to ASP^+ at 37°C and 4°C divided by time of exposure in minutes. Data shown represents mean±SD from n = 3 – 12 experiments

Salbutamol showed little to no effect on ASP^+ uptake with the cell models tested (Figure 4.18). In Calu-3, no difference was visible between racemate and enantiomers of the drug. Reduction to 81±15.5% (100μM) and 65±21.4% (500 μM) for the racemate, 79±18.9% (100 μM) and 74±16.1% (500 μM) for the R-enantiomer and 64±19.1% (100 μM) and 60±19.1% (500 μM) of control for the S-enantiomer were observed. The effects were comparable to those in 16HBE14o- and Caco-2. 16HBE14o-: 92±15.7%, 78±16.5% (100,500 μM R/S); 85±14.1%, 74.7±13.2% (100/500 μM R); 82±20.3%, 72±13.9% (100/500 μM S); Caco-2: 75±15.6%, 72±12.8% (100/500 μM RS); 78±15.1%, 73±13.6% (100/500 μM R); 80±16.6%, 72±16.5% (100/500 μM S) of control. The strongest effect of salbutamol was observed in the A549 model: 96±13.7%; 53±6.3% (100/500 μM R/S); 110±17.5%; 62±17.1% (100/500 μM R); 109±21.4%; 56±17.7% (100/500 μM S). However, no significant inhibition of uptake was detected in the primary model: 103±11.3; 89±11.8% (100/500 μM R/S); 99±17.7%; 92±13.5%; (100/500 μM R); 92±12.5%; 94±9.8 (100/500 μM S).

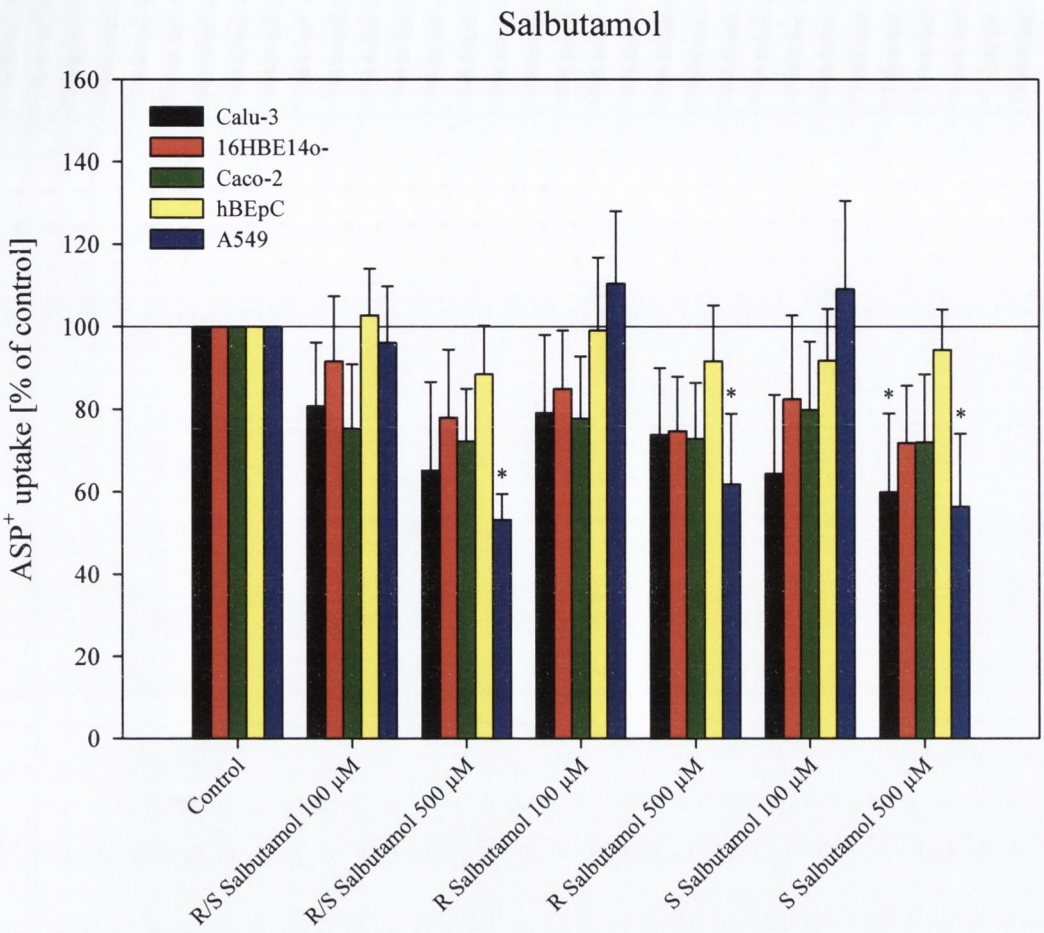

*Figure 4.18 Effect of salbutamol on ASP^+ uptake. Cells were incubated with 10 µM ASP^+ for 20 min at 37°C in all experiments in the presence or absence of the compounds. Control was calculated as the temperature-sensitive (saturable) uptake of ASP^+. Results represent mean±SD (n = 3 – 9 experiments). *P < 0.05 versus control.*

Strongest effects of extracellular pH were observed in the cell models Calu-3 and A549 (figure 4.19) (Calu-3 pH 5.7 40±13.2%, pH 6.5 60±7.7%, pH 7.4 100±4.6%, pH 8.2 84±6.5%; pH 5.7 34±5.3%, pH 6.5 66±12.5%, pH 7.4 100±0.0%, pH 8.2 92±.7% of control). Less, but still noticeable effect was detected with 16HBE14o- (pH 5.7 68±7.0%, pH 6.5 86±5.5%, pH 7.4 100±21.0%, pH 8.2 92±14.6% of control). With Caco-2 and hBEpC, the effect was negligible (Caco-2: pH 5.7

76±14.2, pH 6.5 86±9.9, pH 7.4 100±9.6, pH 8.2 97±13.1; hBEpC: pH 5.7 81±12.1, pH 6.5 85±17.9, pH 7.4 100±5.9, pH 8.2 113±20.8 of control).

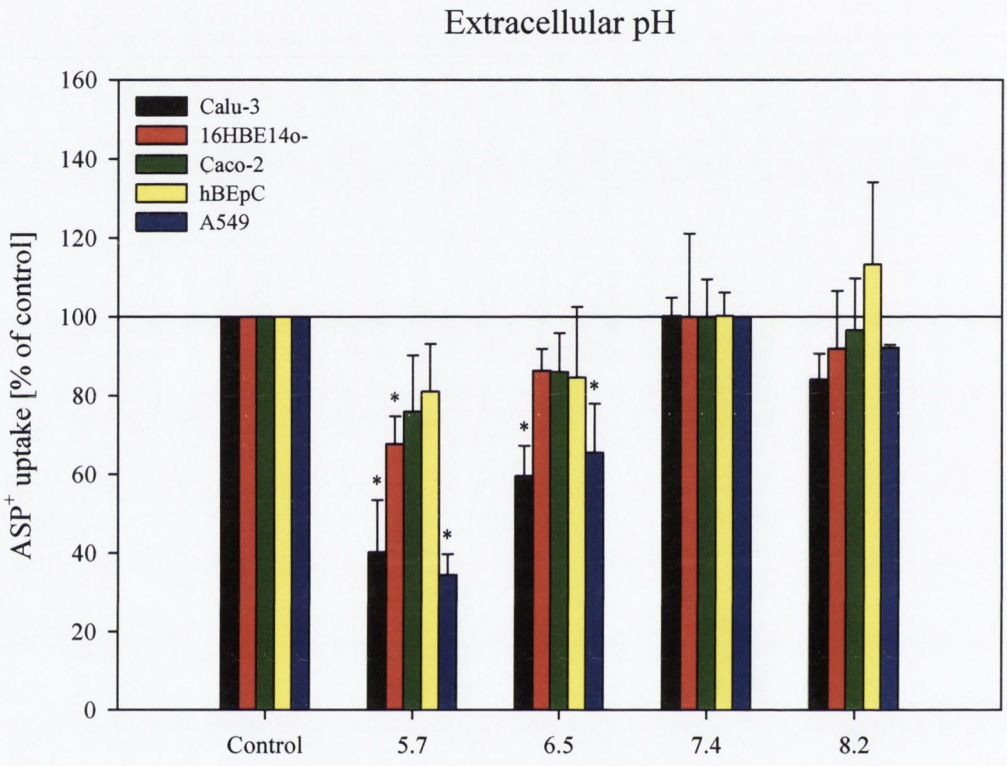

*Figure 4.19 Effect of extracellular pH on organic cation uptake. Cells were incubated with 10 µM ASP^+ for 20 min at 37°C. Control was calculated as the temperature-sensitive (saturable) uptake of ASP^+. Results represent mean±SD (n = 3 – 9 experiments). *P < 0.05 versus control.*

Uptake of ASP^+ was sodium independent for Calu-3, 16HBE14o-, Caco-2 and hBEpC (figure 4.20). However, a significant reduction to 32±2.2% of control was observed with A549 under low sodium conditions.

Negligible to no effect of carnitine on all cell models tested was detected (figure 4.21). Neither L-carnitine nor D-carnitine reduced the uptake of ASP^+ significantly.

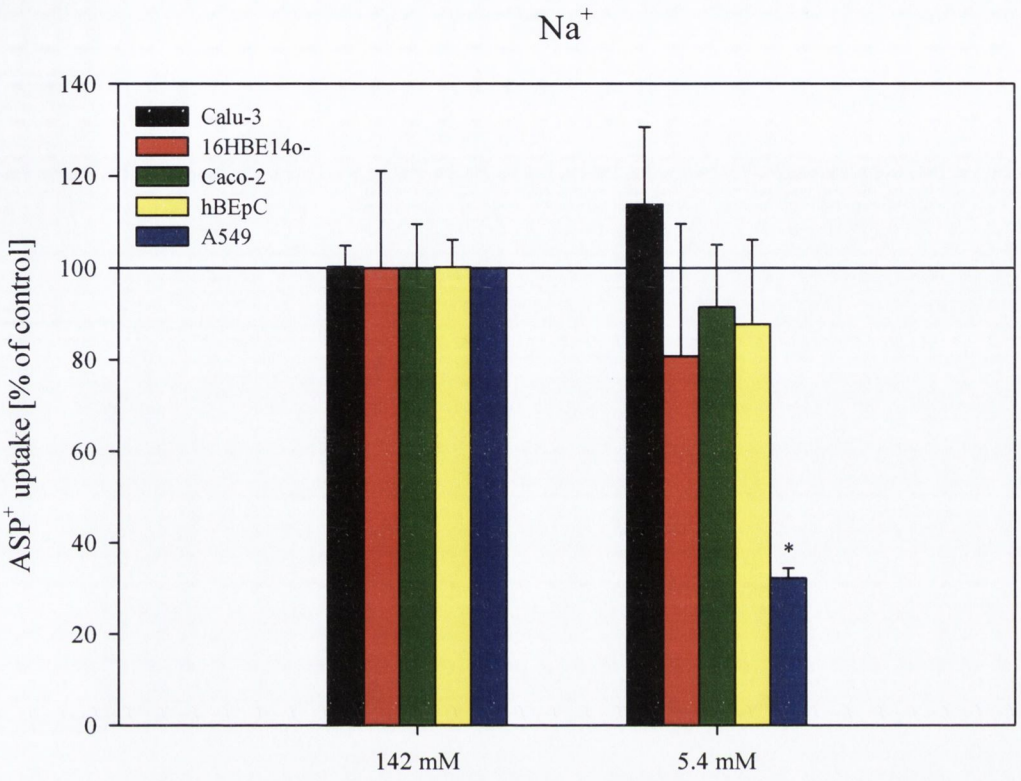

*Figure 4.20 Effect of extracellular sodium concentration on organic cation uptake. Cells were incubated with 10 µM ASP^+ for 20 min at 37°C. Control was calculated as the temperature-sensitive (saturable) uptake of ASP^+. Results represent mean±SD (n = 3 – 9 experiments). *P < 0.05 versus control.*

In A549 cells, formoterol showed the strongest effect on ASP^+ uptake (figure 4.22). Inhibition to 59±14.4%/13±2.9% (100/500 µM RR) and 40±8.3%/6±2.0% (100/500 µM SS) of control revealed a slightly higher potency of the SS-enantiomer. The other cell models showed negligible effect by the RR enantiomer and moderate effect of the SS-formoterol on Calu-3 (100 µM: 64±23.2%, 500 µM: 60±21.9% of control) and 16HBE14o- (100 µM: 71±22.0%, 500 µM: 60±22.8% of control)

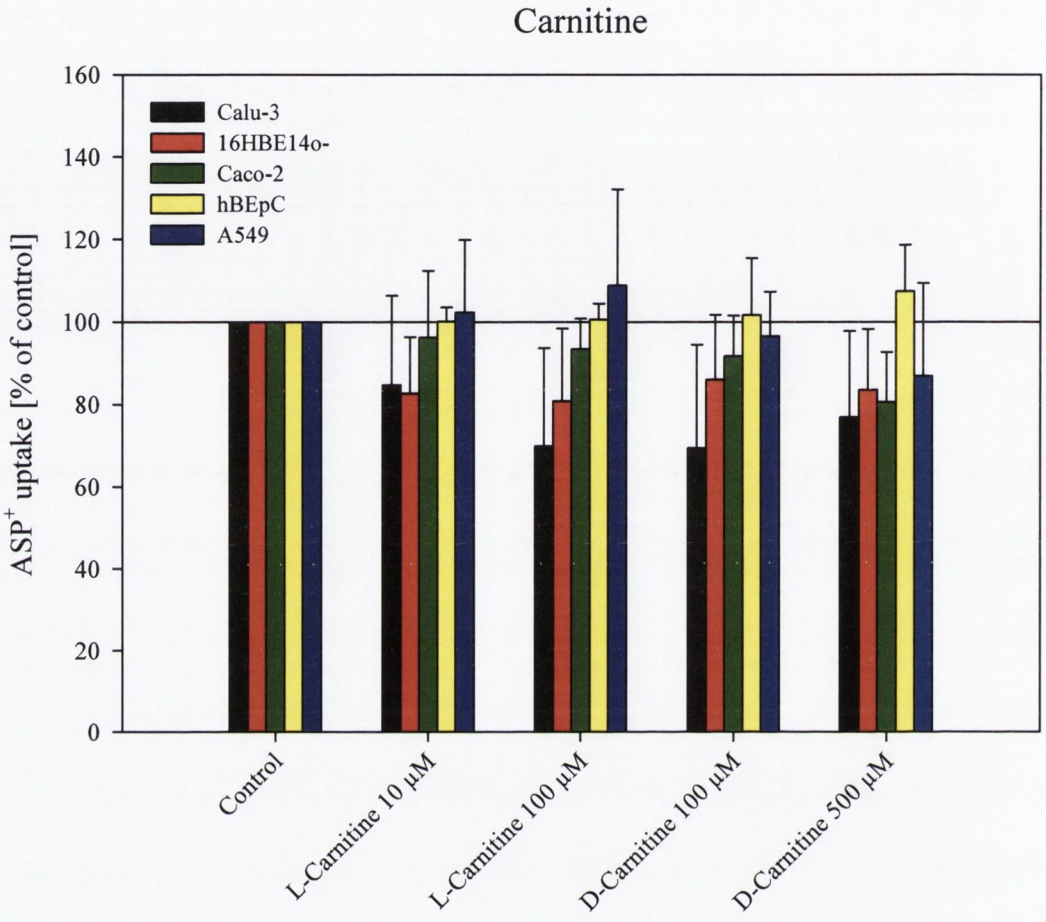

*Figure 4.21 Effect of carnitine on organic cation uptake. Cells were incubated with 10 µM ASP^+ for 20 min at 37°C. Control was calculated as the temperature-sensitive (saturable) uptake of ASP^+. Results represent mean±SD (n = 3 – 9 experiments). *P < 0.05 versus control.*

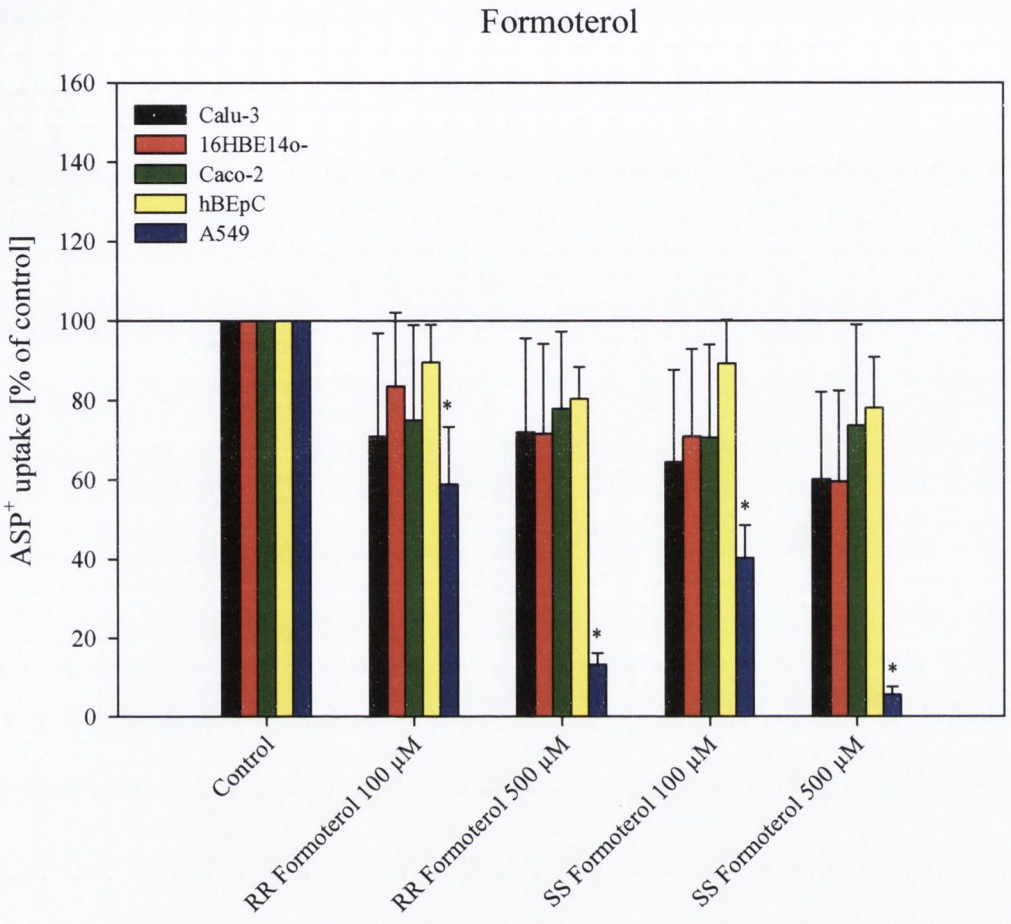

*Figure 4.22 Effect of formoterol on organic cation uptake. Cells were incubated with 10 µM ASP^+ for 20 min at 37°C. Control was calculated as the temperature-sensitive (saturable) uptake of ASP^+. Results represent mean±SD (n = 3 – 9 experiments). *P < 0.05 versus control.*

Amantadine inhibited ASP^+ uptake on a moderate level, with most cell models tested (15-35% inhibition), and stronger with A549 (100/500 µM 65±9.0%, 35±7.7% of control) (figure 4.23). The effect of verapamil was comparable to amantadine, but showed even stronger inhibition with A549 (100/500 µM 72±8.9%, 16±3.3% of control).

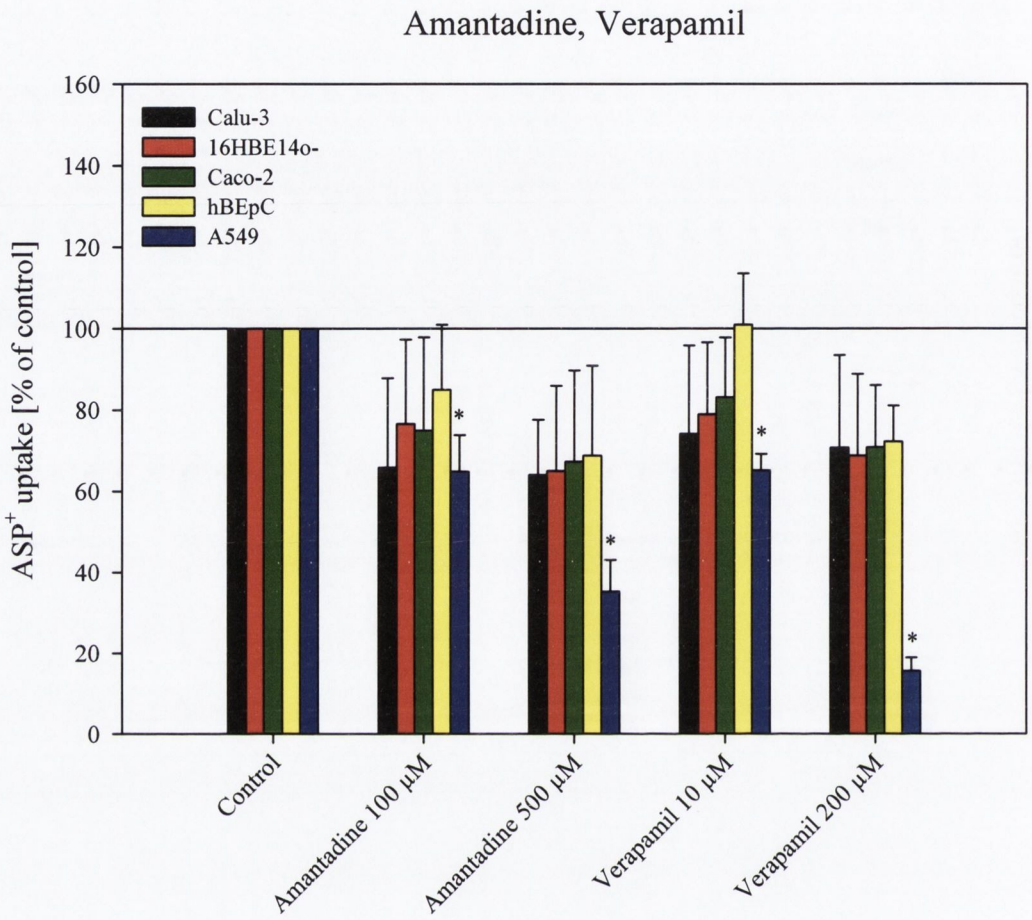

*Figure 4.23 Effect of amantadine and verapamil on organic cation uptake. Cells were incubated with 10 µM ASP^+ for 20 min at 37°C. Control was calculated as the temperature-sensitive (saturable) uptake of ASP^+. Results represent mean±SD (n = 3 – 9 experiments). *P < 0.05 versus control.*

Methanol had a low effect on ASP^+ uptake (figure 4.24). Concentrations up to 1% resulted in insignificant inhibition. Only higher concentration revealed significant inhibition. The effect of ethanol was stronger and proved to be significant at concentrations from 1%. DMSO showed the strongest effect with uptake reduced to less than 20% at concentrations from 5%. Salmeterol showed significant inhibition of ASP^+ uptake (figure 4.25). A reduction to less than 10% could be detected. The low effect of 1% of methanol was negligible.

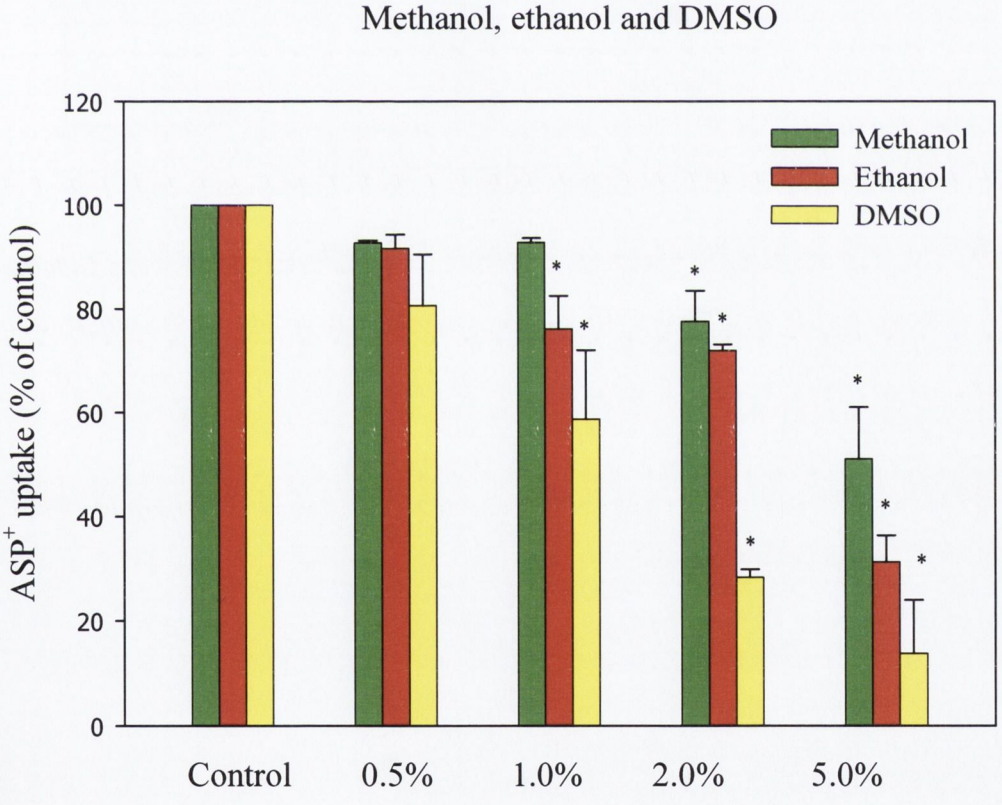

*Figure 4.24 Effect of methanol, ethanol and DMSO on organic cation uptake. A549 were incubated with 10 μM ASP^+ for 20 min at 37°C. Control was calculated as the temperature-sensitive (saturable) uptake of ASP^+. Results represent mean±SD (n = 3 experiments). *P < 0.05 versus control.*

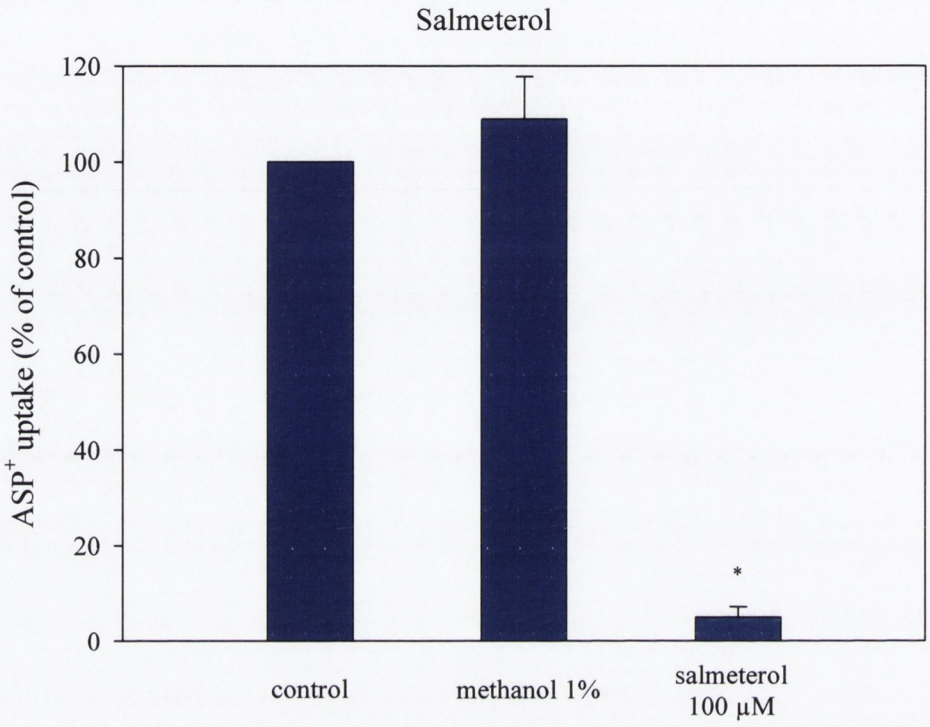

*Figure 4.25 Effect of salmeterol on organic cation uptake. A549 were incubated with 10 µM ASP^+ for 20 min at 37°C. Control was calculated as the temperature-sensitive (saturable) uptake of ASP^+. Results represent mean±SD (n = 3 experiments). *P < 0.05 versus control.*

Budesonide and beclomethasone did not show a significant effect on uptake of ASP^+ (figure 4.26 and 4.27). The light inhibition is similar to the effect by methanol.

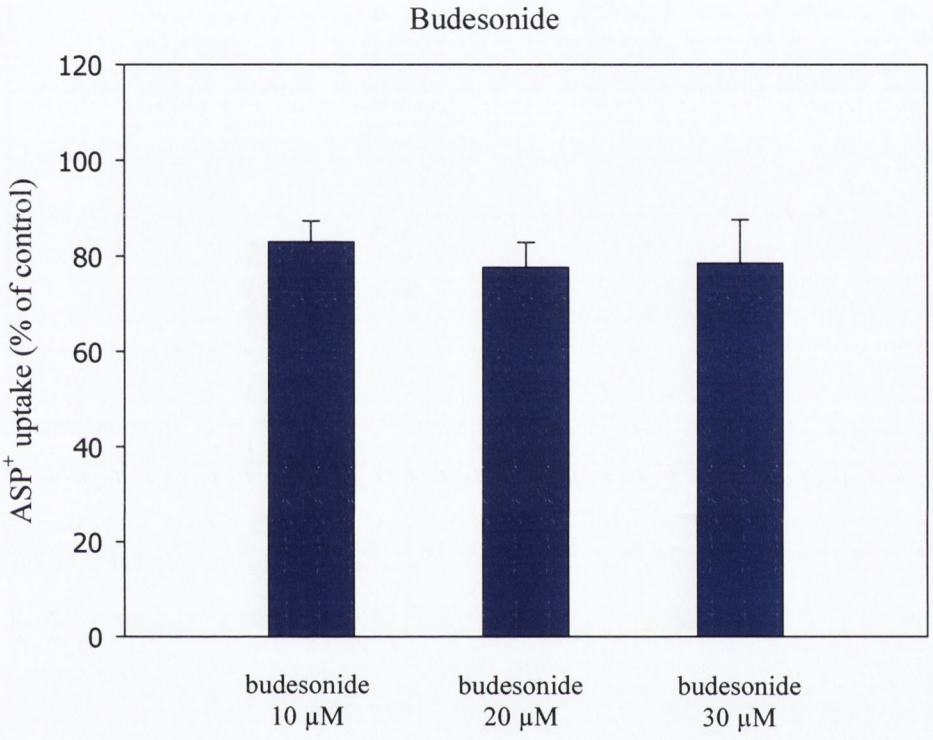

Figure 4.26 Effect of budesonide on organic cation uptake. Cells were incubated with 10 µM ASP^+ for 20 min at 37°C. Control was calculated as the temperature-sensitive (saturable) uptake of ASP^+. Results represent mean±SD (n = 3 experiments).

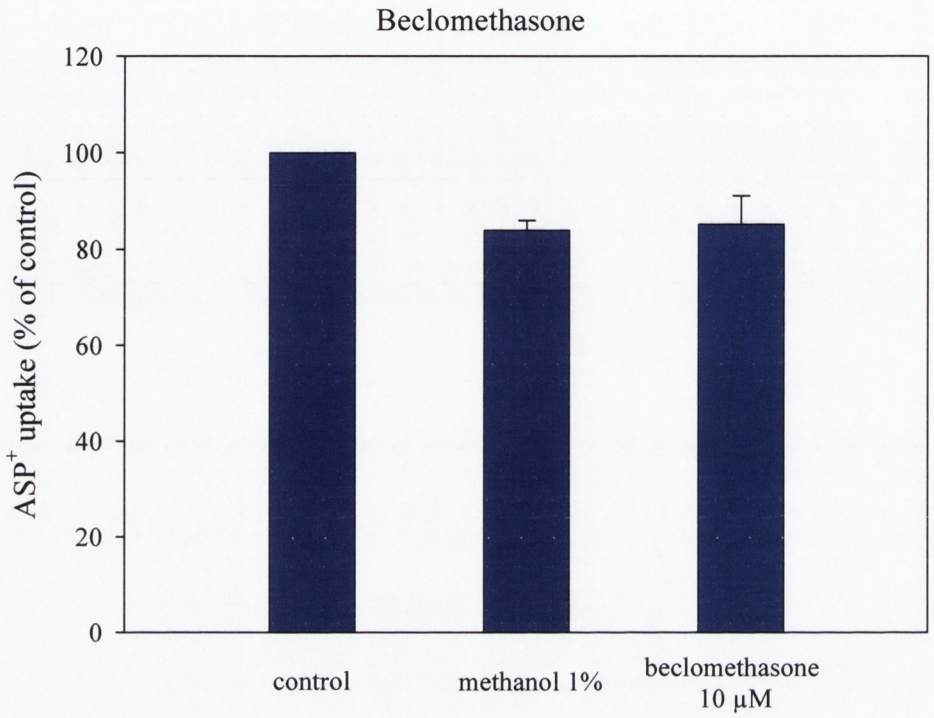

Figure 4.27 Effect of beclomethasone on organic cation uptake. Cells were incubated with 10 µM ASP^+ for 20 min at 37°C. Control was calculated as the temperature-sensitive (saturable) uptake of ASP^+. Results represent mean±SD (n = 3 experiments).

4.4.3 Transport studies

Transepithelial electrical resistance was documented during culture of cells to evaluate confluence and tightness of the monolayers (figure 4.28).

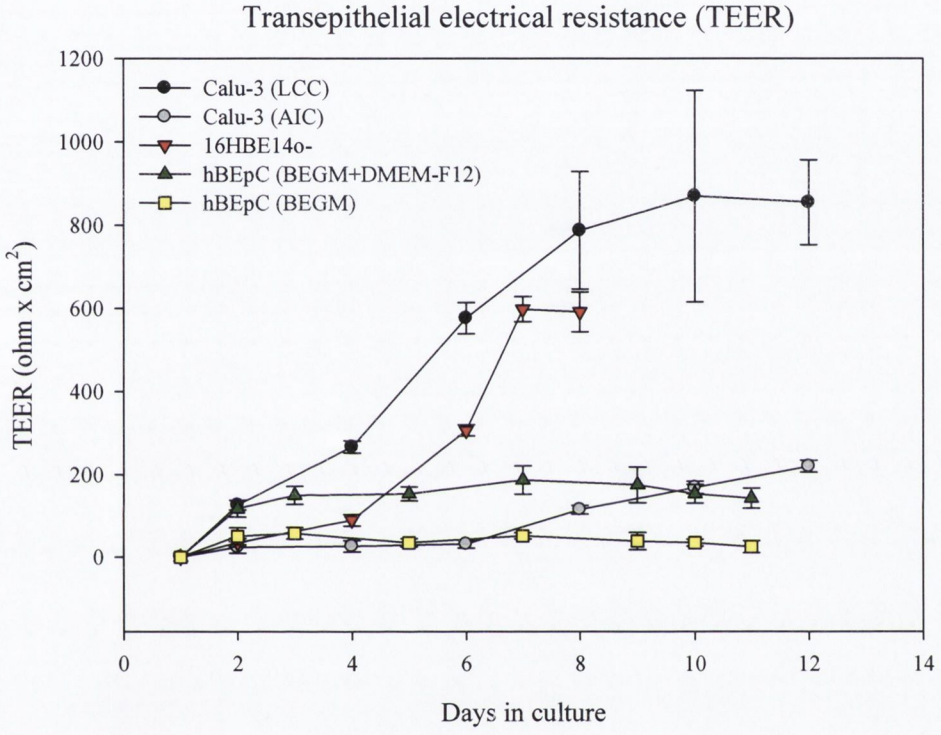

Figure 4.28 Transepithelial electrical resistance (TEER). TEER was measured every 24 or 48 h and corrected for the background value contributed by the Transwell Clear filter and medium. Results represent mean±SD (n = 6 experiments).

At a donor concentration of 500 µM across Calu-3 monolayers, the P_{app} in the apical-to-basolateral (ab) direction was $8.43\pm1.08 \times 10^{-7}$ cm/s, in comparison to $2.71\pm0.22 \times 10^{-6}$ cm/s in the basolateral-to-apical (ba) direction (figure 4.29).

Across 16HBE14o- cell layers, the P_{app} was 5.22±0.19 × 10^{-6} cm/s (ab) vs. 4.02±0.42 × 10^{-6} cm/s (ba). When the donor concentration was reduced to 100 µM, transport studies across Calu-3 monolayers revealed a P_{app} in the ab direction of 3.21±0.21 × 10^{-6} cm/s, in comparison to 1.13±0.10 × 10^{-6} cm/s in the ba direction. Across 16HBE14o- cell layers the P_{app} was 3.21±0.21 × 10^{-7} cm/s (ab) and 1.13±0.10 × 10^{-6} cm/s (ba), respectively (figure 4.30).

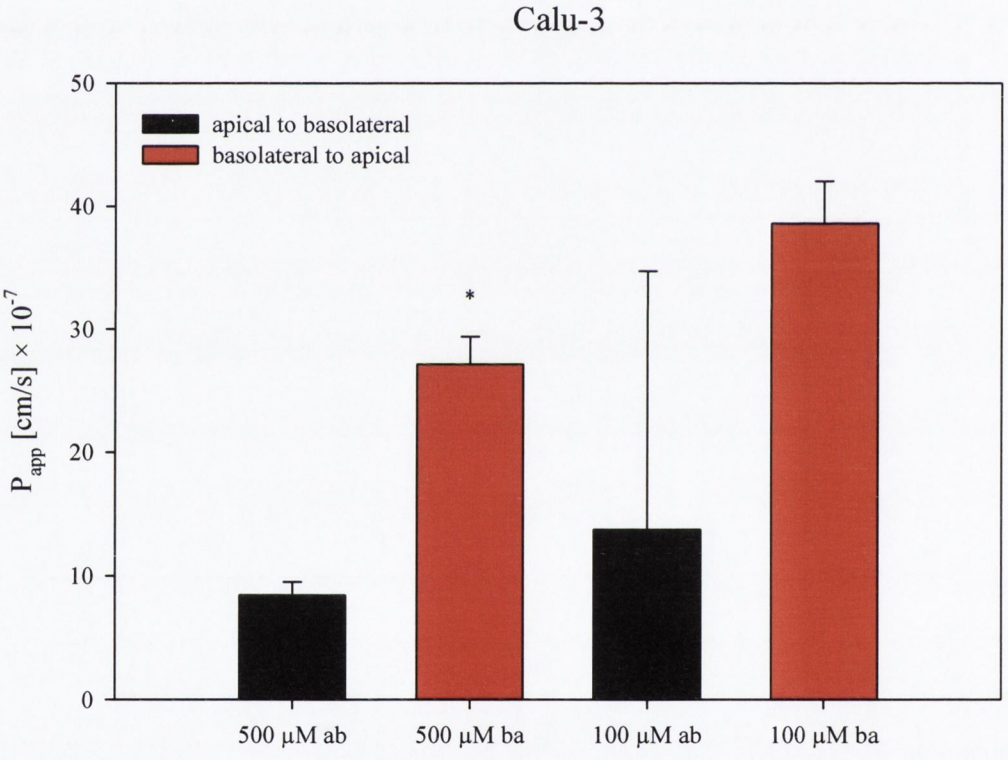

*Figure 4.29 Bi-directional transport studies with the cationic fluorophore ASP^+ indicate a carrier-mediated mechanism in Calu-3. Results represent mean±SD (n = 3 experiments). *Significantly different from the flux measured in the ab direction*

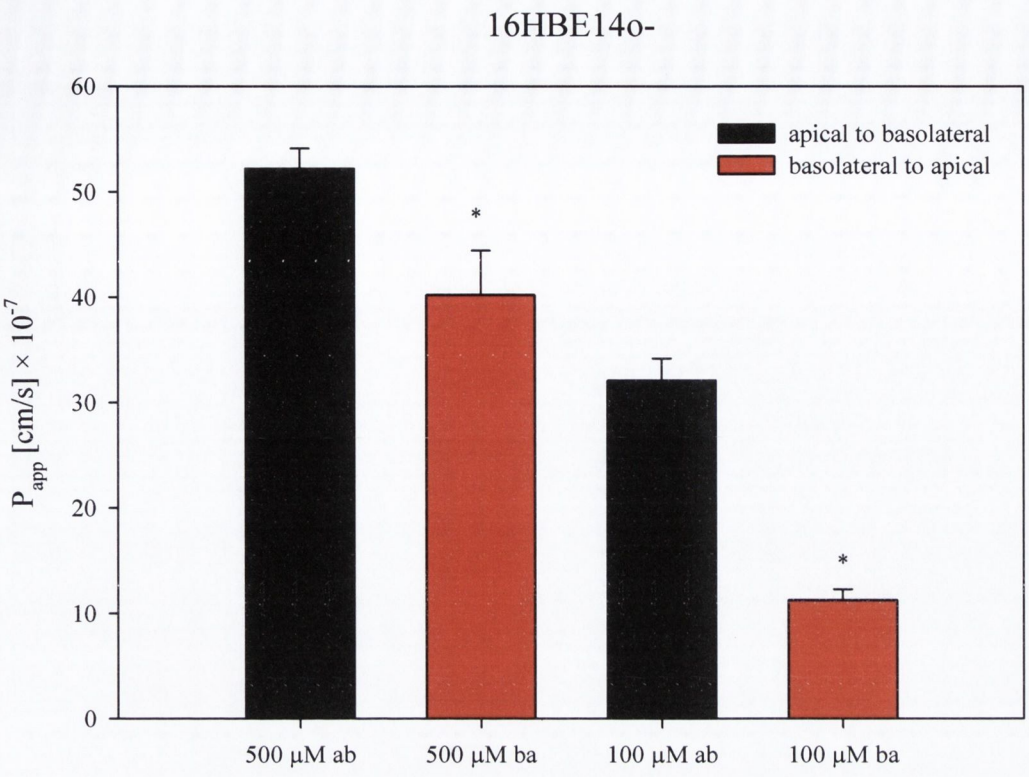

*Figure 4.30 Bi-directional transport studies with ASP^+ indicate a carrier-mediated mechanism in 16HBE14o-. Results represent mean±SD (n = 3 experiments). *Significantly different from the flux measured in the ab direction*

By contrast, hBEpC monolayers did not show any significant difference between ab and ba transport of ASP^+ (figure 4.31). However, growing the cells in different media had an impact on the ASP^+ fluxes. When grown in BEGM, the P_{app} (ab) across hBEpC monolayers was 6.30±1.48 × 10^{-7} cm/s and P_{app} (ba) 6.28±1.41 × 10^{-7} cm/s, whereas cells cultured in BEGM:DMEM-F12 exhibited P_{app} values of 1.39±0.30 × 10^{-7} cm/s (ab) and 1.33±0.52 × 10^{-7} cm/s (ba).

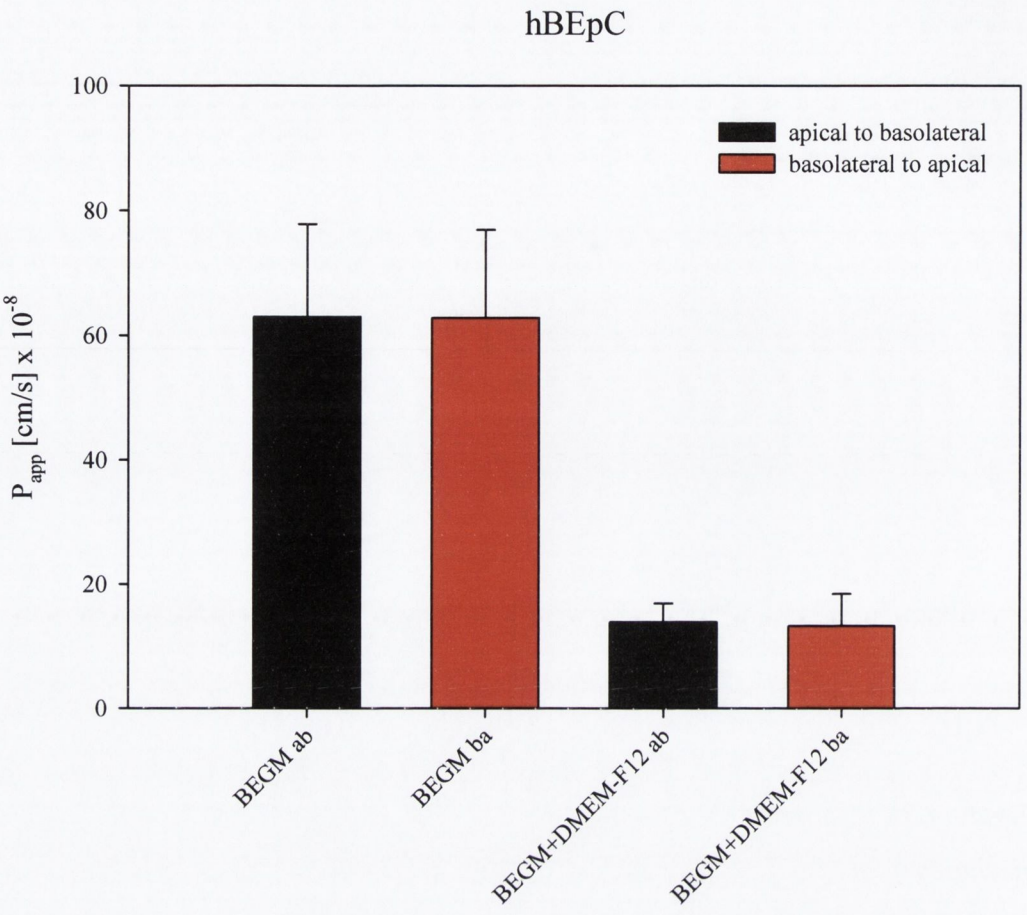

Figure 4.31 Bi-directional transport studies with ASP^+ indicate no carrier-mediated mechanisms in hBEpC. Results represent mean±SD (n = 3 experiments).

4.5 Discussion

4.5.1 Protein expression

Immunofluorescence confocal laser scanning microscopy shows absence of OCT2 in all lung cells tested confirming outcomes on mRNA level (see Chapter 2). This is contrary to results published by Lips and co-workers [2005] who characterised tracheal and bronchial epithelium of rats and human, finding weak staining of the apical membrane of ciliated cells. The differences might be explained by the fact

that this group used different antibodies (raised in rabbits and affinity purified) supplied by Eurogentec (Seraing, Belgium). Another explanation might be a down-regulation of OCT2 under different culture conditions. Caco-2 show low expression of OCT2 which is consistent with data published [Muller et al. 2005; Hilgendorf et al. 2007]. Low expression of OCT1 and OCT3 in all cell models tested confirms data discussed on gene expression level as well as published by Lips and co-workers [2005].

Most cell types showed relatively high expression of OCTN1 and OCTN2. Special attention is drawn to OCTN1, which was absent in hBEpC on mRNA and protein level. This conflicts with findings of Horvath and co-workers, but might be explained by the fact that hBEpC used in this study were purchased frozen and cultured using BEGM and BEGM:DMEM-F12 (50:50), respectively, whereas Horvath and co-workers cultured freshly isolated cells in DMEM-F12 with 10 µg/ml of insulin, 5 µg/ml of transferrin, 0.36 µg/ml of hydrocortisone, 20 ng/ml of triiodothyronine, 7.5 µg/ml of endothelial cell growth supplement, 100 U/ml of penicillin, and 100 µg/ml of streptomycin. Modification of culture medium did affect transepithelial electrical resistance and expression of OCTs. Substitution of 50% BEGM for DMEM:Ham-F12 did result in higher transepithelial electrical resistances.

Fluorescence activated cell sorting did show controversial expression patterns. Although means did vary in the expected dimensions, no difference between expression of organic cation transporters in Calu-3 (LCC and AIC) and 16HBE14o- was significant. Furthermore, the detected expression of OCT2 in all cell models tested lead to the assumption these antibodies are not suitable for

fluorescence activated cell sorting studies. Quantification of organic cation transporters was not possible.

4.5.2 Uptake studies

Data of this work shows uptake in wells of a defined area, which comprise similar numbers of cells and comparable amounts of proteins targeted. Due to the different nature of experiments presented by Horvath and co-workers [2007], who showed uptake into single hBEpC, comparison is rather difficult.

Cell models tested revealed different characteristics in time and temperature dependent uptake. Calu-3 and 16HBE14o- showed similarly low uptake leading to the assumption these two cell lines show similar transporter distribution and provide comparable models of low activity. Uptake of ASP^+ into Caco-2 and A549 was always higher than with the bronchial cell lines, but, whereas A549 could transport ASP^+ quicker in a 10 µM solution, Caco-2 were able to accumulate more ASP^+, showing a much higher saturation limit. Figure 4.17 shows faster uptake with A549 at concentrations up to 50 µM followed by saturation at higher concentrations. Caco-2 could accumulate almost four times more ASP^+ molecules within 20 min at the final concentration of 1 mM. Most discordant data were observed with hBEpC. Whereas time dependent uptake of 10 µM ASP^+ appeared similar to Caco-2, temperature dependent transport revealed lowest activity or rather early saturation.

The pH-dependent transport observed with Calu-3 and A549 supports the theory of a major role for the H^+ dependent transporters OCTN1 and OCTN2, which is consistent with assessments by Horvath and co-workers [2007]. Their studies found

high levels of mRNA and protein in airway epithelial cells of the proximal airway region and pH-dependent ASP^+ uptake that was inhibited by TEA^+, L-carnitine, salbutamol and formoterol, leading to the assumption that cationic drug absorption in the lung is mainly associated with OCTN2. However, this group ignored the potential role of OCT1, OCT2 and OCT3 in their studies. Based on a low level of mRNA of for these transporters, they concluded their absence but did not prove this hypothesis on the protein level. In our studies, uptake by the other cell models, including hBEpC, did not show strong pH-dependency. Furthermore, no significantly higher uptake at pH 8.2 could be observed with any cell model tested. Differences in sodium dependence of the uptake suggest that the models have different transporter activities or distribution. With A549, the mean drops below 35%, whereas all other cell models do not show any significant inhibition under low sodium conditions. Uptake of ASP^+ was not inhibited by carnitine; neither L-carnitine nor D-carnitine had any significant effect. Inhibition of uptake by OCTN1 and OCTN2 should be detectable at concentrations used in this study as Koepsell and co-workers suggest (L-carnitine OCTN2 K_m 11/98 μM and D-carnitine OCTN1 IC50 24 μM, OCTN2 K_m 4.3/4.8 μM) [Koepsell et al. 2007]. Therefore, ASP^+ appears to be transported by additional proteins. However, all K_m and IC50 values published by this group were measured in transfected oocytes of *Xenopus laevis* or transfected epithelial cell lines.

Only A549 showed significant inhibition of ASP^+ uptake by amantadine and verapamil. Amantadine inhibits OCT1 (IC50 236 μM) and OCT2 (K_m 20/27 μM, IC50 28 μM) [Koepsell et al. 2007]. As OCT2 is not detectable in A549, the observed effect could result from inhibition of OCT1.

Verapamil is a multifunctional inhibitor affecting all organic cation transporters tested: OCT1 (IC50 2.9 μM), OCT2 (IC50 206 μM), OCT3 (IC50 24 μM), OCTN1 (IC50 8.4 μM) and OCTN2 (IC50 <50 μM). [Koepsell et al. 2007] Based on these facts, transport by OCTs should be noticeably inhibited at a concentration of 200 μM. However, since means did not go below 60% of control, transport by a different transporter can not be excluded.

Beclomethasone and budesonide did not show a significant inhibition of uptake of ASP^+. Horvath and co-workers [2007] tested the inhibitory potential of corticosterone. As with beclomethasone and budesonide, no reduction of ASP^+ uptake could be detected. Therefore, therapies with these glucocorticoids should not affect active transport of inhaled drugs.

Unlike Horvath et al. [2007] reported, significant inhibition could be observed when A549 were treated with salmeterol. Concentrations of 100 μM were sufficient to reduce the uptake of ASP^+ to less than 20% demonstrating the different nature of this cell line.

These studies show important differences between primary cell cultures and cell lines of different origin. No cell line was comparable to any other cell line. Highest effects were observed with A549. However, this cell line is not polarised, therefore all transporters are expected to be evenly distributed in the membrane.

4.5.3 Transport studies

Functional inconsistencies between cell models may be due to many reasons. One important point is differences between species. Steimer et al. [2007] emphasised that although porcine alveolar epithelial cells (pAEpC) are a promising alternative

to human alveolar epithelial cells (hAEpC), there are still variations between those models. Despite a similar expression of MDR1, confirmed by immunolabelling of the protein, pAEpC did not show secretion behaviour with the MDR1 substrate rhodamine 123 with a ba/ab transport ratio of 1.2, whereas hAEpC revealed a ratio of 3.1 confirming an active efflux of the compound by MDR1. The same studies reported differences between primary cell models and the epithelial cell lines Calu-3, 16HBE14o- and Caco-2. Caco-2, as a cell line of colon carcinoma origin, exposed a far higher transport ratio of 13.2 confirming the assumption that not only the region and accordingly the organ of isolation can lead to a different character of a model, but also variations between cancer and normal tissue include protein expression and/or protein activity.

Studies with bi-directional transport of ASP^+ revealed further differences between the cell lines and primary models. Calu-3, 16HBE14o- and hBEpC did not show similarities in those experiments. Calu-3 showed net secretion behaviour with a ba/ab transport ratio of 3.2 at donor concentration of 500 µM and 2.8 at 100 µM, whereas 16HBE14o-, with transport ratios of 0.8 (500 µM) and 0.4 (100 µM), revealed net absorption of ASP^+. Therefore, organic cation transporters, although similarly expressed in these cell lines, result in an opposing functional character. These differences can be due to alternative distribution of these proteins on the membrane. Since the location of organic cation transporters on apical or basolateral side of cells cultured in these experiments could not be detected with immunofluorescence confocal laser scanning microscopy, this hypothesis can not be proven yet.

With ratios of 1.0, hBEpC cultured under two different conditions showed no directed transport. The difference between these primary models with two media

tested did not consist in direction but rather in higher permeability coefficients for hBEpC cultured in BEGM. Although BEGM is the medium recommended for these cells by the supplier (Lonza), Horvath and co-workers [2007] used DMEM-F12 with 10 µg/ml of insulin, 5 µg/ml of transferrin, 0.36 µg/ml of hydrocortisone, 20 ng/ml of triiodothyronine, 7.5 µg/ml of endothelial cell growth supplement, 100 U/ml of penicillin, and 100 µg/ml of streptomycin to customise their media. Lin and co-workers [2007] cultured hBEpC in T-flasks using BEGM, but then changed medium to BEGM:DMEM-F12 (50:50) for cultures on Transwell inserts resulting in higher TEER values (Figure 4.28). This fact can explain the differences in transport studies of ASP^+ across hBEpC, but lower TEER values describe a less efficient barrier rather than changes in transport activities.

5 Conclusions

This work is an initial step towards a better understanding of the role transporters play in pulmonary drug disposition. It provides fundamental knowledge on expression of key carrier transporters, including 11 ABC transporters, 11 SLC transporters, and 9 SLCO transporters within a wide range of respiratory cell culture models, including established cell lines (A549, Calu-3, 16HBE14o-, BEAS-2B) and freshly isolated cells in primary culture (human bronchial and alveolar epithelial cells), commonly used in biopharmaceutical studies and indeed pharmacological research. Differential transporter expression throughout cell culture models from different regions of the lung as well as disparities when comparing cell lines with primary cell culture models were highlighted. Moreover, a number of variations regarding transporter expression in cell models of pulmonary compared to gastrointestinal origin were discovered. The data provided will help guide the use of particular respiratory cell models and also explain potential differences in results outcome. RT-PCR, immunofluorescence microscopy, uptake and bi-directional transport studies clearly demonstrated the importance of selecting the right cell model.

The presence and activity of MDR1 in hAEpC monolayers was confirmed by Western blotting, by immunofluorescence microscopy and by conducting bi-directional transport studies employing a MDR1 substrate (rhodamine 123) revealing net secretion, which was attenuated in the presence of the MDR1 inhibitor, verapamil. The permeability of fluorescein sodium, a paracellular transport marker, on the other hand, showed no distinct directionality. Alveolar tissue specimens showed MDR1 localised to the luminal membranes of type I pneumocytes. These findings indicate that MDR1 is functionally active in the human alveolar airspace and that hAEpC monolayers might provide a suitable *in*

vitro model for studying MDR1 function mechanistically in the distal human lung. Although primary cells are usually the closest to a situation *in vivo*, this model is relatively high in cost and exhibits limited reproducibility due to inter-individual differences. A cell line reflecting transporter expression *in vivo* provides a more robust model with consistent outcomes.

Characterisation of organic cation transporters in selected cell lines and hBEpC as a primary model confirmed the presence of OCT1, OCT3, OCTN1 and OCTN2 in all cell models tested by immunofluorescence microscopy with highest expression of OCTN1 and OCTN2 in Calu-3 (AIC). However, antibodies used in these studies could only provide a first impression and did not meet the high standards necessary to localise and quantify organic cation transporters. Further studies with more specific, ideally monoclonal, antibodies are essential to provide this information. Unfortunately, there are no suitable antibodies offered for purchase yet.

Uptake of the cationic fluorophore 4-[4-(dimethylamino)-styryl]-N-methylpyridinium (ASP^+) revealed negligible differences between Calu-3 and 16HBE14o- cells. Although A549 showed the strongest effects with inhibitors and strongest pH- and sodium-dependence this cell line is not suitable for transport studies because cells do not polarise and do not form a sufficient barrier. Bi-directional transport studies revealed net secretion with Calu-3 and net absorption with 16HBE14o-, whereas hBEpC did not show any directed transport. Since the organic cation transporters are known to work in both directions, release studies can provide further understanding of their role in the lung.

Even if it seems still unclear which model (Calu-3 or 16HBE14o-) more closely reflects *in vivo* characteristics, and since our hBEpC as the obviously closest model showed unlikely behaviour, based on this study, research with access to freshly

isolated bronchial epithelium will be easily able to choose the appropriate cell model for the drug or substrate to be studied.

Acknowledgements

My eternal gratitude goes to Dr. Carsten Ehrhardt for his enthusiasm, knowledge, encouragement and guidance over this thesis. I would like to thank Patrick Quinlan, Brian O'Reilly, Conan Murphy, Brian Talbot, Betty Daly and Liesa Eckhardt for their support and supply of all the little things that make a big difference in lab and office. Thanks to Leonie Baginski, Stephen Buckley, Fiona Ní Chearúil, Juan Jose Corbalan Penas, Deirdre D'Darcy, Tom Greene, Lenka Horálkova, Jason Horan, Niall Keely, Orla Ní Ógáin, Krzysztof Paluch, Aneta Radziwon, Maria Jose Santos Martinez, Pawel Stasiak and Lidia Tajber for being wonderful colleagues. I would also like to express my gratitude to Dr. Mark Gumbleton, Dr. Paul Buckland, Nicholas Bray, Andrew Hollins, Smitha Sutrala, Christopher Morris, Mathew Smith and Talia Buggins for all their help and support throughout my time in Cardiff. Thanks to Prof. Claus-Michael Lehr and his group for the supply of hAEpC and their support during my studies of this cell model. Thanks to Aoife Gowran for her help with CLSM; and to Serena Germano and Carlos Medina for supporting me during the difficult times with my suboptimal antibodies. My gratitude goes to Prof. Marek Radomski, for his patience and understanding during my writing phase. Thanks to Oliviero Gobbo for being the best office mate I could wish for, and Serena Germano, Ahmad Shawqi Barham, Vincent Caron, Frederic Tewes, Fábio de Sousa Menezes, Shona Harmon, Johanna Salomon and Elena Schwagerus for refreshing and inspiring coffee breaks.

Special thanks go to my family for their love and support, in particular to Jochen Haas for being always by my side, for his love, support and knowledge.

List of abbreviations

16HBE14o-	human bronchial epithelial cell line
A549	a human lung alveolar adenocarcinoma cell line
ab	apical to basolateral
ABC	ATP binding cassette
ACE	Angiotensin-converting enzyme
AIC	air-interphase culture
AP	alkaline phosphatase
ASP^+	4-[4-(dimethylamino)styryl]-N-methylpyridinium iodide
ATI and ATII	human alveolar epithelial type I and II cell
ATP	adenosine triphosphate
AZT	Azidothymidine (INN: Zidovudine)
ba	basolateral to apical
BCECF	2',7'-Bis-(carboxyethyl)-5(6)-carboxyfluorescein
BCRP	breast cancer related protein
BEAS-2B	human bronchial epithelial cell line
BEGM	bronchial epithelial cell growth medium
BPE	Bovine Pituitary Extract
BPI	Bactericidal/permeability-increasing protein
BSA	Bovine serum albumin
BSA-FAF	Bovine Serum Albumin – Fatty Acid Free
BSS	balanced salt solution
Caco-2	line of heterogeneous human epithelial colorectal adenocarcinoma cells
Calu-3	cells derived from a human bronchial adenocarcinoma
cAMP	cyclo-adenosine monophosphate
cDNA	complementary DNA
CF	cystic fibrosis
CFTR	cystic fibrosis transmembrane conductance
cGMP	cyclo-guanine monophosphate
cMOAT	canalicular multispecific organic anion transporter
COPD	chronic obstructive pulmonary disease
d_a	aerodynamic diameter

DAPI	4',6-diamidino-2-phenylindole dihydrochloride
dDAVP	Desmopressin (1-desamino-8-D-arginine vasopressin)
DEPC	diethyl pyrocarbonate
DEPC	Diethylpyrocarbonate (IUPAC: diethyl dicarbonate)
DMEM	Dulbecco's modified Eagle's medium
DNA	deoxyribonucleic acid
dNTP	deoxy-nucleotide-triphosphate (N = A, C, G, T)
DTT	dithiotreitol
EDTA	ethylene diamine tetra-acetic acid
FACS	fluorescence-activated cell sorting
FB	FACS buffer
FBS	foetal bovine serum
FluNa	Fluorescein sodium
FSH	follicle stimulating hormone
GAPDH	D-glyceraldehyde-3-phosphate dehydrogenase
gDNA	Genomic deoxyribonucleic acid
GM-CSF	Granulocyte macrophage-colony stimulating factor
GSH	glutathione
GSSG	oxidized (-S-S-) glutathione
hAEpC	human alveolar epithelial primary cells
HEK 293	Human Embryonic Kidney 293 cells
HeLa cells	cell line, derived from cervical cancer cells taken from patient Henrietta Lacks
HEPES	N-2-hydroxyethylpiperazine-N'-2-ethanesulfonic acid
HIV	human immunodeficiency virus
HMG-CoA	3-hydroxy-3-methylglutaryl-coenzyme A
IgG	Immunoglobulin G
IL-2	Interleukin-2
KRB	Krebs-Ringer buffer
LCC	liquid covered culture
L-DOPA	L-3,4-dihydroxyphenylalanine
LTC_4	Leukotriene C_4
MDR	multidrug resistance protein
MEM	Eagle's minimum essential medium
M-MLV-RT	Moloney Murine Leukemia Virus Reverse Transcriptase

MOAT	multispecific organic anion transporter
MPP^+	1-methyl-4-phenylpyridinium
mRNA	messenger ribonucleic acid
MRP	multidrug resistant protein
MW	molecular weight
NHBE	Normal human bronchial epithelial (cells)
NHE-1	Na^+/H^+ exchanging systems, Sodium-hydrogen antiporter 1
NMDA	N-methyl D-aspartate
OAT	Organic anion transporter
OATP	organic anion transporting polypeptide
OCT	Organic cation transporter
pAEpC	porcine alveolar epithelial cells
PAH	para-aminohippuric acid
P_{app}	apparent permeability coefficient
PBS	phosphate buffered saline
PBS	Phosphate-buffered saline
PCR	polymerase chain reaction
PCR	Polymerase chain reaction
P-gp	P-glycoprotein
PLGA	poly(lactic-co-glycolic acid)
PTH	Parathormone
q-PCR	quantitative polymerase chain reaction
QSAR	quantitive structure-activity relationships
Rh123	rhodamine-123
rhEGF	recombinant human epithelial growth factor
rhG-CSF	recombinant human granulocyte-colony stimulating factor
RNA	ribonucleic acid
rT_3	reverse tri-iodothyronine
RT-PCR	reverse transcription-polymerase chain reaction
SABM	small airway epithelial basal medium
SAGM	small airways growth medium
SD	standard deviation
SDS	Sodium dodecyl sulfate
SLC	solute carrier

SLCO	organic anion transporting polypeptide transporters
SNARF	Seminaphtharhodafluor
SNP	single nucleotide polymorphism
T_4	thyroxine
Taq polymerase	*Thermus aquaticus* polymerase
TBE buffer	TRIS-borate-EDTA buffer
TEA	tetraethylammonium
TEER	transepithelial electrical resistance
THC	Δ-9-tetrahydrocannabinol, dronabinol
TPrA	tetrapropylammonium
TRIS	tris(hydroxymethyl)aminomethane
TSH	Thyroid-stimulating hormone

References

Abulrob, A. G. and M. Gumbleton (1999). Transport of phosphatidylcholine in MDR3-negative epithelial cell lines via drug-induced MDR1 P-glycoprotein. Biochem Biophys Res Commun 262(1): 121-6.

Adachi, H., T. Suzuki, et al. (2003). Molecular characterization of human and rat organic anion transporter OATP-D. Am J Physiol Renal Physiol 285(6): F1188-97.

Anzai, N., Y. Kanai, et al. (2006). Organic anion transporter family: current knowledge. J Pharmacol Sci 100(5): 411-26.

Axiotis, C. A., D. Bani, et al. (1995). P-glycoprotein is expressed in parathyroid epithelium and is regulated by calcium. Calcif Tissue Int 56(2): 170-4.

Ayrton, A. and P. Morgan (2001). Role of transport proteins in drug absorption, distribution and excretion. Xenobiotica 31(8-9): 469-97.

Ayrton, A. and P. Morgan (2008). Role of transport proteins in drug discovery and development: a pharmaceutical perspective. Xenobiotica 38(7-8): 676-708.

Bahadduri, P. M., V. M. D'Souza, et al. (2005). Functional characterization of the peptide transporter PEPT2 in primary cultures of human upper airway epithelium. Am J Respir Cell Mol Biol 32(4): 319-25.

Bakos, E. and L. Homolya (2007). Portrait of multifaceted transporter, the multidrug resistance-associated protein 1 (MRP1/ABCC1). Pflugers Arch 453(5): 621-41.

Bastacky, J., C. Y. Lee, et al. (1995). Alveolar lining layer is thin and continuous: low-temperature scanning electron microscopy of rat lung. J Appl Physiol 79(5): 1615-28.

Bleasby, K., J. C. Castle, et al. (2006). Expression profiles of 50 xenobiotic transporter genes in humans and pre-clinical species: a resource for investigations into drug disposition. Xenobiotica 36(10-11): 963-88.

Bosch, I., K. Dunussi-Joannopoulos, et al. (1997). Phosphatidylcholine and phosphatidylethanolamine behave as substrates of the human MDR1 P-glycoprotein. Biochemistry 36(19): 5685-94.

Campbell, L., A. N. Abulrob, et al. (2003). Constitutive expression of p-glycoprotein in normal lung alveolar epithelium and functionality in primary alveolar epithelial cultures. J Pharmacol Exp Ther 304(1): 441-52.

Cascorbi, I. (2006). Role of pharmacogenetics of ATP-binding cassette transporters in the pharmacokinetics of drugs. Pharmacol Ther 112(2): 457-73.

Chen, J., Z. Chen, et al. (2004). Isolation of highly pure alveolar epithelial type I and type II cells from rat lungs. Lab Invest 84(6): 727-35.

Cordon-Cardo, C., J. P. O'Brien, et al. (1990). Expression of the multidrug resistance gene product (P-glycoprotein) in human normal and tumor tissues. J Histochem Cytochem 38(9): 1277-87.

Cozens, A. L., M. J. Yezzi, et al. (1994). CFTR expression and chloride secretion in polarized immortal human bronchial epithelial cells. Am J Respir Cell Mol Biol 10(1): 38-47.

Daniel, H. and G. Kottra (2004). The proton oligopeptide cotransporter family SLC15 in physiology and pharmacology. Pflugers Arch 447(5): 610-8.

Dean, M., Y. Hamon, et al. (2001). The human ATP-binding cassette (ABC) transporter superfamily. J Lipid Res 42(7): 1007-17.

Demeule, M., J. Jodoin, et al. (2000). P-glycoprotein is localized in caveolae in resistant cells and in brain capillaries. FEBS Lett 466(2-3): 219-24.

Demeule, M., D. Shedid, et al. (2001). Expression of multidrug-resistance P-glycoprotein (MDR1) in human brain tumors. Int J Cancer 93(1): 62-6.

Demling, N., C. Ehrhardt, et al. (2006). Promotion of cell adherence and spreading: a novel function of RAGE, the highly selective differentiation marker of human alveolar epithelial type I cells. Cell Tissue Res 323(3): 475-88.

Ehrhardt, C., E. M. Collnot, et al. (2006). Towards an in vitro model of cystic fibrosis small airway epithelium: characterisation of the human bronchial epithelial cell line CFBE41o. Cell Tissue Res 323(3): 405-15.

Ehrhardt, C., K. J. Kim, et al. (2005). Isolation and culture of human alveolar epithelial cells. Methods Mol Med 107: 207-16.

Ehrhardt, C., K.J. Kim, (eds.) Drug Absorption Studies – In Situ, InVitro and In Silico Models. Biotechnology: Pharmaceutical Aspects Series, 2008: Vol. VII. New York: Springer.

Ehrhardt, C., C. Kneuer, et al. (2002). Influence of apical fluid volume on the development of functional intercellular junctions in the human epithelial cell line

16HBE14o-: implications for the use of this cell line as an in vitro model for bronchial drug absorption studies. Cell Tissue Res 308(3): 391-400.

Ehrhardt, C., C. Kneuer, et al. (2003). 16HBE14o- human bronchial epithelial cell layers express P-glycoprotein, lung resistance-related protein, and caveolin-1. Pharm Res 20(4): 545-51.

Ejendal, K. F. and C. A. Hrycyna (2002). Multidrug resistance and cancer: the role of the human ABC transporter ABCG2. Curr Protein Pept Sci 3(5): 503-11.

Elbert, K. J., U. F. Schafer, et al. (1999). Monolayers of human alveolar epithelial cells in primary culture for pulmonary absorption and transport studies. Pharm Res 16(5): 601-8.

Fetsch, P. A., A. Abati, et al. (2006). Localization of the ABCG2 mitoxantrone resistance-associated protein in normal tissues. Cancer Lett 235(1): 84-92.

Florea, B. I., M. L. Cassara, et al. (2003). Drug transport and metabolism characteristics of the human airway epithelial cell line Calu-3. J Control Release 87(1-3): 131-8.

Forbes, B. and C. Ehrhardt (2005). Human respiratory epithelial cell culture for drug delivery applications. Eur J Pharm Biopharm 60(2): 193-205.

Foster, K. A., C. G. Oster, et al. (1998). Characterization of the A549 cell line as a type II pulmonary epithelial cell model for drug metabolism. Exp Cell Res 243(2): 359-66.

Fuchs, S., A. J. Hollins, et al. (2003). Differentiation of human alveolar epithelial cells in primary culture: morphological characterization and synthesis of caveolin-1 and surfactant protein-C. Cell Tissue Res 311(1): 31-45.

Gao, B., R. D. Huber, et al. (2005). Localization of organic anion transporting polypeptides in the rat and human ciliary body epithelium. Exp Eye Res 80(1): 61-72.

Giard, D. J., S. A. Aaronson, et al. (1973). In vitro cultivation of human tumors: establishment of cell lines derived from a series of solid tumors. J Natl Cancer Inst 51(5): 1417-23.

Glaeser, H., D. G. Bailey, et al. (2007). Intestinal drug transporter expression and the impact of grapefruit juice in humans. Clin Pharmacol Ther 81(3): 362-70.

Greiner, B., M. Eichelbaum, et al. (1999). The role of intestinal P-glycoprotein in the interaction of digoxin and rifampin. J Clin Invest 104(2): 147-53.

Groneberg, D. A., M. Nickolaus, et al. (2001). Localization of the peptide transporter PEPT2 in the lung: implications for pulmonary oligopeptide uptake. Am J Pathol 158(2): 707-14.

Gruenert, D. C., W. E. Finkbeiner, et al. (1995). Culture and transformation of human airway epithelial cells. Am J Physiol 268(3 Pt 1): L347-60.

Hagenbuch, B. and C. Gui (2008). Xenobiotic transporters of the human organic anion transporting polypeptides (OATP) family. Xenobiotica 38(7-8): 778-801.

Hagenbuch, B. and P. J. Meier (2003). The superfamily of organic anion transporting polypeptides. Biochim Biophys Acta 1609(1): 1-18.

Hagenbuch, B. and P. J. Meier (2004). Organic anion transporting polypeptides of the OATP/ SLC21 family: phylogenetic classification as OATP/ SLCO superfamily, new nomenclature and molecular/functional properties. Pflugers Arch 447(5): 653-65.

Hamilton, K. O., G. Backstrom, et al. (2001). P-glycoprotein efflux pump expression and activity in Calu-3 cells. J Pharm Sci 90(5): 647-58.

Higgins, C. F. (1995). Volume-activated chloride currents associated with the multidrug resistance P-glycoprotein. J Physiol 482: 31S-36S.

Hilgendorf, C., G. Ahlin, et al. (2007). Expression of thirty-six drug transporter genes in human intestine, liver, kidney, and organotypic cell lines. Drug Metab Dispos 35(8): 1333-40.

Horvath, G., E. S. Mendes, et al. (2007). The effect of corticosteroids on the disposal of long-acting beta2-agonists by airway smooth muscle cells. J Allergy Clin Immunol 120(5): 1103-9.

Horvath, G., N. Schmid, et al. (2007). Epithelial organic cation transporters ensure pH-dependent drug absorption in the airway. Am J Respir Cell Mol Biol 36(1): 53-60.

Hsiang, B., Y. Zhu, et al. (1999). A novel human hepatic organic anion transporting polypeptide (OATP2). Identification of a liver-specific human organic anion transporting polypeptide and identification of rat and human hydroxymethylglutaryl-CoA reductase inhibitor transporters. J Biol Chem 274(52): 37161-8.

Ishiguro, N., M. Oyabu, et al. (2008). Decreased biosynthesis of lung surfactant constituent phosphatidylcholine due to inhibition of choline transporter by gefitinib in lung alveolar cells. Pharm Res 25(2): 417-27.

Kennedy, B. G. and N. J. Mangini (2002). P-glycoprotein expression in human retinal pigment epithelium. Mol Vis 8: 422-30.

Kim, K. J., Z. Borok, et al. (2001). A useful in vitro model for transport studies of alveolar epithelial barrier. Pharm Res 18(3): 253-5.

Klucken, J., C. Buchler, et al. (2000). ABCG1 (ABC8), the human homolog of the Drosophila white gene, is a regulator of macrophage cholesterol and phospholipid transport. Proc Natl Acad Sci U S A 97(2): 817-22.

Koepsell, H. and H. Endou (2004). The SLC22 drug transporter family. Pflugers Arch 447(5): 666-76.

Koepsell, H., K. Lips, et al. (2007). Polyspecific organic cation transporters: structure, function, physiological roles, and biopharmaceutical implications. Pharm Res 24(7): 1227-51.

Konig, J., Y. Cui, et al. (2000). A novel human organic anion transporting polypeptide localized to the basolateral hepatocyte membrane. Am J Physiol Gastrointest Liver Physiol 278(1): G156-64.

Kool, M., M. de Haas, et al. (1997). Analysis of expression of cMOAT (MRP2), MRP3, MRP4, and MRP5, homologues of the multidrug resistance-associated protein gene (MRP1), in human cancer cell lines. Cancer Res 57(16): 3537-47.

Kool, M., M. van der Linden, et al. (1999). MRP3, an organic anion transporter able to transport anti-cancer drugs. Proc Natl Acad Sci U S A 96(12): 6914-9.

Kruh, G. D. and M. G. Belinsky (2003). The MRP family of drug efflux pumps. Oncogene 22(47): 7537-52.

Kruh, G. D., Y. Guo, et al. (2007). ABCC10, ABCC11, and ABCC12. Pflugers Arch 453(5): 675-84.

Kuhlmann, O., H. S. Hofmann, et al. (2003). Pharmacokinetics of idarubicin in the isolated perfused rat lung: effect of cinchonine and rutin. Anticancer Drugs 14(6): 411-6.

Kullak-Ublick, G. A., B. Hagenbuch, et al. (1995). Molecular and functional characterization of an organic anion transporting polypeptide cloned from human liver. Gastroenterology 109(4): 1274-82.

Kullak-Ublick, G. A., M. G. Ismair, et al. (2001). Organic anion-transporting polypeptide B (OATP-B) and its functional comparison with three other OATPs of human liver. Gastroenterology 120(2): 525-33.

Kummer, W., S. Wiegand, et al. (2006). Role of acetylcholine and polyspecific cation transporters in serotonin-induced bronchoconstriction in the mouse. Respir Res 7: 65.

Kuo, M. T., J. J. Bao, et al. (1996). Frequent coordinated overexpression of the MRP/GS-X pump and gamma-glutamylcysteine synthetase genes in human colorectal cancers. Cancer Res 56(16): 3642-4.

Langmann, T., R. Mauerer, et al. (2003). Real-time reverse transcription-PCR expression profiling of the complete human ATP-binding cassette transporter superfamily in various tissues. Clin Chem 49(2): 230-8.

Laube, B. L. (2005). The expanding role of aerosols in systemic drug delivery, gene therapy, and vaccination. Respir Care 50(9): 1161-76.

Lechapt-Zalcman, E., I. Hurbain, et al. (1997). MDR1-Pgp 170 expression in human bronchus. Eur Respir J 10(8): 1837-43.

Lee, J. and J. L. Boyer (2000). Molecular alterations in hepatocyte transport mechanisms in acquired cholestatic liver disorders. Semin Liver Dis 20(3): 373-84.

Lee, W., H. Glaeser, et al. (2005). Polymorphisms in human organic anion-transporting polypeptide 1A2 (OATP1A2): implications for altered drug disposition and central nervous system drug entry. J Biol Chem 280(10): 9610-7.

Lin, H., H. Li, et al. (2007). Air-liquid interface (ALI) culture of human bronchial epithelial cell monolayers as an in vitro model for airway drug transport studies. J Pharm Sci 96(2): 341-50.

Lips, K. S., A. Luhrmann, et al. (2007). Down-regulation of the non-neuronal acetylcholine synthesis and release machinery in acute allergic airway inflammation of rat and mouse. Life Sci 80(24-25): 2263-9.

Lips, K. S., C. Volk, et al. (2005). Polyspecific cation transporters mediate luminal release of acetylcholine from bronchial epithelium. Am J Respir Cell Mol Biol 33(1): 79-88.

Livak, K. J. and T. D. Schmittgen (2001). Analysis of relative gene expression data using real-time quantitative PCR and the 2(-Delta Delta C(T)) Method. Methods 25(4): 402-8.

Logan, C. and N. O'Sullivan (2008) Detection of Viral Agents of Gastroenteritis: Detection of Gastrointestinal Viruses. Future Virology **3**(1):61-70.

Lu, H. and C. Klaassen (2006). Tissue distribution and thyroid hormone regulation of Pept1 and Pept2 mRNA in rodents. Peptides 27(4): 850-7.

Lu, R., N. Kanai, et al. (1996). Regulation of renal oatp mRNA expression by testosterone. Am J Physiol 270(2 Pt 2): F332-7.

Manford, F., Y. Riffo-Vasquez, et al. (2008). Lack of difference in pulmonary absorption of digoxin, a P-glycoprotein substrate, in mdr1a-deficient and mdr1a-competent mice. J Pharm Pharmacol 60(10): 1305-10.

Manford, F., A. Tronde, et al. (2005). Drug permeability in 16HBE14o- airway cell layers correlates with absorption from the isolated perfused rat lung. Eur J Pharm Sci 26(5): 414-20.

Maubon, N., M. Le Vee, et al. (2007). Analysis of drug transporter expression in human intestinal Caco-2 cells by real-time PCR. Fundam Clin Pharmacol 21(6): 659-63.

Mi, Q., B. Cui, et al. (2001). Pervilleine A, a novel tropane alkaloid that reverses the multidrug-resistance phenotype. Cancer Res 61(10): 4030-7.

Miakotina, O. L., M. Agassandian, et al. (2005). Adenovirus stimulates choline efflux by increasing expression of organic cation transporter-2. Am J Physiol Lung Cell Mol Physiol 288(1): L93-102.

Mikkaichi, T., T. Suzuki, et al. (2004). The organic anion transporter (OATP) family. Drug Metab Pharmacokinet 19(3): 171-9.

Muller, J., K. S. Lips, et al. (2005). Drug specificity and intestinal membrane localization of human organic cation transporters (OCT). Biochem Pharmacol 70(12): 1851-60.

Patton, J. S., C. S. Fishburn, et al. (2004). The lungs as a portal of entry for systemic drug delivery. Proc Am Thorac Soc 1(4): 338-44.

Pavlova, A., H. Sakurai, et al. (2000). Developmentally regulated expression of organic ion transporters NKT (OAT1), OCT1, NLT (OAT2), and Roct. Am J Physiol Renal Physiol 278(4): F635-43.

Pizzagalli, F., B. Hagenbuch, et al. (2002). Identification of a novel human organic anion transporting polypeptide as a high affinity thyroxine transporter. Mol Endocrinol 16(10): 2283-96.

Robey, R. W., K. K. To, et al. (2009). ABCG2: a perspective. Adv Drug Deliv Rev 61(1): 3-13.

Rohen, J. and E. Lütjen-Drecoll (2000). Funktionelle Histologie. Stuttgart, Schattauer.

Sabin, A. B. (1983). Immunization against measles by aerosol. Rev Infect Dis 5(3): 514-23.

Sai, Y. and A. Tsuji (2004). Transporter-mediated drug delivery: recent progress and experimental approaches. Drug Discov Today 9(16): 712-20.

Scheffer, G. L., A. C. Pijnenborg, et al. (2002). Multidrug resistance related molecules in human and murine lung. J Clin Pathol 55(5): 332-9.

Schinkel, A. H. and J. W. Jonker (2003). Mammalian drug efflux transporters of the ATP binding cassette (ABC) family: an overview. Adv Drug Deliv Rev 55(1): 3-29.

Siekmeier, R. and G. Scheuch (2008). Systemic treatment by inhalation of macromolecules--principles, problems, and examples. J Physiol Pharmacol 59 Suppl 6: 53-79.

Sirotnak, F. M., H. G. Wendel, et al. (2000). Co-administration of probenecid, an inhibitor of a cMOAT/MRP-like plasma membrane ATPase, greatly enhanced the efficacy of a new 10-deazaaminopterin against human solid tumors in vivo. Clin Cancer Res 6(9): 3705-12.

Søndergaard, H. B., B. Brodin, et al. (2008). hPEPT1 is responsible for uptake and transport of Gly-Sar in the human bronchial airway epithelial cell-line Calu-3. Pflugers Arch 456(3): 611-22.

Sporty, J. L., L. Horalkova, et al. (2008). In vitro cell culture models for the assessment of pulmonary drug disposition. Expert Opin Drug Metab Toxicol 4(4): 333-45.

Steimer, A., H. Franke, et al. (2007). Monolayers of porcine alveolar epithelial cells in primary culture as an in vitro model for drug absorption studies. Eur J Pharm Biopharm 66(3): 372-82.

Steimer, A., E. Haltner, et al. (2005). Cell culture models of the respiratory tract relevant to pulmonary drug delivery. J Aerosol Med 18(2): 137-82.

Stone, K. C., R. R. Mercer, et al. (1992). Allometric relationships of cell numbers and size in the mammalian lung. Am J Respir Cell Mol Biol 6(2): 235-43.

Stouch, T. R. and O. Gudmundsson (2002). Progress in understanding the structure-activity relationships of P-glycoprotein. Adv Drug Deliv Rev 54(3): 315-28.

Sun, H., E. C. Chow, et al. (2008). The Caco-2 cell monolayer: usefulness and limitations. Expert Opin Drug Metab Toxicol 4(4): 395-411.

Tamai, I., J. Nezu, et al. (2000). Molecular identification and characterization of novel members of the human organic anion transporter (OATP) family. Biochem Biophys Res Commun 273(1): 251-60.

Tamai, I., T. Nozawa, et al. (2001). Functional characterization of human organic anion transporting polypeptide B (OATP-B) in comparison with liver-specific OATP-C. Pharm Res 18(9): 1262-9.

Thomas, G. A., M. A. Barrand, et al. (1994). Expression of the multidrug resistance-associated protein (MRP) gene in human lung tumours and normal tissue as determined by in situ hybridisation. Eur J Cancer 30A(11): 1705-9.

Torky, A. R., E. Stehfest, et al. (2005). Immuno-histochemical detection of MRPs in human lung cells in culture. Toxicology 207(3): 437-50.

Toyoda, Y., Y. Hagiya, et al. (2008). MRP class of human ATP binding cassette (ABC) transporters: historical background and new research directions. Xenobiotica 38(7-8): 833-62.

van der Deen, M., E. G. de Vries, et al. (2005). ATP-binding cassette (ABC) transporters in normal and pathological lung. Respir Res 6: 59.

van der Deen, M., E. G. de Vries, et al. (2007). Cigarette smoke extract affects functional activity of MRP1 in bronchial epithelial cells. J Biochem Mol Toxicol 21(5): 243-51.

van der Deen, M., H. Marks, et al. (2006). Diminished expression of multidrug resistance-associated protein 1 (MRP1) in bronchial epithelium of COPD patients. Virchows Arch 449(6): 682-8.

von Wichert, P. and C. Seifart (2005). The lung, an organ for absorption? Respiration 72(5): 552-8.

Wang, T., J. Li, et al. (2007). Choline transporters in human lung adenocarcinoma: expression and functional implications. Acta Biochim Biophys Sin (Shanghai) 39(9): 668-74.

Weibel, E. R. (1963). Morphometry of the human lung. New York, Academic Press.

Yoneda, K. (1976). Mucous blanket of rat bronchus: an ultrastructural study. Am Rev Respir Dis 114(5): 837-42.

Zhang, L., C. M. Brett, et al. (1998). Role of organic cation transporters in drug absorption and elimination. Annu Rev Pharmacol Toxicol 38: 431-60.

Zhou, S. F. (2008). Structure, function and regulation of P-glycoprotein and its clinical relevance in drug disposition. Xenobiotica 38(7-8): 802-32.